

Diss. ETH No. 14324

# Extending length and time scales of *ab initio* molecular dynamics simulations

A dissertation submitted to the  
Swiss Federal Institute of Technology  
Zurich

for the degree of  
Doctor of Natural Sciences

presented by

**Joost VandeVondele**

Engineer in Physics, Ghent University

born 28.05.1975

Ghent, Belgium

accepted on the recommendation of

Prof. Dr. U. Röthlisberger, examiner

Prof. Dr. M. Parrinello, co-examiner

August, 2001

© 2001

Joost VandeVondele

All Rights Reserved

*To Stephanie*

Seite Leer /  
Blank leaf

Seite Leer /  
Blank leaf

## ACKNOWLEDGEMENTS

Many people have been a part of my graduate education, as friends and colleagues. This thesis would not appear in its present form without their kind assistance and support.

My sincere gratitude goes to my supervisor Ursula Röthlisberger for her support and encouragement. I enjoyed the freedom she gave me to explore different approaches to this inspiring subject. The many discussions we had were invaluable to develop the ideas that are presented in this thesis. Additionally, she provided the resources that were needed to perform the computations and which allowed me to go to several conferences. Going to conferences was a great way to present my results, broadened my view of the field, and provided new ideas.

Special thanks go to Alessandro Laio. Working together with him on the QM/MM code was a joyful and unique experience. The skillful ways in which he derived, integrated, and coded incredible expressions impressed me and contributed significantly to the success of the project. That he failed to serve me a real 'bagnacauda' should not be mentioned.

I would like to thank Tom Woo and Alessandra Magistrato, colleagues of 'the early days'. They taught me many tricks of the trade. The prion project started with the experiments of Sabine Vandoorslaer, Grazia Cereghetti, Rudi Glockshuber, and Arthur Schweiger, and I acknowledge their initiative to contact us. I thank all my other colleagues - Maria Carola Colombo, Karel Doclo, Leonardo Guidoni, Martin Luggen, Patrick Maurer, Stefano Piana, Ute Röhrig, Katrin Spiegel, Andrea Tasso, Otto Anatole von Lilienfeld-Toal, and Martin Zumstein - for the pleasant time we spent both at and after work. Furthermore, I thank Wilfred van Gunsteren, his group and the visitors of our group for the interactions, and Michele Parrinello for accepting to be co-examiner of this thesis.

Most importantly, I'm very grateful to my parents and brother for their continuing encouragement, and to Stephanie Finken for her love and support that makes every day something special and enjoyable.

Seite Leer /  
Blank leaf

# Contents

<b>1</b>	<b>Introduction</b>	<b>19</b>
1.1	<i>Ab initio</i> molecular dynamics simulations . . . . .	20
1.2	Limitations of current MD simulations . . . . .	21
1.3	Assuming locality to extend length and time scales . . . . .	24
1.3.1	Extending the length scales of <i>ab initio</i> MD simulations . . . . .	24
1.3.2	Extending the time scales of <i>ab initio</i> MD simulations . . . . .	25
	Bibliography . . . . .	26
<b>2</b>	<b>Hybrid QM/MM Car-Parrinello simulations</b>	<b>31</b>
2.1	Introduction . . . . .	33
2.2	The QM/MM potential energy and the equations of motion . . . . .	35
2.2.1	The partitioning of the system . . . . .	36
2.2.2	The MM potential . . . . .	38
2.2.3	The QM potential . . . . .	40
2.2.4	Non-bonded QM/MM interactions . . . . .	42
2.2.5	The bonded QM-MM interactions . . . . .	46
2.2.6	Dynamics using the Car-Parrinello method . . . . .	49
2.3	Implementation . . . . .	50
2.4	Copper binding to the structured part of the mouse prion protein . . . . .	51
2.4.1	Prion proteins . . . . .	52

---

2.4.2	The need for QM/MM MD simulations . . . . .	53
2.4.3	A statistical approach to copper binding in proteins . . . . .	54
2.4.4	The computational setup . . . . .	56
2.4.5	Simulation results . . . . .	57
	Bibliography . . . . .	68
<b>3</b>	<b>A Hamiltonian electrostatic coupling scheme for hybrid Car-Parrinello molecular dynamics simulations</b>	<b>73</b>
3.1	Introduction . . . . .	75
3.2	Short range electrostatic interactions . . . . .	79
3.3	Long range electrostatic interactions . . . . .	83
3.4	Potential and forces on the atoms . . . . .	87
	Bibliography . . . . .	90
<b>4</b>	<b>Efficient multidimensional free energy calculations for ab initio molecular dynamics using classical bias potentials</b>	<b>95</b>
4.1	Introduction . . . . .	97
4.2	Bias potentials to increase sampling efficiency . . . . .	99
4.3	Construction of the bias potential . . . . .	100
4.4	A simple example : Methylgroup rotation in ethane . . . . .	102
4.5	The two dimensional free energy surface of peroxy-nitrous acid . . . . .	104
4.5.1	Computational details . . . . .	106
4.5.2	Calculation of the free energy surface from the simulation data . . .	107
4.5.3	Results . . . . .	108
4.6	Conclusions . . . . .	111
	Bibliography . . . . .	112
<b>5</b>	<b>Accelerating rare reactive events by means of a finite electronic temperature</b>	<b>117</b>
5.1	Introduction . . . . .	119



---

5.2	Finite electronic temperature as a chemical driving force . . . . .	123
5.3	Results for reactions in gas and in liquid phase . . . . .	126
5.3.1	Homolytic bond dissociation of $H_2$ . . . . .	129
5.3.2	Rotation around the C-C bond in $C_2H_4$ . . . . .	131
5.3.3	Dissociation of the Lewis acid-base complex of sulfur dioxide and ammonia . . . . .	134
5.3.4	Intramolecular proton transfer between 2-hydroxypyridine and 2-pyridone . . . . .	136
5.3.5	Conrotatory ring opening in cyclobutene . . . . .	138
5.3.6	Peroxynitrous acid . . . . .	140
5.4	Conclusions . . . . .	147
5.5	Acknowledgements . . . . .	148
	Bibliography . . . . .	149
<b>6</b>	<b>Estimating equilibrium properties from non-Hamiltonian dynamics</b>	<b>153</b>
6.1	Introduction . . . . .	155
6.2	Evaluating phase space integrals using ensembles subject to compressible dynamics . . . . .	156
6.3	From ensemble averages to a time average . . . . .	160
6.4	Numerical studies of two model systems . . . . .	162
6.4.1	Estimating free energy differences . . . . .	162
6.4.2	Spatial probability distributions . . . . .	165
6.5	Conclusions . . . . .	169
6.6	Acknowledgements . . . . .	169
	Bibliography . . . . .	170
<b>7</b>	<b>Canonical adiabatic free energy sampling (CAFES): a novel method for the exploration of free energy surfaces</b>	<b>173</b>
7.1	Introduction . . . . .	175
7.2	Formulation of the method . . . . .	178

---

7.3	Determination of the mass ratio . . . . .	180
7.4	The formation of a bromonium ion intermediate and anchimeric assistance in 2-bromoethanol . . . . .	184
7.5	Summary and conclusions . . . . .	187
7.6	Acknowledgements . . . . .	189
	Bibliography . . . . .	189
<b>8</b>	<b>Summary and outlook</b>	<b>193</b>
8.1	Summary . . . . .	194
8.2	Outlook . . . . .	195

**ABSTRACT**

A central goal of *ab initio* molecular dynamics (MD) simulations is the study of complex molecular systems based on parameter-free, quantum mechanical calculations. This method can *in principle* generate a realistic movie (trajectory) at an atomistic level of the physical and chemical processes that are taking place in e.g. biological systems. In this way, unexpected novel mechanisms can be discovered, and quantitative predictions can be made. Using current supercomputers, the dynamics of systems that contain 10-1000 atoms can be calculated for 1-100 picoseconds using the density functional based Car-Parrinello method. This opens a wide range of processes that can be studied, but many systems are still significantly larger, and show e.g. catalytic activity in a time scale of milliseconds to hours. In order to reach the goal of observing reactive events in e.g. enzymes, I developed methods to extend the length and the time scale of *ab initio* molecular dynamics (MD) simulations.

The length scales are extended significantly by implementing the idea of a mixed quantum-classical (QM/MM) description of the system. This approach allows to concentrate the computational effort on the reactive part, while the environment, which can contain ten thousands of atoms, is taken into account with a more expedient classical description based on empirically parametrized force fields. Here, I describe in detail how the interactions between the QM and MM systems have been treated in the hybrid Car-Parrinello/classical MD code that has been developed during my thesis. In particular, a novel scheme that treats the electrostatic interactions in an efficient and accurate manner within a Hamiltonian framework is discussed. Additionally, I present one of the first applications of this QM/MM scheme to a biological problem, namely to a characterisation of possible binding sites of copper ions in the structured part of the mouse prion protein.

In order to overcome the limitations of the short time scales that are typical for *ab initio* MD simulations, I also developed and tested various enhanced sampling methods. These methods provide efficient means to compute thermodynamic information such as relative

stabilities and free energy barriers. Two methods that use bias potentials, a key ingredient of many enhanced sampling techniques, are introduced. I show how the knowledge that has been condensed in a force field can be exploited to enhance the efficiency in sampling an *ab initio* potential energy surface, while maintaining *ab initio* accuracy. In a second approach, the intrinsic information about chemical reactivity that is present in the electronic structure is used explicitly. Chemical reactions are enhanced specifically with the electronic temperature as a driving force as is demonstrated for several systems in gas phase and in solution. In order to increase the flexibility of current sampling algorithms that rely on bias potentials, novel methods that use instead non-Hamiltonian (non-equilibrium) dynamics have also been developed. A statistical theory that can be used to estimate equilibrium properties from a single trajectory of non-Hamiltonian dynamics is presented and tested. Using this theory, biasing forces that do not derive from a (bias) potential can be used to enhance sampling. Finally, a novel method (CAFES) is described that enables the efficient exploration of the free energy surface of a reactive subsystem embedded in an inert environment. The method is based on a combined dynamical, Car-Parrinello-like scheme and uses the temperature of the subsystem as a sampling device. With the new schemes presented here, the sampling efficiency can often be increased by a factor up to  $10^8$  for representative systems.

In this thesis, I have presented a QM/MM Car-Parrinello method and enhanced sampling techniques that can be combined to form a powerful tool to treat reactive events in complex systems that were previously not accessible by *ab initio* molecular dynamics simulations. As an outlook, I present possible future extensions and new developments that might enlarge the range of problems that can be studied even further.

## ZUSAMMENFASSUNG

Ein zentrales Ziel von *ab initio* molekulardynamischen (MD) Simulationen ist die Untersuchung komplexer Systeme mittels parameterfreier quantenmechanischer Berechnungen. Diese Methode kann prinzipiell einen realistischen Film von den Bewegungsabläufen einzelner Atome erzeugen. Dadurch lassen sich physikalische oder chemische Prozesse, die z.B. in biologischen Systemen stattfinden, veranschaulichen. So können unerwartete und neue Mechanismen entdeckt und quantitative Vorhersagen gemacht werden. Mit den heutigen Supercomputern kann mit der auf der Dichtefunktionaltheorie basierenden Car-Parinello Methode die Dynamik von Systemen, die 10 bis 1000 Atome umfassen, für einen Zeitbereich von 1 bis 100 Picosekunden berechnet werden. Dies ermöglicht die Untersuchung einer grossen Klasse von Prozessen. Jedoch sind viele Systeme noch immer bedeutend grösser, und entfalten z.B. ihre katalytische Aktivität im Rahmen von Millisekunden bis Stunden. Um z.B. Enzymreaktionen während einer *ab initio* molekulardynamischen Simulation beobachten zu können, habe ich Methoden entwickelt, die die Systemgrösse und den berechenbaren Zeitraum erweitern. Die Systemgrösse wird signifikant ausgedehnt, indem das System gemischt quantenmechanisch-klassisch (QM/MM) beschrieben wird. Dieser Ansatz ermöglicht die Konzentration der Rechenleistung auf den reaktiven Teil, während die Umgebung, die zehntausende von Atomen enthalten kann, zweckmässig mit empirisch parametrisierten, klassischen Kraftfeldern beschrieben wird. Hier erläutere ich im Detail, wie die Wechselwirkungen zwischen den QM und den MM Systemen im hybriden Car-Parinello/klassischen MD Code, der während meiner Dissertation entstanden ist, behandelt werden. Insbesondere wird ein neuer Ansatz diskutiert, der die elektrostatischen Wechselwirkungen in einer effizienten und genauen Weise innerhalb eines Hamiltonianischen Rahmens behandelt. Weiterhin präsentiere ich eine der ersten Anwendungen dieses QM/MM Schemas auf ein biologisches Problem, nämlich die Charakterisierung von möglichen Kupferbindungsstellen im strukturierten Teil des Prionenproteins der Maus.

Um den kleinen Zeitrahmen, der typisch für *ab initio* MD Simulationen ist, zu vergrössern,

habe ich ausserdem verschiedene verbesserte Absuchmethoden entwickelt und geprüft. Diese Methoden sind effiziente Mittel, um thermodynamische Informationen wie relative Stabilitäten und freie Energiebarrieren zu berechnen. Zwei Methoden, die Verzerrungspotentiale - ein wesentliches Element von verbesserten Absuchmethoden - benutzen, werden vorgestellt. Ich zeige, wie das Wissen, das konzentriert in einem Kraftfeld vorliegt, benutzt werden kann, um die Effizienz beim Abtasten einer *ab initio* Potentialfläche zu steigern, und trotzdem die *ab initio* Präzision beizubehalten. In einem zweiten Ansatz wird die Information über die chemische Reaktivität, die der elektronischen Struktur innewohnt, direkt genutzt, indem chemische Reaktionen durch die treibende Kraft der elektronischen Temperatur spezifisch beschleunigt werden. Dies wird an verschiedenen Beispielen in der Gasphase und in Lösung demonstriert. Weiterhin werden neue Abtastmethoden präsentiert, die sich nicht wie die herkömmlichen auf Verzerrungspotentiale stützen, sondern stattdessen eine flexiblere, nicht-Hamiltoniansche (nicht-Gleichgewichts-) Dynamik benutzen. Es wird eine statistische Theorie vorgestellt und getestet, die auf einer einzigen Bewegungsbahn aus nicht-Hamiltonianischer Dynamik basiert, und zum Abschätzen von Gleichgewichtseigenschaften genutzt werden kann. Diese Theorie ermöglicht es, Verzerrungskräfte zu benutzen, die nicht von einem (Verzerrungs-) Potential hergeleitet werden, um die Abtasteffizienz zu erhöhen. Zum Schluss wird eine neue Methode (CAFES) beschrieben, die die effiziente Untersuchung der freien Energieoberfläche eines reaktiven Subsystems innerhalb einer inerten Umgebung erlaubt. Diese Methode basiert auf einem kombiniert dynamischen, Car-Parrinello-ähnlichen Schema und nutzt die Temperatur als Mittel zur Erhöhung der Absucheffizienz. Mit Hilfe der hier vorgestellten Methoden kann für repräsentative Systeme die Abtasteffizienz um einen Faktor von bis zu  $10^8$  erhöht werden.

In dieser Dissertation habe ich eine QM/MM Car-Parrinello Methode und verbesserte Absuchtechniken beschrieben, die zu einem kraftvollen Werkzeug kombiniert werden können, um reaktive Ereignisse in komplexen Systemen zu behandeln, die vorher *ab initio* MD Simulationen unzugänglich waren. In einem Ausblick zeige ich mögliche zukünftige Erweiterungen und neue Entwicklungen, die das Anwendungsgebiet noch vergrössern können.

## PUBLICATIONS AND PRESENTATIONS

The research that I performed in the group of Prof. Ursula Röthlisberger and that resulted in this thesis, has been published and presented by me orally or as a poster at scientific conferences and seminars.

### Publications

- Joost VandeVondele, Maria Carola Colombo, Alessandro Laio, Leonardo Guidoni, and Ursula Rothlisberger, *Copper binding to the structured part of the mouse prion protein*, manuscript to be submitted.
- Joost VandeVondele, Alessandro Laio and Ursula Rothlisberger, *Mixed QM/MM Car-Parrinello simulation of the CO<sub>2</sub> conversion step in Human Carbonic Anhydrase II*, manuscript to be submitted.
- Ute Röhrig, Alessandro Laio, Joost VandeVondele, Leonardo Guidoni, Imgard Frank, Carla Molteni, Michele Parrinello, and Ursula Rothlisberger, *A QM/MM study of the early steps of the rhodopsin photocycle*, manuscript to be submitted.
- Ute Röhrig, Alessandro Laio, Joost VandeVondele, Jürg Hutter, Imgard Frank, and Ursula Rothlisberger, *A QM/MM calculation of the solvent shift of acetone in aqueous solution*, manuscript to be submitted.
- Carme Rovira, Stefano Piana, Joost VandeVondele, Alessandro Laio, Ursula Rothlisberger, and Michele Parrinello, *A mixed quantum/classical Car-Parrinello study of NO binding to myoglobin*, manuscript to be submitted.
- Alessandro Laio, Joost VandeVondele and Ursula Rothlisberger, *Electrostatic potential derived charges from quantum mechanics/molecular mechanics calculations*, manuscript to be submitted.

- Joost VandeVondele, Alessandro Laio and Ursula Rothlisberger, *Mixed QM/MM Car-Parrinello simulations*, manuscript to be submitted.
- Joost VandeVondele and Ursula Rothlisberger, *Accelerating rare reactive events by means of a finite electronic temperature*, manuscript to be submitted.
- Marialore Sulpizi, Alessandro Laio, Joost VandeVondele, Antonino Cattaneo, Ursula Rothlisberger, Paolo Carloni, *Reaction Mechanism of Caspases, Insights from QM/MM Car-Parrinello simulations*, submitted to J. Biol. Chem.
- Joost VandeVondele and Ursula Rothlisberger, *Canonical adiabatic free energy sampling (CAFES) : a novel method for the exploration of free energy surfaces*, submitted to J. Phys. Chem. B.
- Alessandro Laio, Joost VandeVondele and Ursula Rothlisberger, *A hamiltonian electrostatic coupling scheme for hybrid Car-Parrinello simulations*, submitted to J. Chem. Phys.
- Joost VandeVondele and Ursula Rothlisberger, *Estimating equilibrium properties from non-Hamiltonian dynamics*, J. Chem. Phys. **115**, 7859, (2001).
- Joost VandeVondele, Alessandra Magistrato and Ursula Rothlisberger, *Cis/Trans-Isomerization Triply-Bonded Ditungsten Complexes: A Multitude of Possible Pathways*, Inorg. Chem. **40**, 5780, (2001).
- Alessandra Magistrato, Joost VandeVondele and Ursula Rothlisberger, *Three- and Four-Center Trans Effects in Triply Bonded Ditungsten Complexes: An ab initio Molecular Dynamics Study of Compounds with Stoichiometry  $W_2Cl_4(NHEt)_2(PMe_3)_2$* , Inorg. Chem. **39**, 5553 (2000).
- Joost VandeVondele and Ursula Rothlisberger, *Efficient multidimensional free energy calculations for ab initio molecular dynamics using classical bias potentials*, J. Chem. Phys. **113**, 4863 (2000).



---

**Oral presentations**

- Joost VandeVondele and Ursula Rothlisberger, *A novel dynamical scheme for the exploration of free energy surfaces : observing the formation of the bromonium ion in solution*, Fall meeting of the Swiss chemical society 2001, October 12 2001, Zurich, Switzerland.
- Joost VandeVondele and Ursula Rothlisberger, *Extending length and time scales of ab initio molecular dynamics simulations*, University of California, department of bioengineering, July 27 2001, Berkeley, California.
- Joost VandeVondele and Ursula Rothlisberger, *Extending length and time scales of ab initio molecular dynamics simulations*, University of Washington, department of medicinal chemistry, July 24 2001, Seattle, Washington.
- Joost VandeVondele and Ursula Rothlisberger, *Extending length and time scales of ab initio molecular dynamics simulations*, The Scripps Research Institute, department of structural biology, July 19 2001, La Jolla, California.
- Joost VandeVondele, Alessandro Laio, and Ursula Rothlisberger, *Copper binding to the prion protein*, Ab initio modelling in the biological sciences (CECAM), June 11-13 2001, Lyon, France.
- Joost VandeVondele, Alessandro Laio, and Ursula Rothlisberger, *QM/MM development and the simulation of the prion protein*, Fall meeting of the Swiss chemical society 2000, October 12 2000, Lausanne, Switzerland.
- Joost VandeVondele and Ursula Rothlisberger, *Efficient ab initio multidimensional free energy calculations using classical bias potentials*, Workshop on Simulation of long time scale dynamics (CECAM), June 26-30 2000, Reykjavik, Iceland.

- Joost VandeVondele and Ursula Rothlisberger, *Overcoming the time-scale barrier in ab initio molecular dynamics*, Fall meeting of the Swiss chemical society 1999, October 12 1999, Basel, Switzerland.

### Poster presentations

- Joost VandeVondele and Ursula Rothlisberger, *Canonical adiabatic free energy sampling (CAFES) : a novel way for the exploration of free energy surfaces*, Briding the time scale gap (CECAM), September 10-13 2001, Konstanz, Germany.
- Joost VandeVondele, Alessandro Laio, and Ursula Rothlisberger, *Copper binding to the prion protein*, Davidson Conference, July 21-26 2001, Seattle, Washington.
- Joost VandeVondele and Ursula Rothlisberger, *Efficient ab initio multidimensional free energy calculations using classical bias potentials*, DFT 2000, June 11-14 2000, Menton, France.
- Joost VandeVondele and Ursula Rothlisberger, *Principal component analysis and ab initio molecular dynamics*, Workshop on Computational Sciences and Engineering, May 2-7 1999, Ascona, Switzerland.

## Chapter 1

# Introduction

## 1.1 *Ab initio* molecular dynamics simulations

The term 'molecular dynamics' (MD) is generally used to describe the computer-aided solution of the classical equations of motion for a collection of atoms with the aim of recreating a physical system and its dynamics on a computer. The method is a powerful theoretical approach to study the properties of atoms and molecules. A trajectory generated by a MD simulation provides an atomistic picture (or movie) of all events that occur during the simulation, and hence gives insight in dynamic and thermodynamic properties. Among the properties that can be calculated are e.g. free energy differences, reaction rates, and various space and time correlation functions. The technique was first used in the 50-60s, [1, 2] and is now well established. [3, 4] Molecular dynamics simulations are especially useful in complex systems where an unguided exploration of phase space is important. The fact that a broad range of events can *in principle* occur during a simulation makes MD a truly predictive tool.

'*Ab initio* molecular dynamics' refers to MD simulations, where no empirical parameters have been introduced to describe the interaction between the atoms. This implies that the potential and forces are calculated solving the quantum mechanical Schrödinger equation at every time step. This strategy, which is computationally more demanding than empirical approaches, is particularly appropriate for complex and reactive systems, i.e. for systems where the bonding pattern or the electronic structure changes during the evolution or where interactions that are difficult to parametrize are present. This is for instance the case for many of the systems that play a central role in enzymatic or organometallic catalysis. A particularly successful *ab initio* MD scheme is the Car-Parrinello (CP) method [5, 6] in which the potential and forces on the atoms are calculated using density functional theory (DFT) [9–11] as the underlying quantum theory.

Currently, the CP method allows for the simulation of a few hundred atoms, for tens of picoseconds with an accuracy in the milliHartree range, and the method has found

widespread applications in material science, chemistry and biology. [7, 8] In principle, the method holds special potential for the study of e.g. enzymatic reactions. However, *ab initio* MD simulations are seriously hampered by the large size of the systems (10,000s of atoms are typical), and by the limited time scale that is accessible. In order to fully exploit the potential of this approach, new methodologies have to be developed that allow to bridge the length and time scale gaps.

## 1.2 Limitations of current MD simulations

The limitations of MD methods are to a large extent determined by the following three factors [12] :

- The accuracy of the potential : How well does the potential describe the interactions between the atoms? Are interactions such as bond breaking and polarisation well described, or is a more precise description necessary?
- The size of the model : Are the system and the environment described sufficiently well with the given number of particles? Has e.g. the effect of the protein, solvent, or membrane environment to be taken into account explicitly?
- The length of the simulation : Will the chosen simulation method be able to evolve the system to its equilibrium configuration and yield information about chemical reactions or conformational changes that can happen on the millisecond to hour time scale? Are the observed events statistically meaningful, and the averages converged?

In principle, these problems could easily be solved by using the most accurate quantum chemical methods, for very large systems, and propagate them for very long times. However, the computational cost that is associated with this solution is prohibitive, and typical experimental length, time, and accuracy scales can usually not be reached using a brute

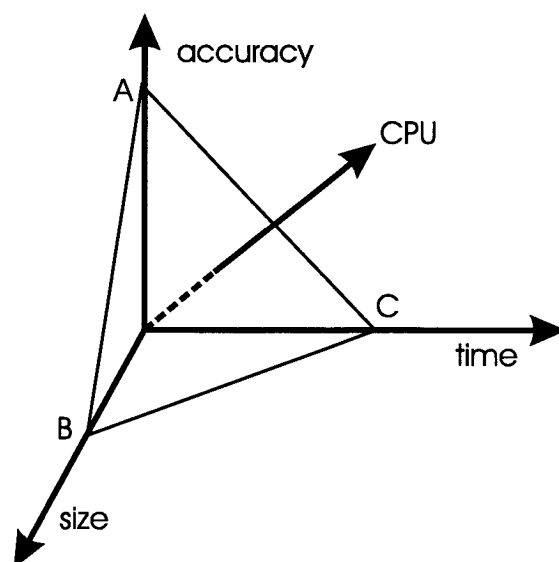


Figure 1.1: The figure shows schematically the three main directions (accuracy, size and time) that can be followed to improve the predictive power of a MD simulation. The CPU time increases along all the three axes, but a plane of constant CPU time is shown to indicate that for a given amount, several different combinations are possible, and the user has to choose the option that yields a simulation that is as realistic as possible. The points A, B, and C indicate the extreme choices.

force simulation technique. 'Improving' the accuracy at one point will usually lead to a compromise for one or both of the other issues. The current limits for these three factors are approximatively given by :

- The accuracy of quantum chemical calculations, such as full configuration interaction (CI) with large basis sets [13]. This method describes all molecular interactions almost perfectly (microHartree errors), but is limited to very small systems such as diatomics of the first row elements. This approach is represented by the point A in Fig. 1.1
- Mesoscopic systems ( $10^6$  atoms) are at the limit of what can be simulated using an explicit atomistic simulation. [14] Moreover, such a study is only feasible with

empirical models and for short (picoseconds) simulation times. This approach is represented by the point B in Fig. 1.1

- Microsecond simulation times can exceptionally be reached for protein simulations based on an atomistic model [15], but for most systems, this is still orders of magnitude lower than what would be needed for obtaining a statistically meaningful sampling of folding and unfolding events. This approach is represented by the point C in Fig. 1.1

The *ab initio* molecular dynamics method that takes a central place in this thesis is one of the possible compromises between these three extremes. The accuracy of the underlying quantum mechanical (QM) method, DFT, is such that basically all elements of the periodic table can be treated on equal footing with relatively reliable energetics. Additionally, DFT is a QM theory that undergoes steady improvements and is expected to become more and more accurate as novel density functionals are being developed. [16–18] The computational cost of a typical DFT calculation scales as  $O(N^3)$  (with  $N$  being the number of atoms) which is relatively moderate in comparison to other quantum chemical approaches (e.g. CCSD(T)  $O(N^7)$  or MP2  $O(N^5)$ ). The largest system sizes that can be treated are therefore in the range of hundreds to a few thousands of atoms. [19] The maximum simulation times that can be reached for small systems (e.g. 10 atoms) are of the order of hundreds of picoseconds. [20] These length and time scales are still many orders of magnitude different from what would be needed for a Car-Parrinello MD study in which all enzymatic reaction steps can be observed spontaneously. The steady increase in computer power due to improvements in chip design and parallelisation is certainly advancing the field of molecular dynamics simulations, but a conservative estimate shows that for a study of such problems twenty orders of magnitude are approximately needed. With the current growth rate, such an increase in computer performance will only be reached in ca. the year 2070. [21] Therefore, novel methods that gain several orders of magnitude by using physically motivated or problem oriented extensions of the standard MD scheme are

needed.

### 1.3 Assuming locality to extend length and time scales

The assumption that underlies most of the methods in this thesis is the locality of the 'interesting events'. For instance, enzymatic reactions often take place in a well defined part of the entire system, i.e. the active site of a solvated protein, and involve only a relatively small, localised subspace that is chemically active. This basic feature is exploited in various ways in the different methods that are presented in this thesis and that are aimed at an extension of the length and time scales of *ab initio* MD simulations.

#### 1.3.1 Extending the length scales of *ab initio* MD simulations

The approach we have adopted to extend the system size is a mixed quantum mechanical/classical (QM/MM) one. In a QM/MM approach, the computationally elaborate QM part is limited to the subsystem that is expected to perform the chemical reactions (e.g. the active site of a protein), and an empirical force field is used to describe the environment (e.g. the protein and the solvent). [22,23] Note that the environment remains in a state in which the electronic structure undergoes only minor changes and can thus be parametrized with simple analytic models that describe it with good accuracy. The method, which dates back to the 70-80s [24,25], holds great promise since (for all practical purposes) the computational cost of simulating a localized chemical event in a large system is essentially independent of the size of the surroundings. Here, a new QM/MM code based on the Car-Parrinello algorithm and the GROMOS96 [26] force field is described in detail in the Chapters 2 and 3. The challenge in designing a hybrid Car-Parrinello MD code lies in an accurate and consistent description of the interaction between the QM and the MM regions. Very satisfying results for test systems have been obtained with the QM/MM



approach that we have developed, and two of the applications are presented in this thesis. The first deals with the problem of copper binding to the prion protein (Chapter 2) and the second is a QM/MM study of the anchimeric assistance in 2-bromoethanol in aqueous solution (Chapter 7).

### 1.3.2 Extending the time scales of *ab initio* MD simulations

Extending the time scale and increasing the sampling efficiency of molecular dynamics simulations has been a major field of research for the past decades, and a selection of the many methods that have been proposed can be found in the references [28–50]. Among these methods are e.g. mass reweighting [32], multiple timestep algorithms [31], constrained dynamics [29, 30], umbrella sampling [28], path sampling [33, 43], essential dynamics [40], subspace integration [41], and bias potential techniques [34–39]. To enhance the sampling of possible reactive events in a system by several orders of magnitude, we decided to refrain from pure dynamic properties and to concentrate instead on an improved statistical description of thermodynamic properties such as free energy differences, reaction paths and rates within transition state theory approximation [27]. This allowed us to develop the new methods presented in Chapters 4, 5, 6, and 7. They are all based on modifications of the dynamics designed in such a way that activated events that are a major bottleneck for most MD simulations occur more frequently. Two methods that are described in this thesis use bias potentials that artificially, but in a well controlled way, modify the potential energy surface. Methods of similar type found their application in classical MD simulations in the 90s [34–36] and are based on principles from statistical mechanics that have been well established. [27, 28] Indeed, as described in Chapter 4, dynamics performed on a biased surface can be directly used to calculate thermodynamics properties of the unbiased ensemble. In this way, rare events that are naturally e.g. in the millisecond range can be observed and characterised during a few tens of picoseconds of dynamics. Especially the method in Chapter 5 is aimed at selectively enhancing the sampling of reactive regions of phase space,

making the method a good candidate for accelerating rare reactive events in complicated systems. A different approach is followed in the Chapters 6 and 7 where the possibilities of non-Hamiltonian (non-equilibrium) dynamics are explored. Non-Hamiltonian dynamics covers a broader class of dynamics than Hamiltonian dynamics, and this freedom can be exploited to devise new algorithms that sample phase space efficiently. In Chapter 6, I show how to connect averages over a single non-Hamiltonian trajectory to equilibrium properties. In Chapter 7, the QM/MM concept of a reactive system in an inert environment is exploited with a scheme that uses the local temperature of a decoupled subsystem to accelerate the reactive dynamics. These last two schemes have a single parameter that can be tuned in order to achieve an accurate description of the equilibrium properties. All the sampling schemes that are presented in this thesis have shown very impressive gains in sampling efficiency (e.g. by a factor of  $10^8$ ) for chemically and biologically relevant systems.

## Bibliography

- [1] B.J. Alder, and T.E. Wainwright, *J. Chem. Phys.* **27**, 1208 (1957).
- [2] A. Rahman, *Phys. Rev.* **136A**, 405 (1964).
- [3] See the corresponding chapters in e.g. M.P. Allen, and D.J. Tildesley, *Computer Simulation of Liquids* (Oxford university press, New York, 1987).
- [4] More recent is the discussion in e.g. D. Frenkel, and B. Smit, *Understanding Molecular Simulation* (Academic press, San Diego, 1996).
- [5] R. Car, and M. Parrinello, *Phys. Rev. Lett.* **55**, 2471 (1985).
- [6] For a recent review of the method see, e.g.: D. Marx, J. Hutter, in *Modern Methods and Algorithms of Quantum Chemistry*, J. Grotendorst (Ed.), John von Neumann Institute for Computing, Jülich, NIC Series, **1**, 301 (2000)

- [7] For a recent review of applications of the Car-Parrinello method see, e.g.: U. Rothlisberger, published in *Computational Chemistry: Reviews of Current Trends*, J. Leszczynsky (Ed.)
- [8] P. Carloni and U. Rothlisberger in *Theoretical Biochemistry - Processes and Properties of Biological Systems*, L. Eriksson (ed.) (Elsevier Science, Amsterdam, 2001).
- [9] P. Hohenberg, and W. Kohn, Phys. Rev B **136**, 864 (1964).
- [10] W. Kohn, and L. J. Sham, Phys. Rev. A **140**, 1133 (1965).
- [11] R. G. Parr, and W. Yang, *Density-Functional Theory of Atoms and Molecules* (Oxford University Press, New York, 1989).
- [12] Additional approximations are related to the quantum nature of the atoms. A classical description of their motion neglects any quantum dynamical effects such as e.g. tunneling and zero point energies.
- [13] A. Szabo, and N.S. Ostlund, *Modern Quantum Chemistry* (Dover publications, New York, 1996).
- [14] See e.g. R.K Kalia, A. Nakano, A. Omeltchenko, K Tsuruta, P. Vahishta, Phys. Rev. Lett. **78**, 2147 (1997).
- [15] Y. Duan, and P. A. Kollman, Science **282**, 707 (1998).
- [16] E.g. novel and extended parametrisations : A. D. Boese, and N. C. Handy, J. Chem. Phys. **114**, 5497 (2001).
- [17] E.g. kinetic energy density dependent functionals : E. Proynov, H. Chermette, and D.R. Salahub, J. Chem. Phys. **113**, 10013 (2000).
- [18] E.g. delocalized exchange : A. D. Becke, J. Chem. Phys. **112**, 4020 (2000).
- [19] See e.g. : J. Hutter, P. Carloni, and M. Parrinello, J. Am. Chem. Soc. **118**, 8710 (1996).

- [20] J. VandeVondele, and U. Rothlisberger, *to be published*. See also Chapter 7.
- [21] Increased cost due to (1) Size : about 100 times larger ( $10^6$ ); (2) Time : going to seconds ( $10^{12}$ ); (3) Accuracy : more costly DFT or wave function schemes ( $10^3$ ); Total increase of the computational cost  $10^{21}$ . If computer performance doubles every year, this will be reached in the year 2070.
- [22] A recent review is given in: P. Sherwood, *Modern Methods and Algorithms of Quantum Chemistry*, J. Grotendorst (Ed.), John von Neumann Institute for Computing, Jülich, NIC Series, **1**, 257 (2000). See also <http://www.kfa-juelich.de/wsqc/proceedings.html>.
- [23] For a monograph see : *Combined quantum mechanical and molecular mechanical methods*, J. Gao, M.A. Thompson (Ed.) (Oxford University Press, 1998).
- [24] A. Warshel, and M. Levitt, *J. Mol. Biol.* **103**, 2227 (1976).
- [25] U.C. Singh, and P.A. Kollman, *J. Comp. Chem.* **11**, 700 (1986).
- [26] W.R.P. Scott, P.H. Hünenberger, I.G. Tironi, A.E. Mark, S.R. Billeter, J. Fennen, A.E. Torda, T. Huber, P. Krüger and W.F. van Gunsteren, *J. Phys. Chem. A* **103**, 3596 (1999).
- [27] D. Chandler, *Introduction to modern statistical mechanics* (Oxford University Press, New York, 1987).
- [28] G. M. Torrie, and J. P. Valleau, *J. Chem. Phys.* **66**, 1402 (1977).
- [29] E. A. Carter, G. Ciccotti, J. T. Hynes, and R. Kapral, *Chem. Phys. Lett.* **156**, 472 (1989).
- [30] M. Sprik, and G. Ciccotti, *J. Chem. Phys.* **109**, 7737 (1998).
- [31] M.E. Tuckerman, and B.J. Berne, *J. Chem. Phys.* **95**, 8362 (1991).
- [32] B. Mao, and A. R. Friedman, *Biophys. J.* **58**, 803 (1990).

- [33] R. Elber, and M. Karplus, *Chem. Phys. Lett.* **139**, 375 (1987).
- [34] T. Huber, A. E. Torda, and W. F. van Gunsteren, *J. Comput.-Aided Mol. Design* **8**, 695 (1994).
- [35] H. Grubmüller, *Phys. Rev. E* **52**, 2893 (1995).
- [36] A. F. Voter, *J. Chem. Phys.* **106**, 4665 (1997).
- [37] A. F. Voter, *Phys. Rev. Lett.* **78**, 3908 (1997).
- [38] M. M. Steiner, P.-A. Genilloud, and J. W. Wilkins, *Phys. Rev. B* **57**, 10236 (1998).
- [39] X. G. Gong, and J. W. Wilkins, *Phys. Rev. B* **59**, 54 (1999).
- [40] A. Amadei, A. B. M. Linssen, and H. J. C. Berendsen, *Proteins: Structure, Function, and Genetics* **17**, 412 (1993).
- [41] B. Space, H. Rabitz, and A. Askar, *J. Chem. Phys.* **99**, 9070 (1993).
- [42] N. Nakajima, H. Nakamura, and A. Kidera, *J. Phys. Chem. B* **101**, 817 (1997).
- [43] C. Dellago, P. G. Bolhuis, F. S. Csajka, and D. Chandler, *J. Chem. Phys.* **108**, 1964 (1998).
- [44] M. Marchi, and P. Ballone, *J. Chem. Phys.* **110**, 3697 (1999).
- [45] K. Kuczera, *J. Comp. Chem.* **17**, 1726 (1996).
- [46] Y. Wang, and K. Kuczera, *Theor. Chem. Acc.* **101**, 274 (1999).
- [47] C. Bartels, and M. Karplus, *J. Comp. Chem.* **18**, 1450 (1997).
- [48] J. Apostolakis, Philippe Ferrara, and A. Caffisch, *J. Chem. Phys.* **110**, 2099 (1999).
- [49] C. Bartels, M. Schaefer, and M. Karplus, *J. Chem. Phys.* **111**, 8048 (1999).
- [50] S. Crouzy, J. Baudry, J. C. Smith, and B. Roux, *J. Comp. Chem.* **20**, 1644 (1999).



## Chapter 2

# Hybrid QM/MM Car-Parrinello simulations

## Abstract

*Ab initio* molecular dynamics (Car-Parrinello) simulations based on density functional theory have become a valuable tool in the investigation of physical, chemical and biological systems. Here, we describe an extension of the Car-Parrinello method into a mixed quantum mechanical/molecular mechanical (QM/MM) scheme in which (i) the electrostatic coupling with the classical environment is based on a fully Hamiltonian approach; (ii) the occurrence of electron-spill out from the QM system onto neighboring classical point charges is impeded by the use of a suitable modification of the Coulomb interactions at short range; (iii) boundary atoms involved in chemical bonds between QM and MM part of the system are treated with empirical monovalent pseudopotentials; and (iv) the exclusion rules of standard (bio)molecular force fields are incorporated in a consistent manner. Our approach enables efficient and robust hybrid Car-Parrinello simulations of extended systems in which the chemically relevant part is treated at an *ab initio* quantum mechanical level while the effects of the surroundings are explicitly taken into account through the embedding in the classical environment. The method is presented in a general way, aimed at the application-oriented reader, and is illustrated with a QM/MM investigation of copper binding to the structured part of the mouse prion protein.



## 2.1 Introduction

The study of chemical processes that take place in large biological systems is a challenging task for which current simulation methodology clearly reaches its limits. Indeed, in order to provide an adequate description of the forming and breaking of chemical bonds, these systems have to be treated within the framework of an electronic structure method. Moreover, the fact that dynamical finite temperature effects can be crucial for enzymatic function necessitates an approach that can take the motion of protein and solvent explicitly into account and allows for a direct determination of the reaction *free* energy. The long characteristic time scales that are involved demand an efficient calculation of both energies and forces, and the ability to capture *at least* several tens of picoseconds of molecular dynamics. In fact, for many systems this limited time scale is by far not sufficient, and appropriately designed enhanced sampling techniques have to be applied for an adequate treatment [1]. The first-principles molecular dynamics method introduced by Car and Parrinello [2] is an efficient way to combine an electronic structure method with a molecular dynamics scheme. This combined approach enables the incorporation of finite temperature effects and the direct simulation of chemical events. It has found widespread use over the last decade and has proven to be a powerful tool in the investigation of complex physical, chemical and biological problems. Nowadays, using massively parallel computer architectures, systems of a few hundred to thousand atoms can be simulated with the Car-Parrinello method for typical time periods of 1-10 picoseconds. Even though the system sizes that can currently be treated are rather impressive, they are still not sufficient for a full quantum mechanical treatment of most biological systems that typically contain few 10,000-100,000 particles. In this article, we present an extension of the Car-Parrinello method into a mixed quantum/classical (QM/MM) scheme. In such a hierarchical hybrid approach, the part of the system that is directly involved in the major rearrangements of the electronic structure is treated at the quantum mechanical level whereas the effects of the environment are taken into account within a classical force field description. In this way, large systems can be

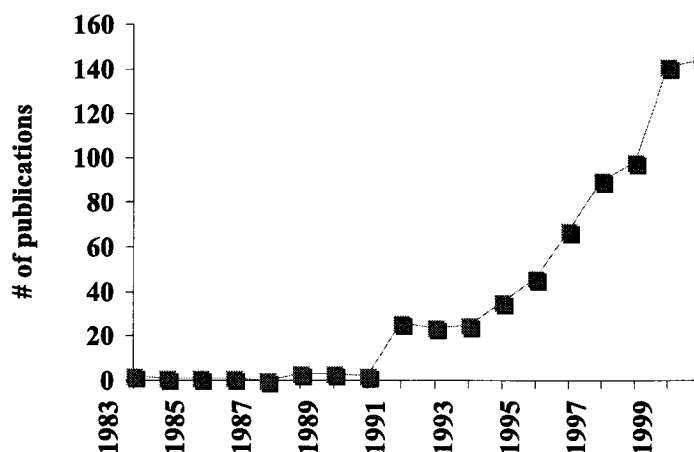


Figure 2.1: Approximate number of publications that use or introduce QM/MM methods for the years 1983-2000 according to a Web of Science search.

studied in their full complexity and the computational effort can be concentrated where it is needed. The computer time gained by treating only a smaller subsystem at the quantum mechanical level can in turn be invested for an improved sampling of the entire system over an extended time scale. QM/MM approaches are thus intuitively appealing, but their accuracy and reliability depends crucially on a rigorous and consistent treatment of the interface between QM and MM parts. Several pitfalls exist in interfacing two methods at such disparate levels as e.g. a first-principles quantum-mechanical approach and a classical force field. We will discuss in detail how our QM/MM method is addressing the various delicate issues inherent to the QM/MM technique in order to generate a reliable and robust hybrid Car-Parrinello scheme that can be applied to a large range of problems in biology and material science.

The original idea of mixing quantum mechanical and classical molecular mechanics approaches dates back to the seventies of last century. [3–5] This appealing idea has found intense renewed interest during the last decade (see Fig. 2.1); and there is currently a highly active research going on to develop novel methods and computer codes that com-

bine various quantum chemical methods and classical force fields using different coupling schemes. [6] [7] The central quantum chemical core of the approach we present here is the Car-Parrinello (CP) method [2] [8] in its standard implementation based on Density Functional Theory (DFT) [9] [10] [11], pseudopotentials, periodic boundary conditions and a basis set of plane waves. We are convinced that DFT, using the current exchange and correlation functionals, provides an excellent compromise between accuracy and computational cost. Furthermore, due to the inclusion of approximate electron correlation effects, DFT also offers a fairly reliable treatment of transition states and is one of the few methods capable of providing an adequate picture of transition metal centers. Additionally, the combination of this theory with the computational efficiency and robustness of the Car-Parrinello algorithm for molecular dynamics simulations constitutes an efficient tool for the study of chemical reactions. DFT and the Car-Parrinello method are now well established, [12] and DFT or CP based QM/MM codes have been implemented. [13] [14] [15] [16] In choosing the combination of a hybrid Car-Parrinello/classical code, we expect to benefit both from the accuracy of the underlying DFT, and the efficiency of the CP method. To this end, the physical soundness of the interaction terms of the QM/MM interface and their computational efficiency have to be considered carefully. In particular, as one of our main objectives is to perform QM/MM dynamics, our approach is fully consistent and energy conserving dynamics can be performed. In this article, we give a general but detailed introduction to our QM/MM method. Its power and performance will be illustrated for a biological application.

## 2.2 The QM/MM potential energy and the equations of motion

In this Section, we describe in detail the potential energy function that is used in our hybrid Car-Parrinello/classical molecular dynamics simulations, and address various general issues

that are of great practical importance for the success of a QM/MM scheme.

### 2.2.1 The partitioning of the system

A central decision in the modelling of any system within a QM/MM approach is the partitioning into QM subsystem and MM environment. A larger QM model increases the accuracy and predictive power of the simulation, however, the computational cost of a QM/MM simulation is almost completely determined by the size of the QM subsystem which, for a typical plane wave based DFT implementation, scales in general with roughly the third power of the system size. An appropriate partitioning strongly depends on the system under study, and on the quality of both the MM model and the quantum mechanical interaction potential. With increasing accuracy of either of the two facets, more challenging problems can be studied with eventually smaller sizes of the QM system. An adequate QM method will be needed to describe all the chemical and physical aspects of molecular interactions that are not taken into account by the MM model. Given the current limitations of classical force fields in describing reactive events such as bond breaking, charge transfer or polarisation, a minimal QM model should at least contain the parts of the system that undergo significant changes in their electronic structure. One of the simplest examples for a possible choice of QM/MM partitioning is a typical solute/solvent system in which the former is treated quantum mechanically and the latter classical. In this specific case, the interactions between the two subsystems do not involve any chemical bonds and can be taken into account as described in Section 2.2.4. The simulation of e.g. enzymatic reactions on the other hand, involves almost invariably a quantum system that is a fraction of a larger, covalently bonded molecule. We will describe in detail in Section 2.2.5 how a covalent bond can be 'cut' and 'terminated', so that the influence of the QM/MM boundary can be kept minimal. As an example of such a more intricate subdivision, we show in Fig. 2.2 a QM/MM model that has been designed with the aim of describing transition metal binding in proteins. Due to their highly complex electronic

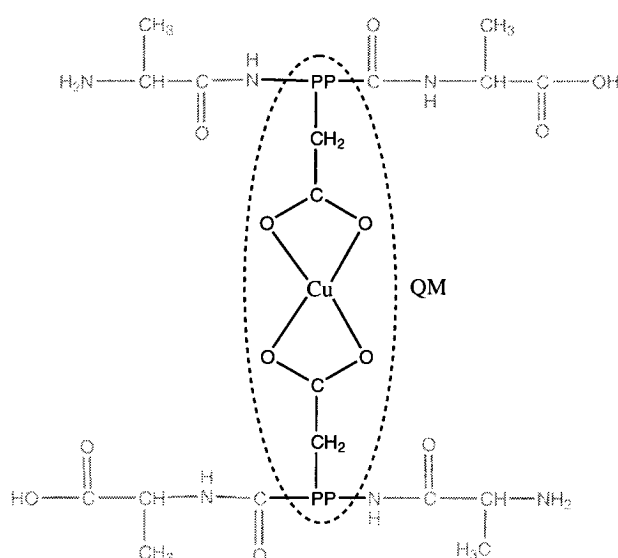


Figure 2.2: Example of a typical QM/MM model. The gray part is the MM system that is treated with a force field, whereas the subsystem that is represented with the black lines is the QM system. In this system, the QM method is mainly used to accurately describe the Cu-O bonding. PP represents a pseudopotential that is needed to describe the boundary atoms as discussed in Section 2.2.5.

properties and their directional nature of bonding, transition metal ions are difficult to parameterize in terms of simple analytic force field models, and hence the metal ion and its direct ligands are more conveniently described at the quantum mechanical (DFT) level. The surrounding protein structure can impose mechanical constraints on the metal binding site or generate an external electrostatic field that can influence the binding properties. Both of these effects can however be modelled accurately with a classical force field.

### 2.2.2 The MM potential

The MM system is in our case described with a simple pairwise-additive potential as used in most biomolecular force fields. A number of such force fields are available that have been carefully parametrized, and their accuracy for standard systems can be remarkable. [17] The MM part of our code is based on the GROMOS96 software [18], but can also run with AMBER 1995 force fields parameters. [19]

$$E_{MM} = \sum_{\text{bonds}} K_r(r - r_{eq})^2 + \sum_{\text{angles}} K_\theta(\theta - \theta_{eq})^2 + \sum_{\text{dihedrals}} \frac{V_n}{2}[1 + \cos(n\phi - \gamma)] + \sum_{\substack{i < j \\ ij \notin \text{excl}}} \left[ \frac{A_{ij}}{r_{ij}^{12}} - \frac{B_{ij}}{r_{ij}^6} + \frac{q_i q_j}{\epsilon r_{ij}} \right] \quad (2.1)$$

A typical form for these force fields is shown in Eq. 2.1 and contains short-range bonded interaction terms for bond stretching, bond angle bending, and torsional angle twisting, involving respectively the distance between two atoms, the angle between three atoms and the dihedral angle between four atoms. Additionally, all particles in the force field are assigned a point charge and two van der Waals parameters (e.g.  $\sigma$  and  $\epsilon$  of a 12-6 Lennard-Jones potential) in order to take into account the non-bonded electrostatic (Coulomb) and steric interactions (van der Waals). Van der Waals and Coulomb interactions between atoms that are involved in direct (1-2) or indirect (1-3, 1-4) bonded interactions might be scaled or excluded from the potential. These exclusions allow in turn for a more accurate parametrisation of the bonded interactions. The functional form and the parameters of

different force fields usually differ only slightly for the bonded interactions, the non-bonded interaction parameters (the assigned point charges and van der Waals parameters) on the other hand can vary considerably.

The GROMOS96 force field in particular, uses an united atom and a charge group concept. In an united atom model, apolar -CH<sub>x</sub> groups are represented as single interaction sites with enlarged van der Waals radii. In this way, non-polar hydrogens can be removed from the model resulting in a reduction of the computational cost. Charge groups are introduced by choosing a point charge assignment that preserves integer charges for local groups (e.g. -CH<sub>3</sub> or -CO-). This allows the use of a molecular (charge group) cutoff for the calculation of the long-range electrostatic interactions and facilitates, as we will show later on, the QM/MM partitioning of the system.

In spite of the fact that the specific choice of parameters can vary distinctly for different force fields, the overall description of e.g. the electrostatic field is often surprisingly similar. For instance, for the prototype system of a Gly-Ala dipeptide in aqueous solution, the classical electrostatic potential generated by the all-atom force field of AMBER (1995) and the united atom force field with charge groups from GROMOS96 is comparable in accuracy, as measured by the RMSD from the quantum electrostatic potential (9 and 13 percent respectively). [20]

Another important issue is the way the long-range interactions are calculated in different classical MD programs. Various schemes exist e.g. atom based/charge group based cutoffs with and without reaction field, Ewald summation and its particle mesh implementations: PME, SPME and P3M. In our QM/MM code, both cutoff based methods with reaction field [18] and a P3M implementation [21] are available.

The most obvious limitation of force fields that are of the common form given in Eq. 2.1 is that they are not able to describe reactive events, since bonds and angles have fixed parameters that cannot adapt to different electronic situations. Additionally, most of the

standard force fields do not contain terms that allow for an explicit polarisation of the MM system. If these aspects are important for the study of certain chemical reactions, a typical QM model would include at least the atoms and functional groups that are covalently bonded to the reactive species, and additionally, one should consider to treat groups that might be strongly polarised (e.g. hydrogen bonding to a charged QM group) at the quantum level.

We would like to point out that it is often necessary to start a QM/MM simulation with an initial classical equilibration run for several hundred picoseconds to nanoseconds. It can be convenient to keep the QM subsystem, for which there might be no good parametrisation, fixed during this initial equilibration phase.

### 2.2.3 The QM potential

The quantum system can be described at various levels of theory, and both semi-empirical [3, 5, 22] (e.g. MNDO, AM1, PM3), and *ab initio* [4, 13–16, 23] (e.g. HF, DFT) methods have been incorporated in QM/MM codes. A discussion of advantages and disadvantages of different QM methods is clearly beyond the scope of this review. Our implementation is based on DFT, [9] [10] [11] since it represents a good compromise between the accuracy needed to describe the structure and energetics of complicated systems such as metallo-proteins, and a modest scaling of its cost with the size of the system. The total QM energy for a set of atomic coordinates  $\{r_j\}$  is given by the minimum value, with respect to the orthonormal Kohn-Sham orbitals  $\{\psi_i\}$ , of the density functional

$$E_{QM}[\{r_j\}, \{\psi_i\}] = T_s[\{\psi_i\}] + \int dr V_{ext}(r)n(r) + \frac{1}{2} \int dr V_H(r)n(r) + E_{xc}[n] + \sum_{i<j} \frac{Z_i Z_j}{r_{ij}}. \quad (2.2)$$



The electronic charge density ( $n(r)$ ) is given by  $n(r) = \sum_i |\psi_i(r)|^2$ , and the various terms are defined as

$$T_s[\{\psi_i\}] = \sum_i \langle \psi_i | -\frac{1}{2}\Delta | \psi_i \rangle \quad (2.3)$$

$$V_{ext}(r) = -\sum_j \frac{Z_j}{|r - r_j|} \quad (2.4)$$

$$V_H(r) = \int dr' \frac{n(r')}{|r - r'|} \quad (2.5)$$

and represent the kinetic energy of the non-interacting reference system, the external potential due to the QM nuclei, and the Hartree potential respectively. The term  $E_{xc}[n]$  in Eq. 2.2 represents the exchange and correlation energy of the electronic system. The success of DFT is based on the fact that good approximations exist for this term even though the exact form of  $E_{xc}[n]$  is unknown. In our calculations, the generalised gradient corrected functionals BLYP and BP are used almost exclusively, since they have proven to be reliable for hydrogen bonding and metallic centers, respectively. [24] [25] [26] Our DFT calculations are based on pseudopotentials and the Kohn-Sham orbitals are expanded in a basis set of plane waves. Plane waves are rather different from e.g. Gaussian orbitals or Slater orbitals, since they are not localised, and hence have different advantages and disadvantages. Among the advantages of plane waves are that they do not suffer from basis set superposition errors; forces can be calculated directly from the Hellman-Feynmann theorem and do not involve Pulay terms; and finally, given their non-localised or diffuse character, allow for any type of polarisation. Additionally, all expensive computational kernels can be coded efficiently with library routines if one exploits the real space and Fourier space representations of the wave functions, and hence, can run with a very high FLOPS (floating point operations per second) rate. Plane wave codes are also easily made parallel if a high communication bandwidth is available for the parallel Fast Fourier Transform (FFT). [8] However, the number of basis functions that is needed can be very large, and hence the computations can be memory-intensive. In order to drastically reduce the number of plane waves that is needed to represent the wave functions, the bare Coulomb potentials of the nuclei in  $V_{ext}$  are replaced by pseudopotentials [27] in order to elimi-

nate the chemically inert and localised core electrons, leading to pseudo wave functions that are identical to the exact ones outside of the core radius of the pseudopotential, and smooth inside. These Kohn-Sham pseudo wave functions can thus be accurately expanded in plane waves with low kinetic energy cutoffs depending on the type of species (typically one uses 70 Ry for a system containing oxygen, carbon, nitrogen and hydrogen). The use of plane waves implies that the shape of the quantum cell is such that it can be repeated periodically. In our implementation, a simple cubic or orthorombic simulation cell can be employed for the quantum system. We remark that this cell is proportional to the size of the quantum system, and is therefore not related to the size of the full (QM + MM) system. The effect of the periodicity can be removed by decoupling the periodic images using either the scheme by Hockney [28] or Martyna et al. [29] to solve the Poisson equation for the Hartree potential. The use of Hockney's method requires that the density is zero at the edges of the box, and hence a QM system that is a few Angstrom away from the edges, whereas Martyna's method requires a box that is double the size of the QM system. For small systems, the method by Martyna et al. is faster, however, in the limit of large systems Hockney's approach becomes more efficient. [8]

#### 2.2.4 Non-bonded QM/MM interactions

So far we have described the form of the separate MM and QM potentials. Here, we present the detailed interaction between the QM and the MM system, focusing on the non-bonded interaction terms. These non-bonded interactions are of primary importance since they can impose additional steric constraints on the QM subsystems, and can significantly stabilise certain states by electrostatic interactions. Furthermore, even the long-range interactions can be directional. We first discuss a simple, computationally inexpensive scheme usually described as 'mechanical coupling', and point out some limitations before we discuss more elaborate electrostatic coupling schemes as implemented in our code.

In the mechanical coupling model, the interaction between QM and MM systems is treated

at the *classical* level. In the spirit of a force field, every quantum atom is assigned a point charge, and van der Waals parameters. Energies and forces due to this interaction are calculated in a straightforward way based on the Hamiltonian:

$$E_{non-bonded-Coulomb}^{mech} = \sum_{i \in QM, j \in MM} \frac{q_i^{QM} q_j^{MM}}{r_{ij}} \quad (2.6)$$

$$E_{non-bonded-vdw}^{mech} = \sum_{i \in QM, j \in MM} \left[ \frac{A_{ij}}{r_{ij}^{12}} - \frac{B_{ij}}{r_{ij}^6} \right] \quad (2.7)$$

We remark that only interactions between the MM and QM system are added, since the internal QM interactions are already treated at the QM level. Effectively, compared to a classical description of the full system, the QM simulation replaces mainly the bonded interaction terms of the force field whereas the electrostatic and van der Waals interactions are still based on an empirical force field description. Van der Waals parameters are to some extent transferable and charges can be assigned to reasonable values for a fixed geometry. There are however serious limitations to this model. They are related to the fact that there is no direct interaction between the electrons of the QM system and the electrostatic field of the MM system. This means that a polar MM environment will not polarise the electron density. Certain systems might be very sensitive to this, and have electrons that are localised on different functional groups depending on the solvent-electron interaction, or it might be the effect of polarisation that turns a specific enzyme into an efficient catalyst. Additionally, a QM/MM simulation will often be used to describe reactive events corresponding to changes in the electron density distribution, and hence assigning a fixed charge to an atom might be a crude approximation that forces the system to remain in the state that resembles most closely the one of the assigned parameters.

In the following, we discuss an approach that overcomes, at least partially, these limitations. Conceptually, instead of treating the QM - MM interaction at a classical level, this interaction will be treated at the QM level, i.e. the MM atoms will explicitly provide an external potential for the QM electrons and nuclei. Ideally, the full interaction between these systems would be described by this potential, i.e. each of the MM atoms would be assigned a pseudopotential that fully describes its interaction with the QM atoms. Our

method is a first step in this direction, explicitly treating the electrostatic interaction at a QM level, while the van der Waals interactions are treated at the classical level. [30] At the lowest level, present in many QM/MM approaches, the electrostatic interaction potential is directly written as the Coulomb potential due to the point charge of the classical atoms. This will directly polarise the electron density, and correctly take into account that the charges on the QM atoms can change during the dynamics, either by polarisation or due to chemical rearrangement. Hence, the main disadvantages of the mechanical coupling model are overcome, and charges for the QM subsystem do not have to be parametrized anymore. However, this method suffers from the well known problem that the electron density of the QM system is typically overpolarised, and might even localise on the MM atoms (i.e. the so called 'spill-out problem'). This problem becomes apparent when a plane wave basis set is employed, since a plane wave basis set allows the density to localise everywhere in space, but might become relevant also when a high quality, flexible, localised basis set is used. The spill-out problem can be attributed to the fact that a bare Coulomb potential is not a good pseudopotential to represent the classical atom since it does not take into account that the partial charge of the classical atom is effectively the result of an electron density distribution. In our approach, as described in Ref. [30], this bare Coulomb potential is modified at short range so that the unphysical singularity is replaced with a smooth potential. The energy can be written as :

$$E_{non-bonded-Coulomb} = \sum_{j \in MM} q_j \int dr \rho^{QM}(r) v_j(r - r_j) \quad (2.8)$$

$$\text{with} \quad v_j(r) = \frac{r_{cj}^4 - r^4}{r_{cj}^5 - r^5}. \quad (2.9)$$

Here  $\rho^{QM}(r)$  is the full QM density, including core density and nucleus, whereas  $v_j(r)$  is a potential that depends on the MM atom  $j$  through  $r_{cj}$ . The latter is a parameter that we have chosen to be the covalent radius of the MM atom. This effectively solves the spill-out and overpolarisation problem. Satisfying results for the radial distribution function of a water solute in a MM solvent have been obtained, without the need to change the classical description such as e.g. the van der Waals parameters. It should be noted that the QM

density can significantly extend into a polar environment, and hence the QM box should be sufficiently large, e.g. strong hydrogen bond acceptors should lie well within the QM box.

The cost of describing the electrostatic interactions with Eq. 2.8 is not small in a plane wave code, since the integral has to be evaluated over a large real space grid, and additionally, the sum includes all classical atoms. Therefore, a more cost effective solution has to be devised. In our approach, the electrostatic interaction is not truncated and neglected after a certain distance, but is taken into account by a long range electrostatic scheme. This might be of importance in enzymes where e.g. the dipole moment of a long  $\alpha$ -helix leads to a sizeable long range electrostatic interaction. This long range electrostatic scheme is based on a multipole expansion of the QM density and effectively couples the monopole ( $C$ ), dipole ( $D^\alpha$ ) and quadrupole ( $Q^{\alpha\beta}$ ) of the quantum system with the far MM atoms ( $LR$ ) by the term

$$E_{non-bonded-Coulomb}^{long-range} = C \sum_{j \in LR} \frac{q_j}{r_j} + \sum_{\alpha} D^\alpha \sum_{j \in LR} \frac{q_j}{r_j^3} \tau_j^\alpha + \frac{1}{2} \sum_{\alpha\beta} Q^{\alpha\beta} \sum_{j \in LR} \frac{q_j}{r_j^5} \tau_j^\alpha \tau_j^\beta \quad (2.10)$$

where  $\tau_j^\alpha = r_j^\alpha - \bar{r}^\alpha$ , and  $\bar{r}$  is the geometric centre of the QM atoms.  $E_{non-bonded-Coulomb}^{short-range}$  is still given by Eq. 2.8 but the sum runs only over the close-by MM atoms (i.e. not in the  $LR$  list). As shown in ref. [30] the polarisation of the QM density due to remote charges is efficiently taken into account if the atoms that are within 8-12 a.u. of the quantum system are described explicitly by Eq. 2.8 and the ones that are further away by Eq. 2.10. We note that the charge group concept in GROMOS96 increases the efficiency of the computation of Eq. 2.8 significantly for hydrophobic active sites, since e.g. united atoms have zero charge and do not appear explicitly in the sum.

One limitation of our method is that it still needs a fixed van der Waals parameter for the QM-MM interactions. QM atoms that undergo a significant change in van der Waals radius cannot be described with a time-independent, classical van der Waals radius. In principle, a pseudopotential that takes into account the van der Waals repulsion could be parametrized for all the MM atom types, as was done in ref. [31] for water. If the

pseudopotential is local, and has a simple analytical form, this could be included in the code without a significant increase of computational cost.

### 2.2.5 The bonded QM-MM interactions

In this Section, we describe the treatment of bonded QM-MM interactions, i.e. how a chemical bond through the QM-MM interface is treated in our approach. This is an important question, and several approaches exist in the literature. A good strategy is to design the cut in such a way that the MM and QM system have, as computed based on the force field charges, an integer charge, since otherwise artifacts in the electrostatic interactions will be introduced. When using the AMBER force field a careful redistribution of the charge might be necessary, since, for example, amino acid side chains do not have an integer charge. Within the charge group concept used in GROMOS96, consistent cuts can be defined more easily since charge neutrality is guaranteed as long as complete charge groups are included in the QM system. We will address how the valence of the quantum system can be saturated, and how the local geometry across the QM-MM interface is kept.

#### Saturating the valence

An unsaturated bond of the QM system is a strong perturbation of the electronic structure. Therefore the valence has to be saturated in such a way as to make this perturbation as small as possible. The simplest solution is to cap this bond with an atom or a group that makes a single covalent bond, e.g. a hydrogen, a fluorine or a methyl group. If a cut through a single, non-polar bond that is far away from the reactive center can be made the effect of those different substituents will be small and the effect of the capping can be understood. If the cut is close to the reactive center, through a conjugated system or a highly polar bond, the effect will be larger. In that case, a careful consideration of the minimum number of unperturbed bonds between the reactive center and the cut will be

necessary.

Although capping with an atom is often performed, the method becomes less attractive in a full QM/MM scheme. Indeed, the capping atom (also called link atom) is an additional atom that is not present in the real system, and that is located in an unphysical location, e.g. a hydrogen between a  $C_\alpha$  and  $C_\beta$ . The correct treatment of this additional atom is not problematic in a mechanical coupling scheme, but might be so in a full electrostatic coupling approach. In our method, one of the boundary atoms of the system is assigned a monovalent pseudopotential. [32–34] The boundary atom is thus a single atom that replaces one of the physical atoms in the system. The pseudopotential is empirical and has only one valence electron. The parametrisation is such that it reproduces binding properties typically found in a generic C-C apolar bond. In the example given above, and shown in Fig 2.2, the  $C_\alpha$  is a boundary atom, whereas the  $C_\beta$  is a physical carbon atom. We remark that from the partitioning point of view, this boundary atom should be considered a quantum atom, and hence is described by Eq. 2.2. The advantages of this approach are that no additional degrees of freedom are introduced and that more accurate pseudopotentials can be parametrized for specific situations. E.g. a boundary  $C_\alpha$  can be parametrized to have electronic properties that resemble more those of the backbone than those of a methyl group. It can be checked that the HOMO, LUMO, electronic gap, proton affinities of the QM/MM system reproduce as good as possible these properties of a reference full QM system. We remark that we have decided to leave a classical van der Waals interaction of the boundary atom with the quantum system (respecting the classical exclusion rules), since this boundary atom is typically an united atom (i.e. representing implicitly the hydrogens) in the GROMOS96 force field, and has an effective size that cannot be accounted for otherwise within a simple pseudopotential scheme.

### Keeping the local geometry

In the boundary pseudopotential approach, the binding geometry over the interface can be kept by the standard bonded terms of the force field. These terms, i.e. bonds, angles, dihedrals, and exclusions are introduced, as soon as one of the atoms involved in these terms belongs to the classical partition. Note that these classical terms have not been parametrized to describe chemical reactions and might have limited accuracy in cases where this boundary is strongly distorted. Rearrangements of the QM system should not be hindered by these boundary terms that might, as in the case of dihedral (1-4) interactions, extend quite far into the quantum region.

Whereas bond, angle and dihedral terms are generally added in the same way also in other approaches, exclusions have received little attention in the literature. We remark that van der Waals exclusions are easy to handle, since this interaction is treated at the classical level. Electrostatic exclusions are only added in a straightforward way in the mechanical coupling case, i.e. when the electrostatic interactions are treated at the classical level. For the electrostatic coupling case, the effect of the nearby charges is significantly more difficult to exclude, since the classical exclusions, that are two-body terms, cannot be univoquely defined in the QM case since the interaction of the classical point charge is with the full QM density. We remark that setting the classical charges to zero is not a good solution, since this is equivalent to neglecting their interaction with the full (quantum) system [32], and this might be to crude an approximation. In our approach, the exclusions can be introduced by having an additional term

$$E_{excl} = - \sum_{excl} \frac{q_{ESP} q_{MM}}{r}. \quad (2.11)$$

The charge  $q_{ESP}$  is determined by a variational RESP fit at every time step [20], and since it depends explicitly on the density, the forces due to this term also act on the density in the form of a compensating field. [35] In the total energy, these boundary bonds, angles, dihedrals and van der Waals exclusions are taken into account by specifying them in Eq. 2.1, the electrostatic exclusion is given by Eq. 2.11.



### 2.2.6 Dynamics using the Car-Parrinello method

In order to calculate the dynamics of the system the Car-Parrinello method [2] is employed. The Car-Parrinello method has been reviewed extensively [8] [12], and here we present only the essence of the method, indicating the small changes that are necessary for performing QM/MM dynamics. The efficiency and robustness of the CP method is related to the fact that electronic structure calculation is done using a dynamical scheme where both the electronic degrees of freedom (the wave function coefficients) and the ionic degrees of freedom (the classical and the quantum atoms) are propagated simultaneously, in such a way that the density remains close to the minimum of the density functional and that the dynamics of the ions is an accurate approximation to the exact Born-Oppenheimer dynamics. This combined evolution is based on the following Lagrangian

$$\begin{aligned} \mathcal{L}_{CP}[\{r_i\}, \{\psi_i\}] = & \sum_i \frac{1}{2} m_i \dot{r}_i^2 + \sum_i \frac{1}{2} \mu \int dr \psi_i^* \dot{\psi}_i - E_{MM} - E_{QM} - \\ & E_{non-bonded-vdw} - E_{non-bonded-Coulomb}^{short-range} - E_{non-bonded-Coulomb}^{long-range} - \\ & E_{excl} + \Lambda_{ij} \left( \int dr \psi_i^* \psi_j - \delta_{ij} \right) \end{aligned} \quad (2.12)$$

As can be noted, this Lagrangian does not only contain the ionic coordinates, but also the wave functions are propagated in a classical, fictitious dynamics. The last term in the equation contains the Lagrangian multipliers  $\Lambda_{ij}$  that are introduced to fulfil the orthonormality constraint of the Kohn-Sham orbitals. The resulting dynamics has the property that, if one starts from the optimised wave functions and if the dynamics of the wave functions is adiabatically separated from the ionic motion, the ions will perform an approximate but accurate microcanonical dynamics on the Born-Oppenheimer surface since the wave functions remain at all times close to the minimum of  $E_{QM}$ . The adiabatic separation between the electronic degrees of freedom and the ionic degrees of freedom is guaranteed if there is a large gap between the highest ionic frequency (e.g. an O-H bond stretch), and the lowest electronic frequency ( $\propto \sqrt{\frac{E_{gap}}{\mu}}$ ). This can be obtained by making the fictitious electronic mass  $\mu$  small. The high frequency motion of the wave functions requires a smaller time step than is typical for classical MD. Typically,  $\mu = 200 - 1200$  a.u., and  $\Delta t = 4 - 8$  a.u.

(0.1 - 0.2 fs). The dynamics based on Eq. 2.12 samples the microcanonical ensemble if the wave function degrees of freedom are adiabatically separated, and if the ionic system is ergodic. Additionally, the canonical ensemble can be sampled employing the Nosé-Hoover method [36–38]. It is also possible to efficiently obtain free energy differences by performing various types of constrained molecular dynamics. [39] [40]

## 2.3 Implementation

Our implementation of the QM/MM dynamics is based on the programs CPMD [41] and GROMOS96 [18]. Both codes are highly complex constructs, with a long development history, written currently in FORTRAN 77. The complexity of a classical code lies, to a large extent, in features that are not obvious from the inspection of Eq. 2.1, such as the construction and parsing of the topology file (i.e. the description of all the terms in Eq. 2.1), the construction of a neighboring list (i.e. to calculate the short range van der Waals interactions), and the use of P3M for the long range electrostatics. The complexity of the quantum code is not only related to the complexity of Eq. 2.2, but also to the large amount of data (i.e. the plane wave expansion of the wave functions), and the parallelisation. In our implementation we decided to use CPMD as the central driver for the molecular dynamics, and call GROMOS96 routines to calculate the classical energies and forces, and to perform the initialisation of the classical part of the code, i.e. parse the topology. There are several reasons for this: a) CPMD is able to calculate ionic dynamics and needs relatively few modifications to accommodate the classical atoms although a few changes are needed since the number of atoms (typically  $O(10,000)$ ) is large. b) The wave function dynamics is implemented in CPMD, and must be done in parallel given the large number of degrees of freedom (typically  $O(1,000,000)$ ). c) Apart from the calculation of forces and energies, system properties such as NMR spectra, Wannier orbitals, and atomic charges are directly accessible through CPMD. d) The interface is integrated in CPMD, and hence evolves with the code. We have decided to have a tightly coupled interface between

CPMD and GROMOS96, i.e. there is a single executable, for reasons of efficiency and ease of use. In particular, the communication is through function calls or by directly using the GROMOS96 data structures, avoiding disk I/O. The implementation is thus more efficient, but more programming effort is required upon change of the classical code. An advantage from the user point of view is that changes to the quantum model can be made rapidly, since the code will, at runtime, automatically perform the changes needed to the classical topology, based on a list of quantum atoms that are assigned a pseudopotential. Given (equilibrated) initial coordinates and the corresponding topology, a QM/MM simulation can be set up within minutes.

The calculations for the QM forces and the QM/MM interaction are performed in parallel, whereas the classical force calculation is done serially. The user can decide to have the classical calculation performed by a separate node, or on a node that also does part of the QM force calculation. Depending on the size of the QM system, and on the number of nodes that is available, one of the strategies may be more efficient from a timing or memory point of view. Since the cost of even a small QM system dominates by a sufficient factor (e.g 100) the total cost of the calculation, it is in practise sufficient not to parallelise the MM calculation. The electrostatic QM/MM interaction as given by Eq. 2.8 is the computationally most expensive term of the interaction, but can be well parallelised since the field has to be calculated on the real space grid, that can be distributed.

## 2.4 Copper binding to the structured part of the mouse prion protein

We illustrate the performance of our QM/MM method with an application to a representative biological problem, namely copper binding in the structured part of the mouse prion protein.

### 2.4.1 Prion proteins

Prions are infectious agents that consist of a single protein, and are thus devoid of any nucleic acid information. [42] [43] They play a central role in a group of invariably fatal, neurodegenerative diseases affecting animals such as sheep (scrapie) or cattle (BSE), and humans (e.g. variants of the Creutzfeldt-Jacob disease). It is now widely established that these diseases are caused by an abnormal isoform  $PrP^{Sc}$  of the normal cellular prion protein  $PrP^C$ . The formation of  $PrP^{Sc}$  leads to an aggregation into insoluble amyloid fibrils in the brain, which accompanies neuronal damage and eventual loss of neuronal function. [44] [45] The detailed mechanisms involved in prion diseases are still poorly understood, but a first fundamental basis for an understanding at the molecular level has been established in 1996 when the first NMR structure of the mouse prion protein was determined. [46] Comparable structural data for the abnormal isoform has not yet been measured, but this form is characterized by a high  $\beta$ -sheet content. [47] The biological function of the normal cellular form, present in animals and humans, is largely unknown. However, recent experiments, both *in vivo* and *in vitro*, indicate that prions are able to bind  $Cu^{2+}$ , and that they have an antioxidant activity. [48] [49] It has been suggested that  $Cu^{2+}$  could bind in the histidine-rich unstructured part and that copper binding could influence the stability of the prion protein. [50] [51] Interestingly, recent pulse EPR and ENDOR experiments suggest [52] [53] that copper binds with higher affinity in the structured part (amino acids residues 125-228). Three copper binding sites have been found in this part, and they change relative population as a function of pH. Although it is not known which residues bind to the copper ion for any of the binding sites, the EPR data shows that there is dominant oxygen ligation for the low pH (pH < 7) complex, that the intermediate pH (pH 3-8) complex, for which the most detailed experimental data is available, involves binding of one of the three histidines present in the structured part, and that the high pH (pH 7-8) complex has the highest nitrogen content. Given the importance of the prion protein, the interest in its stability and its biological function, the availability of an accurate structure, and detailed experimental data on copper binding, we decided to model potential copper binding sites

in the structured part of the prion protein. This work, in collaboration with the authors of ref. [52, 53], is still in progress, and the results presented here are an illustration of the performance of the hybrid Car-Parrinello / Classical code that we have developed.

### 2.4.2 The need for QM/MM MD simulations

Locating copper ions in the prion protein structure is a particularly challenging problem. Not only because the system is complex, and requires advanced modeling techniques, but more importantly it is *a priori* not known what ligands are involved in binding, i.e. what the active site is. Both solvent and protein need to be modeled in order to take into account e.g. the nonhomogenous electrostatic field of the protein and the fact that the solvent can even act as a potential ligand of the copper ion. The large system size of more than 10,000 atoms, implies that part of the system has to be described classically. On the other hand, a high level of quantum theory is mandatory to describe the binding of the copper ion to the protein. Indeed, we can't make an *a priori* assumption about the possible ligands or their binding geometry, and thus we can't easily parametrize an empirical method for this purpose. The use of DFT has the advantage that a much larger part of the potential energy surface can be exploited with good accuracy, since the system can form bonds and change, in a reactive way, its conformation around the binding site. It turns out to be crucial to perform molecular dynamics simulations in the course of this local relaxation. Indeed, local geometry optimisations did not relax the system sufficiently, and chemically much more sound configurations were only obtained after a few picoseconds of molecular dynamics simulations. However, with simulation times of a few ps, the configurational space can be exploited only partially. In particular, it is not clear if the relaxation times of the coordination sphere are sufficiently short so that the local geometry can be considered as converged. The final states represent chemically reasonable and stable geometries, and hence we believe that the QM/MM method employed here, combined with a short-time dynamical relaxation, is indeed able to find relevant minima on the free energy surface.

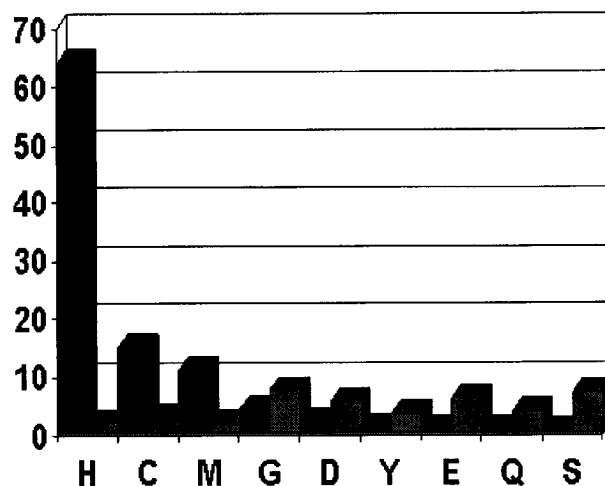


Figure 2.3: Relative abundance of the amino acids bound to copper in proteins (dark shading for each amino acid), compared with their natural abundance (gray shading). There is a clear preference for Histidine, Cysteine, and Methionine

### 2.4.3 A statistical approach to copper binding in proteins

A global search for binding sites by molecular dynamics simulations cannot be performed with current supercomputing power. An additional tool needs to be employed in order to perform a global and unbiased search for reasonable binding sites. We have combined the experimental data in Ref. [52] and [53] with a statistical analysis of known copper proteins in order to find the residues in the protein structure that are most likely to bind a copper ion. For this purpose, 111 PDB structures of copper proteins that are known at relatively high resolution ( $< 2.0 \text{ \AA}$ ) have been analysed, yielding information about 216 copper binding sites and involving bonding to 928 donor atoms. These numbers indicate that some of the copper sites are undercoordinated in the PDB structures, and that some of the e.g. water molecules that bind to copper ions might not have been resolved in the x-ray structures. The relative probability of the amino acids that are involved in

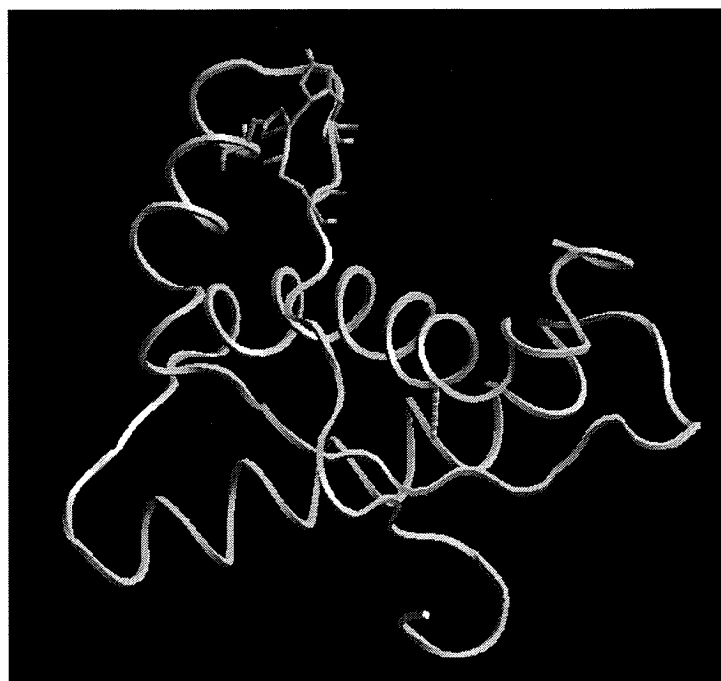


Figure 2.4: Ribbon diagram of the mouse prion protein, the binding site that is discussed in the text is shown with cylinders. This site is located in the top of the first  $\alpha$ -helix of the structure, and involves Met 138, His 140, and Asp 147.

copper binding is shown in Fig. 2.3, together with their natural abundance. This statistical analysis clearly shows that histidine is the most probable copper ligand, and provides in this way a confirmation of the experimental suggestion that one of the copper complexes probably involves a histidine ligand. Additionally, this analysis shows that the two sulfur containing amino acids cysteine and methionine are more likely than any of the residues with oxygen donors. These three residues together are providing about 80 percent of the copper ligands, whereas their natural abundance on the other hand is less than 7 %. Additionally, it should be noted that aspartic acid and glutamic acid are only as likely as the somewhat more abundant glycine and tyrosine. This can be attributed to the fact that copper is relatively 'soft'.

Using this data, the structured part of the mouse prion protein, was scanned, and a number

of candidate binding sites were found. Every site involves, by construction, one of the three histidine residues of the structured part of the prion. Additional ligands were included if their distance to the histidine or to any of the other potential ligands was less than 8 Angstrom, this large distance is used in order to take into account the flexibility of the protein structure and possible structural relaxation upon copper coordination. A ranking of the sites found in this way has been made, based on the likelihood of the involved residues. Two of the highly ranked sites, both located in the first  $\alpha$ -helix, and a closeby site that involves only aspartic acid residues have been simulated so far. The location of these sites in the first  $\alpha$ -helix is interesting, since the stability of this helix, which is supposed to be involved in the early stages of the conversion of the cellular form of the prion protein to the scrapie form, could be changed significantly by the presence of the copper ion. In the following, we describe the computational setup and the simulation results for one binding site that involves the residues methionine 138, histidine 140, and aspartic acid 147 as shown in Fig. 2.4 together with a ribbon diagram of the protein backbone.

#### 2.4.4 The computational setup

The average NMR structure of the structured part of the protein, residues 124 to 226, has been solvated using 4087 SPC water molecules at normal density, and the water has been equilibrated with a fixed protein structure, including one copper ion, for 150 ps at 300 K, with a box of  $4.5 \times 5.9 \times 5.2$  nm<sup>3</sup>. We used the GROMOS96 force field to represent the protein structure, using all flexible bonds, and P3M with a  $64^3$  grid for the electrostatics. The neighboring list, with a 0.9 nm cutoff, was updated every 2.5 fs. The quantum system was described with the local spin density approximation, using the BLYP functional. The pseudopotentials were of the Martins-Trouillers type and in particular, for the copper ion a previously tested copper pseudopotential [55] was employed with an 80 Ry plane wave cutoff. The charged QM system was decoupled from the images using the method due to Tuckerman and Martyna. The fictitious electron mass was 800 a.u. and the time step



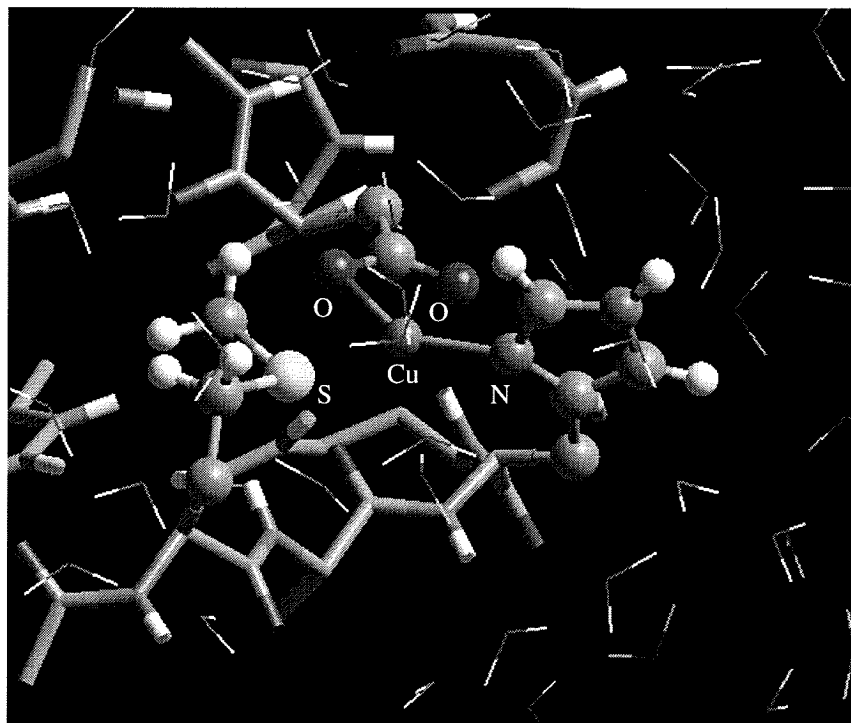


Figure 2.5: Frame from the QM/MM dynamics. The QM system is represented with balls and sticks, the visible part of the protein structure with cylinders, the solvent with lines. See the text for a description.

5 a.u. The electrostatic coupling used the modified potential and the long-range scheme as described above, with a distance cutoff of 10 a.u. The interacting residues were updated every 200 steps.

### 2.4.5 Simulation results

The simulation of this site has been performed for a total of about 5 ps, and some interesting snapshots are shown in Fig. 2.5-2.10. The first four frames are described with a relatively small QM model (23 atoms), where the boundary pseudopotentials are located on the  $C_{\beta}$  of the involved residues. The first frame (Fig. 2.5) shows the initial configuration, where

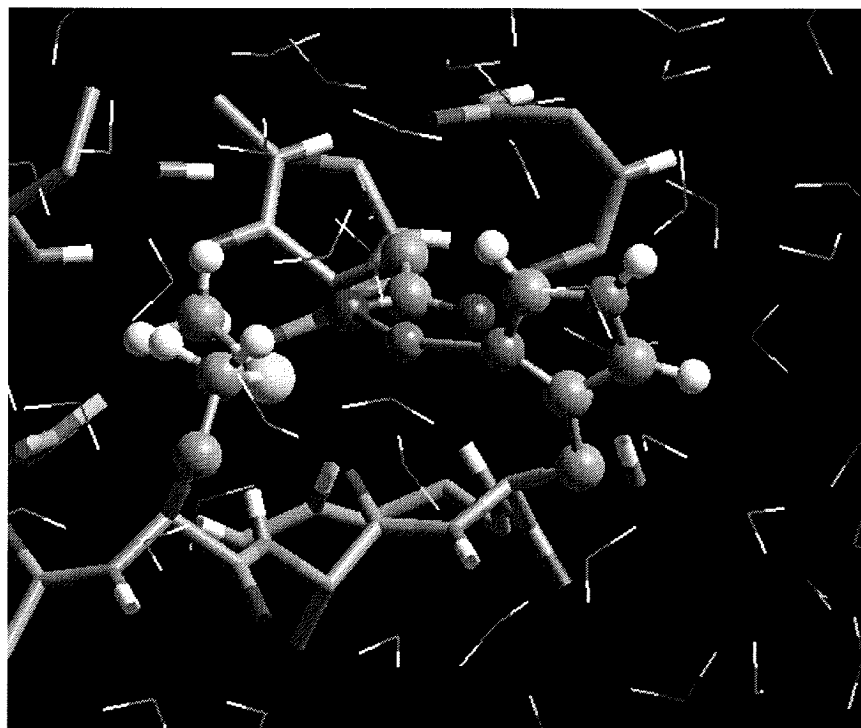


Figure 2.6: Frame from the QM/MM dynamics. The QM system is represented with balls and sticks, the visible part of the protein structure with cylinders, the solvent with lines. See the text for a description.

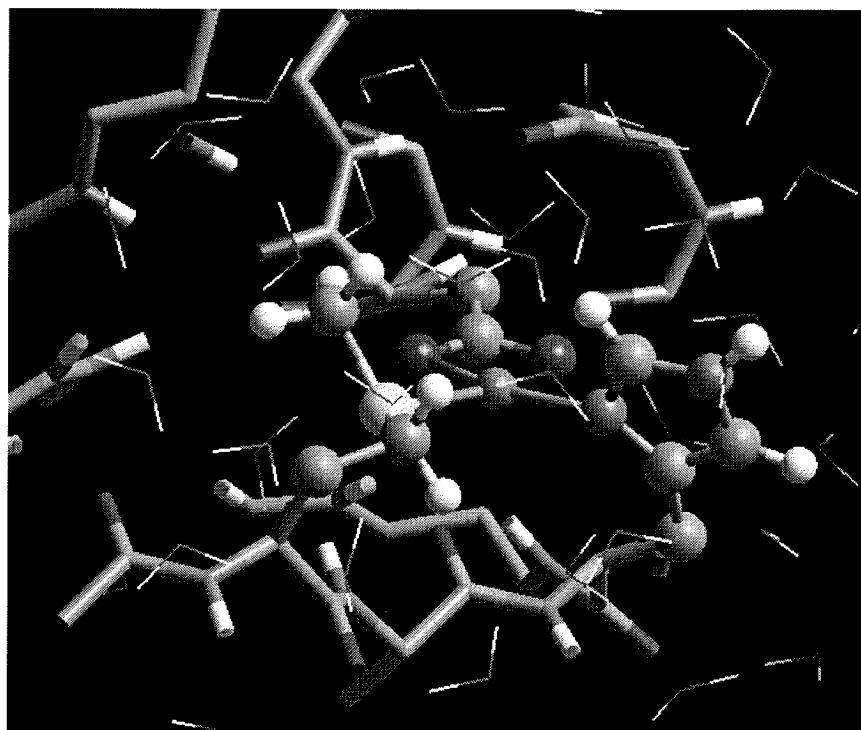


Figure 2.7: Frame from the QM/MM dynamics. The QM system is represented with balls and sticks, the visible part of the protein structure with cylinders, the solvent with lines. See the text for a description.

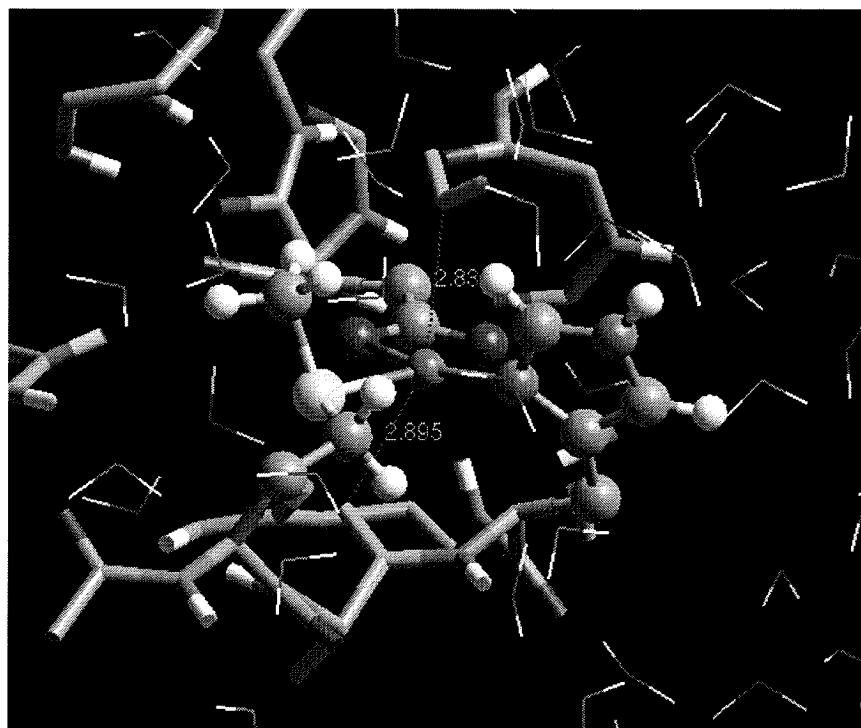


Figure 2.8: Frame from the QM/MM dynamics. The QM system is represented with balls and sticks, the visible part of the protein structure with cylinders, the solvent with lines. See the text for a description.

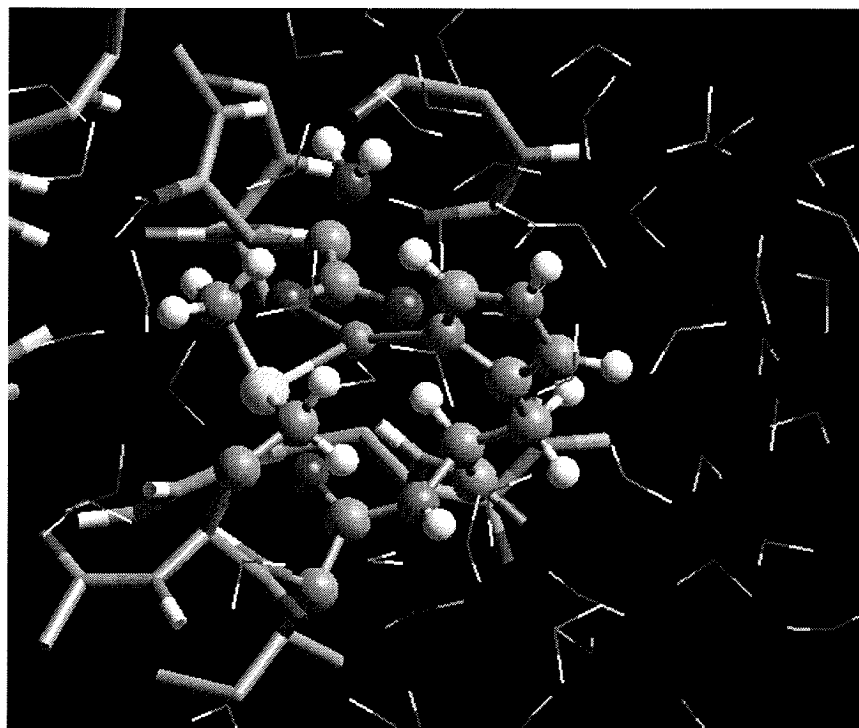


Figure 2.9: Frame from the QM/MM dynamics. The QM system is represented with balls and sticks, the visible part of the protein structure with cylinders, the solvent with lines. See the text for a description.

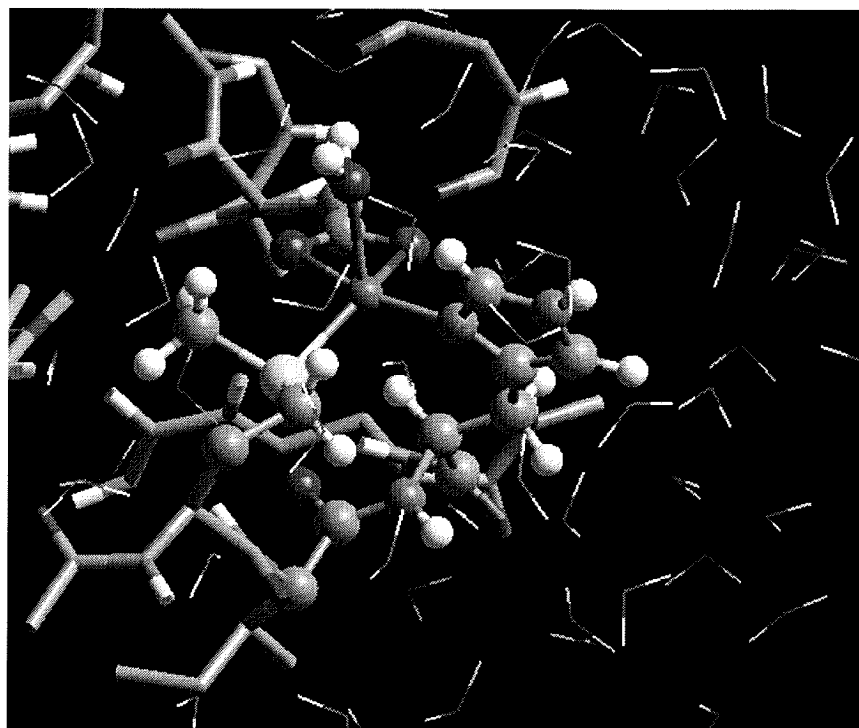


Figure 2.10: Frame from the QM/MM dynamics. The QM system is represented with balls and sticks, the visible part of the protein structure with cylinders, the solvent with lines. See the text for a description.

the residues are not yet relaxed. In particular, the methionine residue is in an unfavourable orientation when considering the lone pairs of the sulfur atom and their overlap with the copper orbitals. The second frame (Fig. 2.6) shows the configuration that results from 2500 steps of geometry optimisation. An initial geometry optimisation is necessary to optimise the bonded interactions within the QM system, and to relax the hydrogens that have to be added to the united atoms. Interestingly, the geometry of the sulfur atom is almost unchanged with respect to the initial configuration. In the third frame (Fig. 2.7) we show the configuration after only 250 steps of dynamics. Significant changes have taken place, including a favourable orientation of the sulfur atom, made possible by a torsional transition involving Cysteine  $C_\gamma$ . This indicates that the geometry optimisation was trapped in an unfavourable local minimum, and also points to the relatively high efficiency of the dynamical scheme in relaxing the structure. During 1.4 ps of equilibration, it was observed that two classical oxygen atoms, one belonging to a solvent molecule, and one to the backbone of Ile 139 (colored differently in the fourth frame, Fig. 2.8), came into an axial position, in bonding distance to the copper ion. The quantum system was increased to allow the system to select either of the two ligands. The extended system, which has 36 QM atoms, is shown in the fifth frame (Fig. 2.9), and involves the solvent molecule, and a part of the backbone, starting at the  $C_\alpha$  of Ile 139, and ending with the backbone carbon of His 140. The time evolution of the distances of the two potential oxygen ligands is shown Fig. 2.11. The upper panel of the figure shows clearly that the classical description cannot provide information about which of the two ligands is preferred for copper binding, since their distance fluctuates around approximately the same average value. This is not surprising, since the QM/MM interface cannot describe a chemical interaction of copper with the ligands. During the dynamics where these ligands are described quantum mechanically, a rapid binding and equilibration of the water molecule takes place, whereas the backbone oxygen drifts away from the copper ion, and stabilizes around 5 Å away from the copper ion. The dynamics was continued for 2.5 ps, and a stable configuration was observed. The sixth frame (Fig. 2.10) shows a typical configuration of the system, and one can clearly see the square planar geometry of the aspartic acid, the

Ligand	bond length (Å)	width (Å)
Met 138	2.37	0.10
His 140	1.93	0.04
Asp 147a	1.98	0.05
Asp 147b	2.27	0.03
Sol	2.26	0.05

Table 2.1: Average bond lengths for each of the copper ligands based on the final 2 ps of the dynamics, and the width ( $1 \sigma$ ) of the thermal distribution of this bond.

histidine, and the methionine, and the water molecule in an axial position. From the dynamics run, detailed structural information about the binding site can be extracted.

In Fig. 2.12 we show the copper-ligand bond lengths. This data not only provides precise geometrical information of the binding site, but in principle also allows for the parametrisation of a force field that can be used for a long time, classical, simulation of the prion protein in the copper binding state. In Tab. 2.1, average bond lengths, and the Gaussian width of the distribution of this length, which is directly related to the force constant of the bond, is provided. Note that the aspartic acid, that has both oxygen atoms involved in binding, has the shortest bond for the oxygen that is trans to the histidine.

A clear advantage of a quantum mechanical simulation is that the electronic properties are directly accessible. As an example we show in Fig. 2.13 the spin density of the copper site. This quantity is directly related to the experimental EPR measurements. Already at a qualitative level, the experimental observation of an unexchangeable proton signal could, if our binding site corresponds with the experimental one, be explained by the significant amount of spin density on the sulfur atom. [54] The binding site is in agreement with the experimental data of ref. [52] [53], and hence demonstrates that a combined statistical and *ab initio* approach can be used to suggest possible binding sites and their geometry, and provide a feedback for further experimental work.



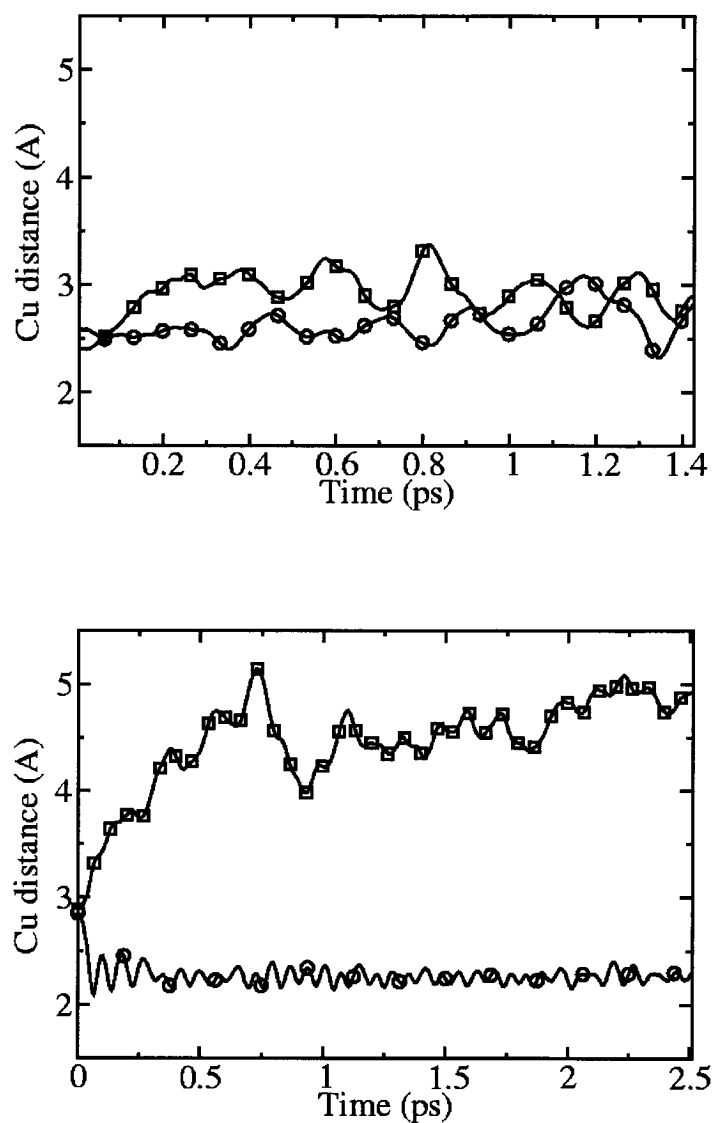


Figure 2.11: Distance of the water oxygen (circles) and the isoleucine backbone oxygen (squares) to the copper ion during the dynamics. The upper panel shows the data for the small QM model, where the oxygen atoms are treated classically. The lower panel shows the data for the larger QM model that includes these atoms as well.

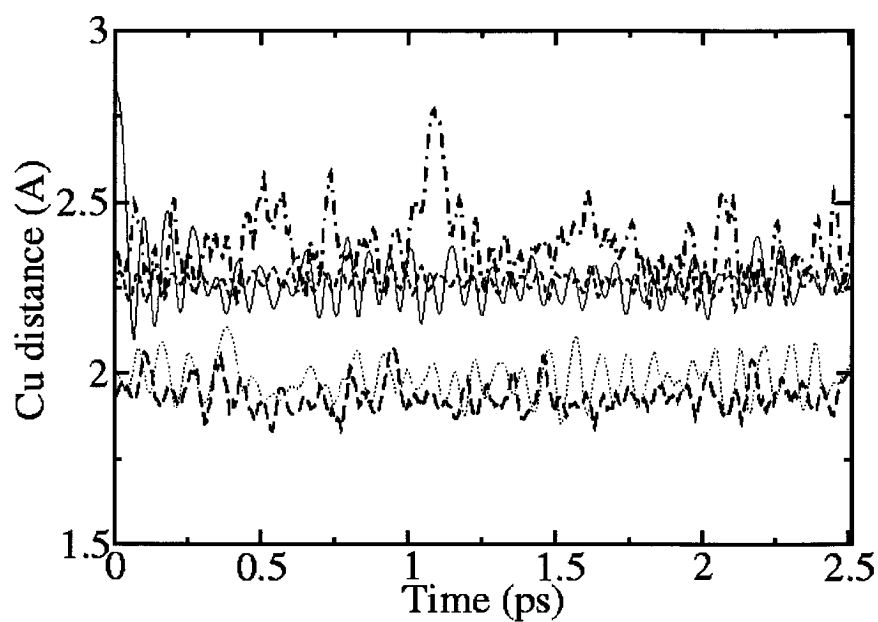


Figure 2.12: Copper - ligand binding distance during the last 2.5 ps of the simulation. The lower two lines represent the histidine (thick dashed) and the aspartate oxygen (thin dotted) distances, whereas the upper three lines represent the water (thin solid), the methionine (thick dash-dotted) and the second aspartate oxygen (dashed).

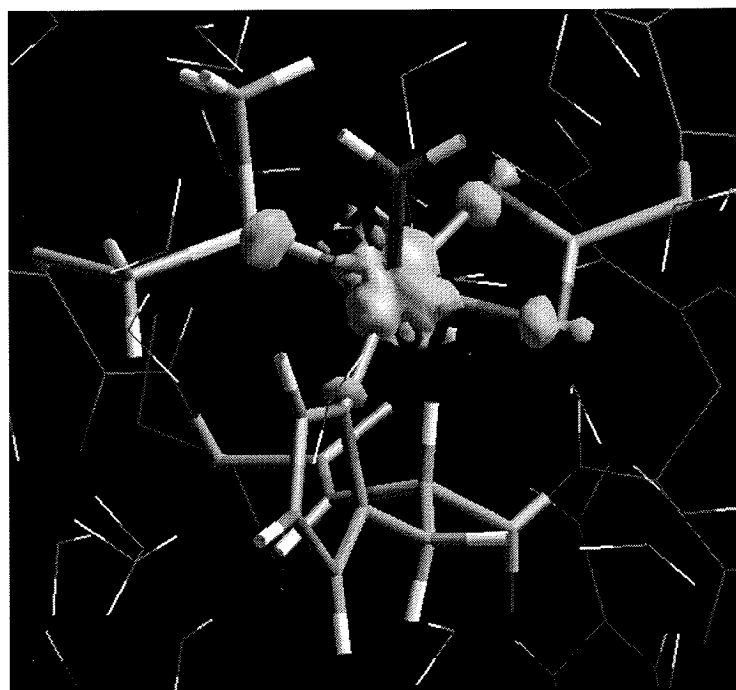


Figure 2.13: Spin density (contour at 0.012 a.u.) of the equilibrated copper complex. Note that this density is visible on all ligands in the plane, and in particular on the sulfur atom.

## Bibliography

- [1] See e.g. G. M. Torrie and J. P. Valleau, *J. Chem. Phys.* **66**, 1402 (1977); T. Huber, A. E. Torda, and W. F. van Gunsteren, *J. Comput.* **8**, 695 (1994); H. Grubmüller, *Phys. Rev. E* **52**, 2893 (1995); A. F. Voter, *Phys. Rev. Lett.* **78**, 3908 (1997); M. M. Steiner, P.-A. Genilloud, and J. W. Wilkins, *Phys. Rev. B* **57**, 10236 (1998); J. VandeVondele and U. Rothlisberger, *J. Chem. Phys.* **113**, 4863 (2000).
- [2] R. Car, and M. Parrinello, *Phys. Rev. Lett.* **55**, 2471 (1985).
- [3] A. Warshel, and M. Levitt, *J. Mol. Biol.* **103**, 2227 (1976).
- [4] U.C. Singh, and P.A. Kollman, *J. Comp. Chem.* **11**, 700 (1986).
- [5] M.J. Field, P.A. Bash, and M. Karplus, *J. Comp. Chem.* **7**, 700 (1990).
- [6] A recent review is given in: P.Sherwood, *Modern Methods and Algorithms of Quantum Chemistry*, J. Grotendorst (Ed.), John von Neumann Institute for Computing, Jülich, NIC Series, **1**, 257 (2000). See also <http://www.kfa-juelich.de/wsqc/proceedings.html>.
- [7] For a monograph see : *Combined quantum mechanical and molecular mechanical methods*, J. Gao, M.A. Thompson (Ed.) (Oxford University Press, 1998).
- [8] For a recent review of the Car-Parrinello method see, e.g.: D. Marx, J. Hutter, in *Modern Methods and Algorithms of Quantum Chemistry*, J. Grotendorst (Ed.), John von Neumann Institute for Computing, Jülich, NIC Series, **1**, 301 (2000)
- [9] P. Hohenberg, and W. Kohn, *Phys. Rev B* **136**, 864 (1964).
- [10] W. Kohn, and L. J. Sham, *Phys. Rev. A* **140**, 1133 (1965).
- [11] R.G. Parr, and W. Yang, *Density-Functional Theory of Atoms and Molecules* (Oxford university press, New York, 1989).

- [12] For a recent review of applications of the Car-Parrinello method see, e.g.: U. Rothlisberger, in *Computational Chemistry: Reviews of Current Trends*, J. Leszczynsky (Ed.) World Scientific (in press)
- [13] D. Wei, and D.R. Salahub, *Chem. Phys. Lett.* **224**, 291 (1994).
- [14] R.V. Stanton, L.R. Little, and K.M. Merz, *J. Phys. Chem.* **99**, 17344 (1995).
- [15] M. Eichinger, P. Tavan, J. Hutter, and M. Parrinello, *J. Chem. Phys.* **110**, 10452 (1999).
- [16] T.K. Woo, P.M. Margl, L. Deng, and T. Ziegler, in *it Combined quantum mechanical and molecular mechanical methods*, J. Gao, M.A. Thompson (Ed.) (Oxford University Press, 1998).
- [17] J. Wang, P. Cieplak, P.A. Kollman, *J. Comp. Chem.* **21**, 1049 (2000).
- [18] W.R.P. Scott, P.H. Hünenberger, I.G. Tironi, A.E. Mark, S.R. Billeter, J. Fennen, A.E. Torda, T. Huber, P. Krüger and W.F. van Gunsteren, *J. Phys. Chem. A* **103**, 3596 (1999).
- [19] W.D. Cornell, P. Cieplak, C.I. Bayly, K.M. Gould, K.M. Merz, D.M. Ferguson, G.L. Seibel, U.C. Singh, P.K. Weiner, and P.A. Kollmann, *J. Am. Chem. Soc.* **117**, 5179 (1995).
- [20] A. Laio, J. VandeVondele, and U. Rothlisberger, *to be published*.
- [21] P. Hünenberger, *J. Chem. Phys.* **23**, 10464 (2000).
- [22] See e.g. H. Liu, F. Müller-Plathe, and W.F. van Gunsteren, *J. Mol. Biol.* **261**, 454 (1996). P. L. Cummins, and J.E. Gready, *J. Comp. Chem.* **18**, 1496 (1997). G. A. Kaminski, and W. L. Jorgensen, *J. Phys. Chem. B*, 1787 (1998).
- [23] See e.g. P. D. Lyne, M. Hodoscek, and M. Karplus, *J. Phys. Chem. A.* **103**, 3462 (1999). Y. Zhang, H. Liu, and W. Yang, *J. Chem. Phys.* **112**, 3483 (2000).

- [24] A.D. Becke, Phys. Rev. A **38**, 3098 (1998).
- [25] J.P. Perdew, Phys. Rev. B **33**, 8822 (1986).
- [26] C. Lee, W. Yang, R. G. Parr, Phys. Rev. B **37**, 785 (1988).
- [27] N. Trouiller, and J.L. Martins, Phys. Rev. B **43**, 1993 (1991).
- [28] R.W. Hockney, Methods Comp. Phys. **9** 136 (1970).
- [29] G. Martyna, and M. Tuckermann, J. Chem. Phys. **110**, 1810 (1999).
- [30] A. Laio, J. VandeVondele, and U. Rothlisberger, *to be published*.
- [31] S. Chalmet, and M.F. Ruiz-López, Chem. Phys. Lett. **329**, 154 (2000).
- [32] Y. Zhang, T.-S. Lee, and W. Yang, J. Chem. Phys. **110**, 46 (1999).
- [33] I. Antes, and W. Thiel, J. Phys. Chem. A **104**, 9290 (1999).
- [34] U. Rothlisberger et al. *to be published*.
- [35] A. Laio, J. VandeVondele, and U. Rothlisberger, *to be published*.
- [36] S. Nosé, J. Chem. Phys. **81**, 511 (1984).
- [37] W.G. Hoover, Phys. Rev. A **31**, 1695 (1985).
- [38] G.J. Martyna, M.L. Klein, and M. Tuckerman, J. Chem. Phys. **97**, 2635 (1992).
- [39] E.A. Carter, G. Ciccotti, J.T. Hynes, and R. Kapral, Chem. Phys. Lett. **156**, 472 (1989).
- [40] M. Sprik, and G. Ciccotti, J. Chem. Phys. **109**, 7737 (1998).
- [41] CPMD, J. Hutter, A. Alavi, T. Deutsch, M. Bernasconi, St. Goedecker, D. Marx, M. Tuckerman, M. Parrinello, MPI für Festkörperforschung and IBM Zurich Research Laboratory 1995-1999

- [42] S.B. Prusiner, *Science* **252**, 1515 (1991).
- [43] for a review see : S.B. Prusiner, *Science* **278**, 245 (1997).
- [44] iC. Weissmann, *FEBS Lett.* **389**, 3 (1996).
- [45] A.L. Horwich, and J.S. Weissman, *Cell* **89**, 499 (1997).
- [46] R. Riek, S. Hornemann, G. Wider, M. Billeter, R. Glockshuber, and K. Wütrich, *Nature* **382**, 180 (1996).
- [47] K. Pan, M. Baldwin, J. Nguyen, M. Gasset, A. Serban, D. Groth, I. Mehlhorn, Z. Huang, R.J. Fletterik, F.E. Cohen, S.B. Prusiner, *Proc. Nat. Acad. Sci. USA* **90**, 10962 (1993).
- [48] D.R. Brown, K. Qin, J.W. Herms, A. Madlung, J. Manson, R. Strome, P.E. Fraser, T.A. Kruck, A. von Bohlen, W. Schulz-Schaeffer, A. Giese, D. Westaway, and H.A. Kretzschmar, *Nature* **390** 684 (1997).
- [49] D.R. Brown, C. Clive, and S.J. Haswell, *J. Neurochem.* **76**, 69 (2001).
- [50] E. Sulkowski, *FEBS Lett.* **307**, 129 (1992).
- [51] J.H. Viles, F.E. Cohen, S.B. Prusiner, D.B. Goodin, P.E. Wright, and H.J. Dyson, *Proc. Nat. Acad. Sci. USA* **96**, 2042 (1999).
- [52] S. Van Doorslaer, G. M. Cereghetti, R. Glockshuber, and A. Schweiger, *J. Phys. Chem. B* **105**, 1631 (2001).
- [53] S. Van Doorslaer, et. al, *to be published*.
- [54] S. Van Doorslaer, *private communication*.
- [55] U. Rothlisberger, P. Carloni, K. Doclo, and M. Parrinello, *J. Biol. Inorg. Chem.* **5** 236 (2000).





## Chapter 3

# A Hamiltonian electrostatic coupling scheme for hybrid Car-Parrinello molecular dynamics simulations

## Abstract

We present a fully Hamiltonian and computationally efficient scheme to include the electrostatic effects due to the classical environment in a Car-Parrinello mixed Quantum Mechanics/ Molecular Mechanics (QM/MM) method. The polarization due to the MM atoms close to the quantum system is described by a Coulombic potential modified at short range. We show that the functional form of this potential has to be chosen carefully in order to obtain the correct interaction properties and to prevent an unphysical escape of the electronic density to the MM atoms (the so-called spill-out effect). The interaction between the QM system and the more distant MM atoms is included by a Hamiltonian term explicitly coupling the multipole moments of the quantum charge distribution with the classical point charges. Our approach remedies some of the well known deficiencies of current electrostatic coupling schemes in QM/MM methods, allowing molecular dynamics simulations of mixed systems within a fully consistent and energy conserving approach.

## 3.1 Introduction

Atomistic simulations of chemical reactions in extended complex systems such as biomolecules are one of the major challenges of computational chemistry. The description of chemical reactions requires highly accurate methods for electronic structure determination, which are also able to describe unstable intermediate states, such as transition states. Moreover, since the majority of chemical processes are activated and the relaxation in structured molecular systems is usually slow, simulations over long periods of time are needed. Density functional (DFT) based *ab initio* molecular dynamics techniques, such as the Car-Parrinello (CP) method [1,2], provide us with accurate computational tools to study chemical reactions in liquids and solids [3]. However, bio-relevant molecular environments, such as proteins, are usually too large and complex for a straightforward application of this method, and the requirements on system size, accuracy and duration of a run are difficult to reconcile.

This has led, already some time ago [4–6], to the idea of partitioning the system into a chemically active part, that is treated by quantum chemical methods (QM) and a larger environment, assumed to be chemically inert, that is modelled by a classical force field (MM) [7]. This approach is particularly appealing since the computational effort can be concentrated on the region where the chemical reaction is expected to happen (e.g. the active site of an enzyme), while taking advantage of the computational efficiency of classical force fields, that provide a more expedient description of the biomolecule far from the active site.

The QM subsystem can be described at different levels of quantum mechanical approximation applying semi-empirical or *ab initio* methods. The generalization to a hybrid calculation is most natural for semi-empirical methods and already considerable experience exists in this field [4–6,8–11]. A similar development of fusing and adapting electronic structure methods and classical modelling techniques has been initiated in the *ab initio*

world, using HF or DFT [12–20]. Although similar to the problems encountered when using semi-empirical methods, the compatibility problems in *ab initio* implementations are more critical as a consequence of the increased complexity and flexibility of the basis sets and of the larger difference in the level of approximation between the MM and the QM subsystems.

The central question in hybrid methods concerns the way in which the quantum and the classical subsystems are interfaced. As a consequence of the form of standard biomolecular force fields, the interactions coupling QM and MM degrees of freedom can be grouped in bonded and non-bonded. Bonded interactions arise when the QM/MM boundary cuts through a chemical bond of a molecule. In that case, one or more QM atoms are joined to MM atoms by incomplete covalent bonds which leave the QM atoms with unsaturated valence orbitals. The problem of interfacing across bonds has received special attention [21–25]. The common solution is to "cap" the QM site with a link atom (frequently an hydrogen atom) or an empirically parametrized boundary atom, e.g. described by a suitable pseudopotential. An alternative is provided by the so-called frozen orbital approach, consisting in saturating the valence with suitable orbitals located on the MM atoms. These orbitals are included in the KS (or HF) Hamiltonian, but are not evolved during the simulation [26–28]. However, such an approach, though physically sound, implies a significant increase in computational cost within a plane-wave (PW) based scheme. The remaining bonded interactions, in particular angular and dihedral terms involving MM and QM atoms are taken into account by the classical force field.

Following the classification used in biomolecular force fields, the non-bonded interactions between the QM system and the MM atoms can be divided into steric and electrostatic environment effects. The steric interactions due to the Pauli repulsion and the dispersion interactions are usually taken into account in a straight forward way by retaining the van der Waals interaction as described by the classical force field [7]. The electrostatic interaction between the QM density and the point charges representing the charge distribution

in the MM system often constitutes the main environmental effect on the QM system and is technically more subtle.

Here, we will discuss a novel scheme to include electrostatic interactions between MM and QM subsystems in a PW-based CP molecular dynamics code. A natural choice for the non-bonded interaction Hamiltonian, extensively used in most of the advanced QM/MM approaches, is of the type

$$H_{non-bonded} = \sum_{i \in MM} q_i \int dr \frac{\rho(r)}{|r - r_i|} + \sum_{\substack{i \in MM \\ j \in QM}} v_{vdw}(r_{ij}) \quad (3.1)$$

where  $r_i$  is the position of the MM atom  $i$ , with charge  $q_i$ ,  $\rho$  is the total (electronic plus ionic) charge of the quantum system and  $v_{vdw}(r_{ij})$  is the van der Waals interaction between atom  $i$  and atom  $j$ . The core charge of the QM atom  $j$  is represented, in our approach, by a Gaussian charge distribution of magnitude  $Z_j$  (the valence of the quantum atom  $j$ ) and radius  $r_g$ . Since the ionic charge distribution is explicitly coupled with the external field through (3.1),  $r_g$  has to be chosen carefully in order to recover as close as possible the physical core charge distribution.

The form (3.1) for the electrostatic interaction Hamiltonian poses serious theoretical and technical problems, related to both its short range and its long range behavior. A first issue is related to the fact that positively charged classical atoms can act as traps for the electron if the basis set is flexible enough to allow for this. In fact, the Pauli repulsion from the electron cloud that would surround the classical atoms is absent, and the electron density is therefore overpolarized at short range by an incorrect purely attractive potential, giving rise to the so-called *electron spill-out* problem. This effect is particularly pronounced in a plane-wave basis-set approach, in which the electrons are fully free to delocalize, but can be of relevance also in schemes using localized basis sets, especially if extended basis sets with diffuse functions are used.

A second problem is related to the computational cost to compute the first term of the interaction Hamiltonian (3.1) within a plane-wave scheme. The number of operations that

would be required for a direct evaluation of (3.1) is of the order of  $N_r N_{MM}$ , where  $N_r$  is the number of real space grid points (of the order of  $100^3$ ) and  $N_{MM}$  is the number of classical atoms (usually of the order of 10000 or more in systems of biochemical relevance). In a real system, a straightforward computation of (3.1) would therefore increase the computational cost by several orders of magnitude. This serious bottleneck can be avoided employing techniques like the hierarchical multipole (HMP) method, an approach that has been developed in the framework of classical molecular dynamics simulations [29]. A suitable extension of the HMP allows for the calculation of the electrostatic potential on the grid at an affordable computational cost [17]. This technique is accurate when used to compute the potential for a given configuration of MM atoms. However, in the current QM/MM implementation [17], the forces on the MM atoms due to the electron charge distribution are estimated as ordinary Coulomb forces from auxiliary charges located on the QM atoms (electrostatic potential derived charges), and this leads to a non-Hamiltonian description.

Here, we present a method to include the electrostatic interactions in PW-based QM/MM calculations that does not suffer from any of the problems outlined above. In particular, within our scheme (i) the short range interactions are accurately described without any spill-out of the electron density onto the MM atoms and without any need to reparametrize the classical force-field; (ii) the long range electrostatic interaction can be taken into account within a fully Hamiltonian scheme; (iii) the inclusion of the electrostatic coupling to the environment does not significantly change the computational cost of the simulation (for a straightforward implementation, the computational overhead is only of the order of 10% to 50%, and could be reduced further by employing multiple time step techniques in which the electrostatic interaction is updated on an ionic time scale).

The method we present here has been developed as a part of an interface between the Car-Parrinello code CPMD [31] and the classical molecular dynamics package GROMOS96 [30]. A suitable decoupling technique [32] is used to eliminate the effect of the periodic images of

the QM charge density generated as a consequence of using a PW basis. The electrostatic interaction between classical atoms is taken into account by the P3M method [33].

## 3.2 Short range electrostatic interactions

In this Section, we will discuss a method to treat non-bonded short-range interactions between QM and MM atoms within a fully Hamiltonian scheme. A consistent description of the electrostatic interaction between the QM subsystem and the nearest classical atoms is crucial in order to obtain an accurate prediction of the electronic and structural properties at the QM/MM interface. The MM atoms in the immediate vicinity of the quantum system are responsible for a large part of the polarization. For instance, the incorrect description of the energetics of a hydrogen bond between a QM and a MM atoms can lead to large errors that might frustrate any attempt to accurately treat the relevant but weaker longer range interactions. This problem has repeatedly been pointed out in the literature as a possible source of errors in QM/MM simulations [34]. A direct inclusion of the Coulomb potential in the Kohn-Sham (or the Hartree-Fock) Hamiltonian as in (3.1) is widely applied in schemes based on localized basis sets. However, this leads to a model that is intrinsically unphysical since part of the electron density can artificially localize on positively charged MM atoms. In a localized basis set approach this problem might be less severe, but the unphysical nature of the interaction is present at any level of description, and is doomed to get worse if the basis set is extended. The severe shifts in the radial distribution functions and the large errors in the hydration enthalpies observed in QM/MM simulations of liquid water in which a single water is treated as a quantum fragment [34, 35] are possible manifestations of this effect. One suggested remedy to this problem is a reparametrization of the van der Waals radii of the classical atoms in order to compensate for this effect, but this *ad hoc* procedure does not eliminate the overpolarization of the electron cloud or the incorrect localization behavior of the electrons. Moreover, this approach does not always succeed, as demonstrated by Tu et al [34], who have reparametrized the force field in order to reproduce

the structural properties of a QM/MM water dimer with no apparent improvement for the pair correlation functions of liquid water.

Here, we employ a computationally more expedient and physically sound alternative, in the spirit of an empirical pseudopotential-like approach. The Coulomb potential is replaced with a suitable function  $v_j(r)$  (depending on the MM atom  $j$ ) such that  $v_j(r)$  goes to  $1/r$  for large  $r$  and to a finite value for small  $r$ . The first term in the interaction Hamiltonian (3.1) is thus replaced by

$$H_{el} = \sum_{j \in MM} q_i \int dr \rho(r) v_j(|r - r_j|). \quad (3.2)$$

For a given functional form  $v_j(r)$ , the forces on the MM atoms are obtained by a straightforward differentiation with respect to atomic coordinates (see eqn. (3.11)). The forces can be computed together with the potential for the QM system in a single loop over the real space grid, without a significant computational overhead, leading to a fully Hamiltonian description.

The electronic and mechanical properties of the mixed QM/MM system critically depend on the choice of the function  $v_j(r)$ . The most sensitive interactions are, in general, the direct contact interactions between QM and MM atoms, in particular the hydrogen bonds. In our approach, like in most of the other QM/MM approaches [7], we have chosen to retain a steric (van der Waals) interaction between the nuclei of the quantum and classical atoms described by the classical force field. Given this choice, an accurate description of hydrogen bond distances and energetics can be obtained choosing a  $v_j(r)$  saturating to  $1/r$  at a distance  $r_{c_j}$  from the MM atom  $j$ , and smoothly going to a constant for small  $r$ . In particular, we take

$$v_j(r) = \frac{r_{c_j}^n - r^n}{r_{c_j}^{n+1} - r^{n+1}} \quad (3.3)$$

where  $n=4$  and  $c_j$  is the covalent radius of the atom  $j$ . This functional form is resembling the form obtained by smearing the MM point charges into Gaussians charge distributions with finite width [17, 36]. Among other alternative choices for  $v_j(r)$ , we tested functions



with a repulsive core for small radius and functions going to zero for  $r \rightarrow 0$ . In all these cases, we obtained unsatisfying results. The influence of  $r_c$  on the pair correlation functions between QM and MM atoms has been probed by performing a QM/MM simulation of a quantum water molecule in a box of classical water.

The radial distribution functions for various choices of the cutoff radii  $r_{c,j}$  are summarized in Figure 3.1a and 3.1b for the oxygen-hydrogen and in Figure 3.1c for the oxygen-oxygen pair correlation functions. All simulations were performed starting from a thermalized box of 256 classical SPC water molecules at normal density and at a temperature of 300 K. Data have been collected for 10 ps after 5 ps of QM/MM thermalization. The QM water molecule is modelled with a cutoff of 70 Ry and the BLYP approximation [37, 38] for exchange and correlation. The influence of the functional form of  $v_j(r)$  on the bonding properties of the system can be dramatic. If, e.g.,  $r_c$  of  $0.8 \text{ \AA}$  is chosen for all the classical atoms the first peak in the oxygen-hydrogen pair correlation function disappears, indicating that the hydrogen bond between the quantum oxygen and the classical hydrogen is essentially lost and the solvation structure has almost entirely disappeared. If  $r_c$  is chosen to be equal to the van der Waals radius ( $\sim 0.8 \text{ \AA}$  for hydrogen and  $\sim 1.4 \text{ \AA}$  for oxygen) also the oxygen-oxygen peak is strongly shifted and smeared out, showing that with this choice, the quantum water molecule interacts too weakly with the classical water. The correlation functions computed without modification of the Coulombic interactions cannot be consistently defined within our approach, since, if this functional form is chosen a fraction of the electron density localizes on the classical hydrogens. Additionally, if no smearing is applied to the Coulombic interaction, the electrons heat up significantly during the simulation (see Fig. 3.2), showing that the system is unstable with a typical choice for the fictitious mass of the electrons. Pair correlation functions consistent with the full quantum [39] and the full classical (SPC) results could instead be obtained by choosing  $r_c$  sufficiently close to the covalent radius (i.e.  $\sim 0.4 \text{ \AA}$  for hydrogen and  $\sim 0.7 \text{ \AA}$  for oxygen), as shown in Fig. 3.1. With this choice, the position and the size of the peaks predicted by the QM/MM model is in close agreement with the classical and the full QM results.

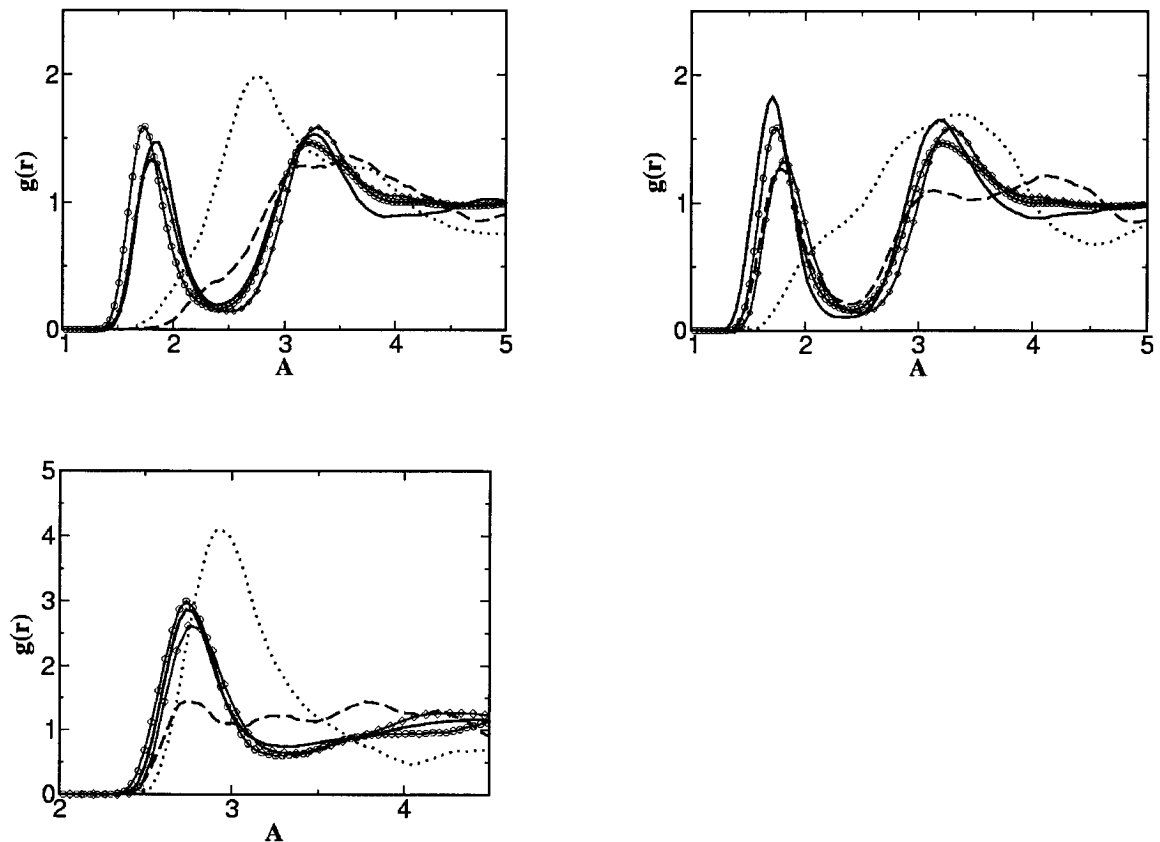


Figure 3.1: Pair correlation functions for a quantum water in a box of classical (SPC) waters compared with full classical SPC water (continuous line with circles) and full quantum [39] (continuous line with diamonds) results. Continuous line:  $r_c$  in equation (3.3) for oxygen and hydrogen are 0.8 and 0.4 Å respectively; dashed line:  $r_c$  for oxygen and hydrogen are 0.8 and 0.8 Å; dotted line:  $r_c$  for oxygen and hydrogen are 1.4 and 0.8 Å. (a): quantum oxygen-classical hydrogen pair correlation function. (b): quantum hydrogen-classical oxygen pair correlation function. (c): quantum oxygen-classical oxygen pair correlation function

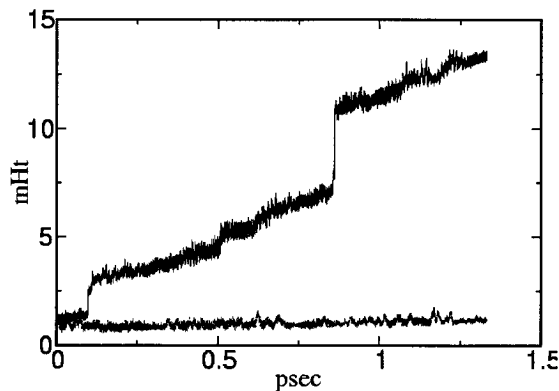


Figure 3.2: Fictitious electronic kinetic energy [1] as a function of time for a simulation of a quantum water in a box of classical (SPC) waters at 300K and normal density. The time step is 6. a.u. Continuous line: no modification of the Coulomb potential of classical point charges is applied. Dotted line: the Coulomb potential is modified according to Eq. (3.3) with  $r_c = 0.8 \text{ \AA}$  for oxygen and  $r_c = 0.4 \text{ \AA}$  for hydrogen.

Moreover, we have checked that the pair correlation functions are unchanged (within the noise of a limited simulation of 10 ps) if  $r_c$  is changed throughout a range between a factor of 0.6 to 1.2 of the covalent radius.

In conclusion, our choice (3.3) for the modified Coulombic interaction provides accurate results for the structural properties of a quantum water molecule in a box of classical water without any *ad hoc* reparametrization of the force-field.

### 3.3 Long range electrostatic interactions

A direct computation of the interaction Hamiltonian (3.2) with the summation running over all the charges of the MM system would be too expensive within a plane-wave based approach. In this Section, we introduce a method that allows, within a fully Hamiltonian

scheme, an accurate and computationally efficient computation of (3.2). In the coupling scheme we present in this article, the Coulombic electrostatic field is included exactly only for a set of MM atoms in the vicinity of the QM system. This set of atoms (NN atoms) is defined in such a way as to include all (non-neutral) atoms belonging to charge groups ([30]) with at least an atom inside a shell of thickness  $R_c$  around any quantum atom. Hence, care is taken that charge groups are included (or excluded) as a whole from the direct interaction with the quantum system.

The electrostatic field on the MM atoms that do not belong to the NN set is calculated by a multipolar expansion of the full interaction given in Eq. (3.2). In fact, since the charge density of the quantum system is localized (e.g., inside a sphere of radius  $R_q$  around the geometrical center of the quantum system), up to quadrupolar order, the electrostatic field due to  $\rho$  at the position  $r_j$  of the MM atom  $j$  is given by

$$\int dr \frac{\rho(r)}{|r - r_j|} = C \frac{1}{|r_j - \bar{r}|} + \sum_{\alpha} D^{\alpha} \frac{(r_j^{\alpha} - \bar{r}^{\alpha})}{|r_j - \bar{r}|^3} + \frac{1}{2} \sum_{\alpha\beta} Q^{\alpha\beta} \frac{(r_j^{\alpha} - \bar{r}^{\alpha})(r_j^{\beta} - \bar{r}^{\beta})}{|r_j - \bar{r}|^5} + \mathcal{O}\left(\frac{R_q}{|r_j - \bar{r}|}\right)^4 \quad (3.4)$$

where  $\bar{r}$  is the origin of the multipolar expansion (in our implementation the geometrical center of the quantum system) and  $C$ ,  $D^{\alpha}$  and  $Q^{\alpha\beta}$  are the total charge, the dipole and the quadrupole of the quantum charge distribution  $\rho$ .  $C$ ,  $D^{\alpha}$  and  $Q^{\alpha\beta}$  are respectively given by

$$\begin{aligned} C &= \int dr \rho(r) \\ D^{\alpha} &= \int dr \rho(r) (r^{\alpha} - \bar{r}^{\alpha}) \\ Q^{\alpha\beta} &= \int dr \rho(r) \left[ 3(r^{\alpha} - \bar{r}^{\alpha})(r^{\beta} - \bar{r}^{\beta}) - \delta^{\alpha\beta} |r - \bar{r}|^2 \right] \end{aligned} \quad (3.5)$$

where greek indices are assumed to run from 1 to 3. Since for  $|r - r_j| \gg r_c$ ,  $v(r - r_j) \simeq \frac{1}{|r - r_j|} \left(1 + \mathcal{O}(r_c/|r - r_j|)^4\right)$  for all atoms  $j$  outside the NN set, using (3.4) the electrostatic interaction (3.2) can be expressed, neglecting terms of the order of  $\mathcal{O}(R_q/\min_{j \in NN} |r_j - \bar{r}|)^4$ ,

as

$$H_{el} = \sum_{j \in NN} q_j \int dr \rho_e(r) v_j(|r - r_j|) + H_{lr} \quad (3.6)$$

where  $H_{lr}$  is given by

$$H_{lr} = C \sum_{j \notin NN} \frac{q_j}{\tau_j} + \sum_{\alpha} D^{\alpha} \sum_{j \notin NN} \frac{q_j}{\tau_j^3} \tau_j^{\alpha} + \frac{1}{2} \sum_{\alpha\beta} Q^{\alpha\beta} \sum_{j \notin NN} \frac{q_j}{\tau_j^5} \tau_j^{\alpha} \tau_j^{\beta} \quad (3.7)$$

with

$$\tau_j^{\alpha} = r_j^{\alpha} - \bar{r}^{\alpha}.$$

Since the MM atoms are divided, except for physically charged groups, into globally neutral clusters [30], the error can be reduced further using two different cutoffs for uncharged and charged units. If a sufficiently large cutoff is used for the comparably few charged groups, the first term neglected in the multipolar expansion is an octupole-dipole term with the neutral groups at  $R_c$ , hence the error is of the order  $\mathcal{O}\left(\frac{R_q}{R_c + R_q}\right)^5$ . The convergence of  $H_{lr}$  to the Hamiltonian (3.2) can be systematically improved by including multipoles of higher order with very small additional computational cost.

The only free parameter in the present approach is the thickness  $R_c$  of the shell of MM atoms explicitly coupled to the quantum system. The convergence of the results with respect to  $R_c$  can be checked directly comparing the results obtained for finite  $R_c$  with the values obtained with the full interaction Hamiltonian(3.2). As test case we have considered a QM/MM calculation of the mouse prion protein [40] in solution with a single peptide unit (Gly126) as the QM part. The system is terminated by three dummy carbons represented by monovalent pseudopotentials [25], as shown in Fig. 3.3 (one located on the  $C_{\beta}$  of the side chain, an aspartate in the particular case, and the other two located respectively on a  $C_{\alpha}$  and on the backbone carbonyl carbon atom of the following peptide unit).

The prion protein is a good test system to probe the performance of an electrostatics coupling scheme, since it has a strongly dipolar charge distribution and hence long range electrostatic effects have a sensitive influence on the properties of the system [41]. For an arbitrarily chosen snapshot configuration of a MD run, we have computed, as a function

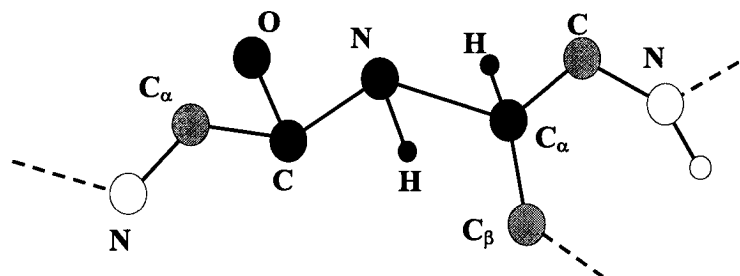


Figure 3.3: The quantum atoms for the system used to test the behaviour of the interaction Hamiltonian (3.6). Black circles: quantum atoms described by ordinary pseudopotentials. Gray circles: carbon atoms described by a monovalent pseudopotential [25] to compensate the valence of the quantum atoms. Empty circles: classical atoms.

of  $R_c$ , the total energy  $E_{lr}$ , and the dipole  $D_{lr}$  of the system. In particular, the values at finite  $R_c$  are compared with the ones obtained for very large  $R_c$ , for which the full protein is explicitly coupled to the quantum system by (3.2). Moreover, denoting by  $\rho_{R_c=\infty}$  and by  $\rho_{R_c}$  the density for the finite and very large  $R_c$ , we have computed the charge polarization

$$\mathcal{P} = \int dr |\rho - \rho_{R_c=\infty}| \quad (3.8)$$

The differences in energy, dipole moments and polarization are a measure of the approximation that is done when using Hamiltonian (3.6) instead of Hamiltonian (3.2). The results are reported in Table 3.1. As it is apparent,  $E_{lr}$  and  $D_{lr}$  converge quickly, as a function of  $R_c$ , to the value obtained using the full Hamiltonian(3.2) and  $\mathcal{P}_{lr}$  converges rapidly to zero. For a comparison, we calculate the total energy  $E_{mc}$ , the dipole  $D_{mc}$  and the charge polarization  $\mathcal{P}_{mc}$  in the case in which the long range interaction is taken into account by a classic Coulomb interaction. In this case  $H_{lr}$  in (3.6) is replaced by

$$H_{mc} = \sum_{\substack{i \notin NN \\ j \in QM}} \frac{q_j q_i}{r_{ij}} \quad (3.9)$$

i.e. the long range electrostatic interaction is treated within a "mechanical coupling" scheme [7, 8] ( $q_j$  is the force field charge of the QM atom  $j$ ). As it is apparent in Table 3.1, using a mechanical coupling scheme for the interaction between the QM atoms and

$R_c$	$E_{lr}$	$E_{mc}$	$D_{lr}$	$D_{mc}$	$\mathcal{P}_{lr}$	$\mathcal{P}_{mc}$
5	0.33875	17.4755	4.666	4.428	0.0203	0.0306
10	2.70004	23.7623	4.587	3.926	0.0097	0.0214
14	0.109596	15.9611	4.625	4.573	0.0063	0.0171
20	0.478235	-10.7304	4.586	4.601	0.0042	0.0059
25	0.259044	3.47717	4.587	4.728	0.0030	0.0050
60	0.	0.	4.592	4.592	0.	0.

Table 3.1: Total energies  $E$ , dipole  $D$  and polarization  $\mathcal{P}$  (as given by Eq. (3.8)) as a function of the cut-off radius for the explicit electrostatic interaction  $R_c$  for the system of Fig. 3.3. Values labelled "lr" and "mc" are respectively obtained if the long range interaction is described by (3.7) and by (3.9). Energies are in a.u.  $10^{-3}$ . The zero of the energy and the reference value for the density are defined by the value of the total energy and of the density obtained if an interaction Hamiltonian of the form (3.2) is used.  $R_c$  is in a.u. Dipoles are in Debye.  $\mathcal{P}$  in elementary charge units is calculated as given by (3.8)

the MM atoms not included in the NN set implies a significant error on the total energy, dipole moment and charge polarization of the system even for rather large values of the cut-off radius  $R_c$ .

### 3.4 Potential and forces on the atoms

In our approach, the non-bonded interaction between the QM and the MM system is described by an Hamiltonian of the form

$$H_{non-bonded} = H_{el} - \sum_{\substack{i \in MM \\ j \in QM}} \frac{Z_j q_i}{r_{ij}} + \sum_{\substack{i \in MM \\ j \in QM}} v_{vdw}(r_{ij})$$

with  $H_{el}$  given by (3.6). Energy conserving dynamics can be performed if the potential and the forces are calculated consistently. The potential is obtained by taking the functional

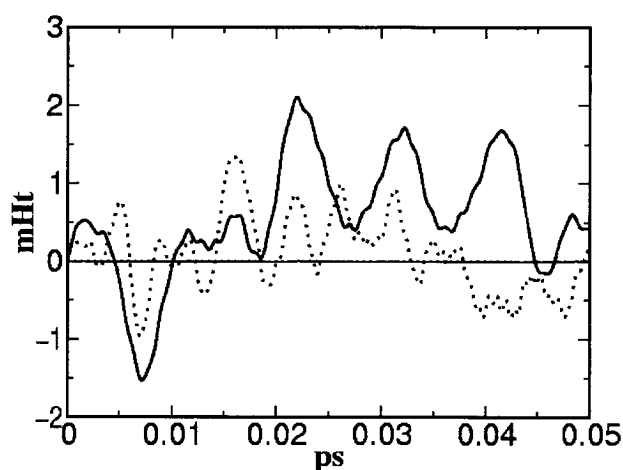


Figure 3.4: Total energy (thick lines) and potential energy (thin lines) as a function of time for the simulation of a quantum water in a box of classical water molecules at 300 K (continuous lines) and for the QM/MM simulation at 300 K of the system described in Figure 3 (dashed lines). The energy are divided by the square root of the number of particles (648 and 11279 respectively for the two systems). Moreover, the value of the initial energy is subtracted.



derivative of (3.6) with respect to  $\rho$  :

$$V(r) = \frac{\delta H_{el}}{\delta \rho} = \sum_{j \in NN} q_j v_j (|r - r_j|) + V_{lr}(r) \quad (3.10)$$

with

$$\begin{aligned} V_{lr}(r) = \frac{\delta H_{lr}}{\delta \rho} = & \sum_{j \notin NN} \frac{q_j}{\tau_j} + \sum_{\alpha} (r^{\alpha} - \bar{r}^{\alpha}) \sum_{j \notin NN} \frac{q_j}{\tau_j^3} \tau_j^{\alpha} + \\ & + \frac{1}{2} \sum_{\alpha\beta} \left[ 3(r^{\alpha} - \bar{r}^{\alpha})(r^{\beta} - \bar{r}^{\beta}) - \delta^{\alpha\beta} |r - \bar{r}|^2 \right] \sum_{j \notin NN} \frac{q_j}{\tau_j^5} \tau_j^{\alpha} \tau_j^{\beta} \end{aligned}$$

Since this potential is explicitly included in the Kohn-Sham Hamiltonian, the electron density is polarized up to any multipolar order by the atoms in the NN set and up to quadrupolar order by the rest of the MM atoms.

The forces on the atoms are obtained by taking the derivative of (3.6) with respect to the atomic positions. For  $j$  in the NN set the forces are given by

$$F_j^{\alpha} = q_j \int dr \rho(r) g_j (|r - r_j|) \frac{r^{\alpha} - r_j^{\alpha}}{|r - r_j|} \quad (3.11)$$

where  $g_j(r) = dv/dr$ . The forces on a MM atom not belonging to the set NN is

$$F_j^{\gamma} = -q_j \left[ \left( -\frac{C}{\tau_j^3} - 3\frac{1}{\tau_j^5} \sum_{\alpha} D^{\alpha} \tau_j^{\alpha} - \frac{5}{2} \frac{1}{\tau_j^7} \sum_{\alpha\beta} Q^{\alpha\beta} \tau_j^{\alpha} \tau_j^{\beta} \right) \tau_j^{\gamma} + \frac{D^{\gamma}}{\tau_j^3} + \frac{1}{\tau_j^5} \sum_{\alpha} Q^{\alpha\gamma} \tau_j^{\alpha} \right] \quad (3.12)$$

Finally, the forces on the quantum atoms deriving from (3.7) are (independently of the atom)

$$F_j^{\gamma} = \frac{1}{N_Q} \left[ -\frac{5}{2} \sum_{\alpha\beta} Q^{\alpha\beta} \sum_{k \notin NN} \frac{q_k}{\tau_k^7} \tau_k^{\alpha} \tau_k^{\beta} \tau_k^{\gamma} + \sum_{\alpha} Q^{\alpha\gamma} \sum_{k \notin NN} \frac{q_k}{\tau_k^5} \tau_k^{\alpha} \right] \quad (3.13)$$

where  $N_Q$  is the number of quantum atoms. Moreover, the quantum ions are subject to the forces due to the potential (3.10). If  $\rho_G^j (|r - r_j|)$  is the Gaussian density used to represent the core charge distribution of the quantum atom  $j$ , we have

$$F_j^{\alpha} = - \int dr V(r) \frac{d\rho_G^j}{dr} \Big|_{r=|r-r_j|} \frac{r^{\alpha} - r_j^{\alpha}}{|r - r_j|}.$$

The computation of the forces on the atoms and of the potential due to (3.6) is computationally relatively inexpensive. The computational bottleneck is the evaluation of the

first term in (3.6), requiring the calculation of the distances between every grid point and all the NN atoms. The evaluation of the potential and the forces derived from the second term in (3.6) is instead inexpensive, since it requires only the calculation of the distances between all MM atoms and all grid points from a *single* point (the geometrical center of the quantum system). The correctness of the implementation can be directly verified by monitoring the conservation of energy for a MD simulation. Some typical examples are shown in Fig. 3.4. In these cases the drift is only  $10^{-6}$  a.u. per picosecond and per particle.

**Acknowledgments.** We are thankful to Maria Lore Sulpizi for her precious help, to Philippe Hünenberger for useful discussions and for kindly making a P3M version of GRO-MOS available and to Pierluigi Silvestrelli for providing the data on the full quantum pair correlation function of water.

## Bibliography

- [1] R. Car, and M. Parrinello, *Phys. Rev. Lett.* **55**, 2471 (1985).
- [2] For a recent review of the method see, e.g.: D. Marx, J. Hutter, in *Modern Methods and Algorithms of Quantum Chemistry*, J. Grotendorst (Ed.), John von Neumann Institute for Computing, Jülich, NIC Series, **1**, 301 (2000)
- [3] For a recent review of applications of the Car-Parrinello method see, e.g.: U. Rothlisberger, published in *Computational Chemistry: Reviews of Current Trends*, J. Leszczynsky (Ed.) World Scientific (in press)
- [4] A. Warshel and M. Levitt, *J. Mol. Biol.*, **103**, 227 (1976).
- [5] U. C. Singh, P. A. Kollman, *J. Comp. Chem.* **7**, 718 (1986).
- [6] M. J. Field, P. A. Bash, and M. Karplus, *J. Comput. Chem.* **11**, 700 (1990).

- [7] A recent review is given in: P. Sherwood, published in *Modern Methods and Algorithms of Quantum Chemistry*, J. Grotendorst (Ed.), John von Neumann Institute for Computing, Jülich, NIC Series, **1**, 257 (2000).
- [8] D. Bakowies and W. J. Thiel, *J. Phys. Chem.* **100**, 10580 (1996).
- [9] H. Liu, F. Müller-Plathe, W. van Gunsteren, *J. Mol. Biol.* **261**, 454 (1996).
- [10] P. Cummins, J. Gready, *J. Comp. Chem.* **18**, 1496 (1997).
- [11] F. J. Luque, N. Reuter, A. Cartier, M. F. Ruiz-Lopez, *J. Phys. Chem. A* **104** 10923 (2000)
- [12] Z.H. Deng, G. J. Martyna, and M. L. Klein, *J. Chem. Phys.* **100**, 7590, (1994).
- [13] D. Wei, D. Salahub, *Chem. Phys. Lett.*, **224**, 291 (1994).
- [14] I. Tunon, M. T. C. Martins-Costa, C. Millot, M. F. Ruiz-Lopez, *J. Mol. Model.*, **1**, 196 (1995).
- [15] R. V. Stanton, L. R. Little, and K. M. Merz Jr. , *J. Phys. Chem.* **99**, 11266 (1996).
- [16] U. Rothlisberger, *Combined Quantum Mechanical and Molecular Mechanical Methods*, ACS Symposium Series 712, Ed. J. Gao and M. A. Thompson, Am. Chem. Soc., Washington, DC (1998).
- [17] M. Eichinger, P. Tavan, J. Hutter, M. Parrinello, *J. Chem. Phys.* **21**, 10452- (1999).
- [18] P. Lyne, M. Hodosceck, M. Karplus, *J. Phys. Chem. A* **103**, 3462 (1999).
- [19] G. Pioda, T. K. Woo, U. Röthlisberger, A. Togni, *Organometallics* **19**, 2144 (2000).
- [20] R. Hall, S. Hindle, N. Burton, I. Hillier, *J. Comput. Chem.* **16**, 1433 (2000).
- [21] J. Gao, P. Amara, C. Alhambra, M. J. Field, *J. Phys. Chem. A*, **102**, 4714 (1998).
- [22] I. Antes and W. Thiel, *J. Phys. Chem. A*, **103**, 9290 (1999).

- [23] Y. Zhang, T.-S. Lee, W. Yang, *J. Chem. Phys.* **110**, 46 (1999).
- [24] N. Reuter, A. Dejaegere, B. Maigret, M. Karplus, *J. Phys. Chem. A* **104**, 1720 (2000).
- [25] U. Rothlisberger, to be published
- [26] G. Monard, M. Loos, V. Thery, K. Baka, J.-L. Rivail, *Int. J. of Quantum Chem.*, **58**, 153 (1996).
- [27] V. Kairys and J. Jensen, *J. Phys. Chem. A* **104**, 6656 (2000).
- [28] R. Murphy, D. Philipp, R. Friesner, *J. Comp. Chem.* **21**, 1442 (2000).
- [29] C. Niedermeier and P. Tavan, *J. Chem. Phys.*, **101**, 734 (1994).
- [30] W. van Gunsteren *et al*, *Biomolecular Simulations: The GROMOS96 Manual and User Guide*, Vdf Hochschulverlag AG, ETH Zurich, Universitetstrasse 6, CH-8092, Zurich, 1996.
- [31] CPMD, J. Hutter, A. Alavi, T. Deutsch, M. Bernasconi, St. Goedecker, D. Marx, M. Tuckerman, M. Parrinello, MPI für Festkörperforschung and IBM Zurich Research Laboratory 1995-1999.
- [32] G. Martyna, M. Tuckerman, *J. Chem. Phys.* **110**, 1810 (1999).
- [33] P. Hünenberger, *J. Chem. Phys.* **23**, 10464 (2000).
- [34] Y. Tu, A. Laaksonen, *J. Chem. Phys.* **16**, 7519 (1999).
- [35] I. Tunon, M. Martins-Costa, C. Millot, M. Ruiz-Lopez, *Chem. Phys. Lett.* **241**, 450 (1995).
- [36] K. P. Eurenius, D. C. Chatfield, B. R. Brooks, M. Hodosek, *Int. J. of Quantum Chem.*, **60**, 1189 (1996).
- [37] A. D. Becke, *Phys. Rev. B* **38**, 3098 (1988).

- 
- [38] C. Lee, W. Yang, R. G. Parr, *Phys. Rev. B* **37**, 785 (1988).
- [39] P. L. Silvestrelli, M. Parrinello, *J. Chem. Phys.* **111**, 3572 (1999).
- [40] R. Riek, S. Hornemann, G. Wider, M. Billeter, R. Glockshuber, K. Wüthrich, *Nature* **382**, 180 (1996).
- [41] J. Zuegg, J. E. Gready, *Biochemistry*, **38** 13862 (1999).



## Chapter 4

# Efficient multidimensional free energy calculations for ab initio molecular dynamics using classical bias potentials

## Abstract

We present a method for calculating multidimensional free energy surfaces within the limited time scale of a first-principles molecular dynamics scheme. The sampling efficiency is enhanced using selected terms of a classical force field as a bias potential. This simple procedure yields a very substantial increase in sampling accuracy while retaining the high quality of the underlying ab initio potential surface and can thus be used for a parameter free calculation of free energy surfaces. The success of the method is demonstrated by the applications to two gas phase molecules, ethane and peroxy-nitrous acid, as test case systems. A statistical analysis of the results shows that the entire free energy landscape is well converged within a 40 picosecond simulation at 500 K, even for a system with barriers as high as 15 kcal/mol.



## 4.1 Introduction

Ab initio molecular dynamics (AIMD) [1] is gradually becoming a well established tool for the study of physical [2], chemical [3] and biochemical [4] systems. With density functional theory (DFT) [5, 6] as the underlying electronic structure method, an accurate potential energy surface can be obtained at a correlated level for systems up to few hundreds of atoms. A particular advantage is that, in contrast to conventional electronic structure calculations, AIMD allows for a direct study of dynamic and thermodynamic properties at finite temperature. Thus, in principle, it is possible to use ab initio molecular dynamics for a parameter free calculation of free energy differences, or more general, of free energy surfaces. Clearly, the calculation of the relative free energy is of primary importance because it is the quantity that contains all the fundamental information for the prediction of the stability of different forms, the most likely reaction pathways, and, in the transition state theory approximation, the corresponding rate constants [7]. Since the free energy of a specific configuration is directly related to the probability of observing it in an ensemble, its relative free energy can be calculated from the fraction of time it has been observed during a molecular dynamics run [7]. It is however necessary that the phase space trajectory is sufficiently long so that it samples all relevant configurations in a statistically meaningful way. This implies that for a system with large barriers and, consequently, small rate constants for the transitions between different minima, long simulation times will be needed before free energy estimates can be made. Typical activation barriers in (bio)chemical reactions, for example, can be of the order of 10 - 30 kcal/mol, corresponding to reaction times in the range of ms to hours. These time scales undoubtedly exceed the length of typical AIMD simulations that currently span at most 100 ps. Clearly, a technique that enhances sampling by several orders of magnitude is compulsory.

Here, we present and test a method that is designed for enhancing the AIMD sampling of multidimensional free energy surfaces by several orders of magnitude. This enhancement results from the application of a bias potential derived from selected terms of a classical

force field. It is important to point out that this approach differs from methods that are based on classical force fields for the estimation of the free energy. The method presented here has the advantage that the converged values for the free energies do not depend on the classical force field, and are thus of *ab initio* quality. Only the rate of convergence depends on the quality of the force field, or more precisely, on the fact of how closely the classical force field matches the *ab initio* results.

We tested such a biased sampling approach on two systems. As a first test case, we calculated the one dimensional free energy profile for rotation of the methyl groups in ethane. As an illustration of the severe time scale barrier inherent to *ab initio* MD, we show that, even at 500 K, where ethane can often be regarded as a free rotator, direct *ab initio* molecular dynamics fails to sample the three symmetry equivalent minima homogeneously. Through the application of the classical bias method presented here these shortcomings can be fully overcome. The second test system is more demanding and involves the calculation of the free energy surface in the two dimensional torsional space of peroxyntrous acid (ONOOH). ONOOH is an interesting test system for our purpose as it is small, but at the same time fairly complex. The potential energy surface of this molecule has three different minima and six transition states. The minima are all within few kcal/mol and are thus all significantly occupied even at a temperature of 500K. The different forms can be interconverted through rotation around the two central bonds. Rotation around the oxygen-oxygen bond has a low barrier of  $\approx 2$  kcal/mol. Rotation around the central nitrogen-oxygen bond on the other hand, implies a partial breaking of the conjugated system and involves a barrier of  $\approx 15$  kcal/mol. Thus *cis-trans* isomerisation can be expected to occur approximately in the ms time range. In view of the typical time scale implied by *ab initio* MD, this system is therefore a challenging test case.

## 4.2 Bias potentials to increase sampling efficiency

Many different methods for enhanced sampling have been suggested in the context of classical MD simulations. The most dramatic speedup is achieved by methods that modify the Hamiltonian of the system in some way [8–22] although other approaches exist [23–27]. A modification of the Hamiltonian is possible because thermodynamic properties can be evaluated as a phase-space integral of a time independent function and the dynamics of the system serves only as a sampling device of the relevant phase-space. The challenge lies in how to modify the Hamiltonian, and in defining a consistent way to correct back for the properties of the original system. The changes made to the Hamiltonian should be such that the computed averages converge much faster for the modified system than for the original one. One of the simplest versions of such an approach is the rescaling of the particle masses. Rescaling the masses might help in sampling phase space more efficiently, and since free energy differences in a classical system do not depend on the masses of the particles, no correction is necessary. Another well established technique is umbrella sampling [8], that introduces a bias potential, i.e. an attractive potential  $V$  near the barrier of the system, to enhance the sampling of a region where statistics would otherwise be very poor. Recently, it was suggested that it is also possible to modify the potential energy surface near the minimum [17–22], that is, decreasing the depth of the minimum by adding a repulsive potential. This has the advantage that only the location of the minimum has to be known, and that it gives additional freedom to the system to cross different barriers and choose several reactive pathways. If transition state theory can be applied, one can estimate that for a decrease in depth of the potential by  $V_{bias}$  the rate constant increases exponentially by  $\approx e^{\beta V_{bias}}$ . The same exponential acceleration can be expected in the convergence of the free energy. The application of a biasing potential is not restricted to the regions of minima or transition states. In the most general case, the full potential energy surface, or an arbitrary part of it, can be biased. Furthermore, we note, that it is always possible to obtain the corrected results for the original system if one

changes the Hamiltonian ( $H$ ) and inverse temperature ( $\beta$ ) of a system to  $H'$  and  $\beta'$ . The thermodynamic average of a function  $f(p, q)$  can be manipulated as follows:

$$\begin{aligned}
 \langle f(p, q) \rangle_{\beta H} &= \lim_{\Delta t \rightarrow \infty} \frac{1}{\Delta t} \int_0^{\Delta t} f(p(t), q(t)) dt \quad \text{where } p(t), q(t) \text{ derive from } H \\
 &= \frac{\int \int f(p, q) e^{-\beta H(p, q)} dp dq}{\int \int e^{-\beta H(p, q)} dp dq} \\
 &= \frac{\int \int [f(p, q) e^{\beta' H' - \beta H}] e^{-\beta' H'} dp dq}{\int \int e^{-\beta' H'} dp dq} \frac{1}{\frac{\int \int [e^{\beta' H' - \beta H}] e^{-\beta' H'} dp dq}{\int \int e^{-\beta' H'} dp dq}} \\
 &= \langle f(p, q) e^{\beta' H' - \beta H} \rangle_{\beta' H'} \frac{1}{\langle e^{\beta' H' - \beta H} \rangle_{\beta' H'}}
 \end{aligned} \tag{4.1}$$

The last equality shows that the average of the function  $f$  of the system with Hamiltonian  $H$  ( $\langle f(p, q) \rangle_{\beta H}$ ) can be obtained as a function of the averages of two different functions,  $f(p, q) e^{\beta' H' - \beta H}$  and  $e^{\beta' H' - \beta H}$ , of a system based on the Hamiltonian  $H'$ . If  $H'$  is chosen in an appropriate way the new averages  $\langle f(p, q) e^{\beta' H' - \beta H} \rangle_{\beta' H'}$  and  $\langle e^{\beta' H' - \beta H} \rangle_{\beta' H'}$  converge faster than the original one. The technique will work efficiently as long as sufficiently many configurations sampled with the Hamiltonian  $H'$  are also significant for the system with Hamiltonian  $H$ , so that the reweighting factor  $e^{\beta' H' - \beta H}$  is non-vanishing during a considerable part of the trajectory.

### 4.3 Construction of the bias potential

A variety of applications in classical MD have demonstrated convincingly (see e.g. references [8], [14], and [19]) that the use of a bias potential can accelerate the convergence of the thermodynamic averages in an impressive manner. However, the efficiency of the approach depends on the appropriate choice of the bias potential. Here, we construct bias potentials that, although general in nature, are especially useful for applications in the context of ab initio MD.

The properties of an efficient bias potential will certainly be system dependent, however,

some general ideas apply:

- (i) An ideal bias potential should be sufficiently strong (at least larger than  $kT$ ) as to be effective. Optimally, the height of the bias potential should be of the order of  $E_a$ , the activation energy for escaping from a minimum configuration. However, if the bias potential is too strong and thus changes the potential energy surface too drastically, the sampled ensemble becomes irrelevant since there is no overlap with the unbiased ensemble anymore.
- (ii) The bias potential should also not introduce new barriers or increase existing barriers by more than  $kT$ . The latter can be avoided if not only the height, but also the shape adapts to the underlying potential, being more narrow for stiff degrees (such as bond vibrations), and more extended for flexible degrees of freedom (such as torsional motions).
- (iii) Optimally, the bias should be adapted to the free energy surface. This might be particularly important for systems with a very rugged energy landscape, with many small barriers, as e.g. for molecules in solution. In such a case, local information of the potential energy surface, such as the gradient, Hessian and higher order derivatives might no longer be a good base for the construction of a bias potential. In this case preliminary sampling [18] and an iterative construction [13] can be necessary.
- (iv) The sampling time required grows exponentially with the dimensionality of the bias potential. Therefore, only those degrees of freedom for which a homogeneous sampling is needed in order to construct the free energy surface should be biased strongly [28].
- (v) The calculation of the potential and the corresponding forces should be computationally inexpensive. We remark that 'inexpensive' should be compared to the possible exponential savings in sampling convergence. Still, for a quantum mechanically calculated surface it may be too expensive to calculate third derivatives at every time step as needed in some schemes [19].

In the present work, we propose to use selected terms of a classical force field, in order to construct efficient bias potentials for AIMD simulations. This simple approach satisfies all of the five criteria (i)-(v) mentioned above: Clearly, if the force field is sufficiently close to the ab initio results then the resulting potential ( $V' = V + V_{bias}$ ) will be nearly flat, and the trajectory can visit all points in space without having to cross potential energy barriers. Since only a few terms of a force field are needed, the parameterization effort can be kept to a minimum. Furthermore, for many systems, adequate classical force fields are already available and some of them have been constructed with a special emphasis on reproducing free energy differences [29]. The configurational space can be restricted by including only specific terms of a force field (such as e.g. torsional potentials). Finally, the bias potential presented here is inexpensive in both computational time, and implementation effort. All the ab initio MD simulations have been performed with the program CPMD [30] that has been modified to account for the classical bias.

#### 4.4 A simple example : Methylgroup rotation in ethane

An illustration of the severe time scale barrier inherent to current AIMD simulations, is provided by a calculation of the torsional free energy profile of ethane. For this system, the barrier for rotation, that is the energy difference between the eclipsed and the staggered conformation, is  $\approx 2.6$  kcal/mol [31]. At a temperature of 500K, the system is often considered to rotate almost freely. However, the free energy profile calculated from our AIMD simulation of about 30 ps (Figure 4.1) fails to represent the symmetry equivalence of the three rotational minima. In order to improve sampling a bias potential was constructed. The easiest approach, and the one adopted here, is to take an estimate for the rotational barrier, and construct explicitly a torsional potential of the form  $\frac{1}{2}V_0(1 - \cos(3\phi))$  [28, 32]. This bias potential, the original potential and the resulting total potential are shown in Figure 4.2. For this biased system we performed a simulation of 30 ps. The distribution of the torsional angles sampled during the simulation is shown in Figure 4.3, together with

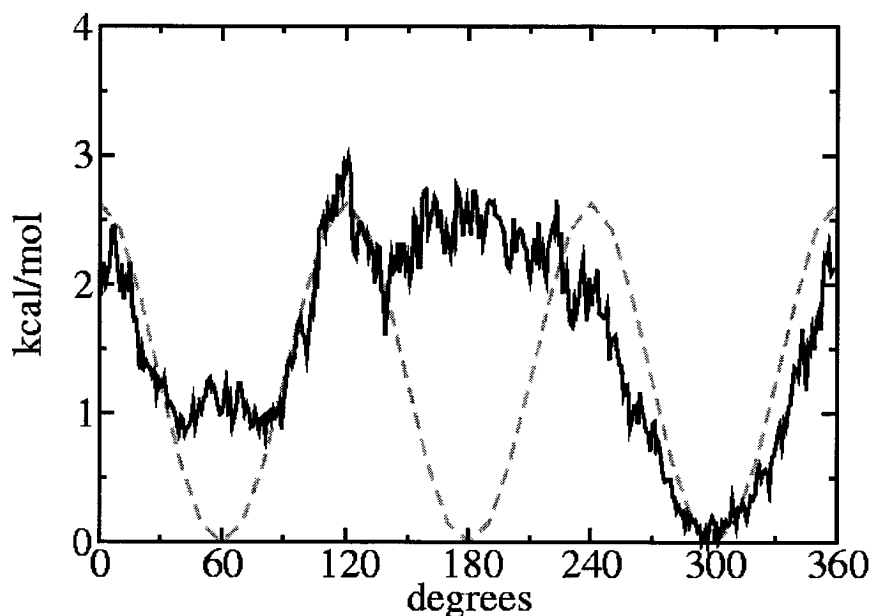


Figure 4.1: Free energy profile for methyl group rotation in ethane, as obtained from an unbiased AIMD run at 500K (full line). The dashed curve is the potential energy calculated on a grid of  $10^\circ$  and is given for comparison.

the corrected distribution as obtained using Eq. 4.1. Clearly, the three equivalent minima are now sampled almost equally. Additionally, the sampling is sufficiently homogeneous, so that also the region near the barrier is well sampled. The free energy  $F$  is obtained from  $F(x) = -kT \ln(P(x))$ , where  $P$  is the sampled probability distribution. This free energy profile is shown in Figure 4.4 together with the potential energy profile. By inspecting the deviation from three-fold symmetry we can estimate that the sampling accuracy is better than 0.5 kcal/mol over the whole profile. Extending the simulation length to 100 ps reduces the error to less than 0.3 kcal/mol. Thus, the statistical error is certainly smaller than the error due to the approximations currently made to the exchange and correlation functional in DFT, and the neglect of the quantum nature of the hydrogens. For many systems it would be already very gratifying to have an accuracy in the free energy of the

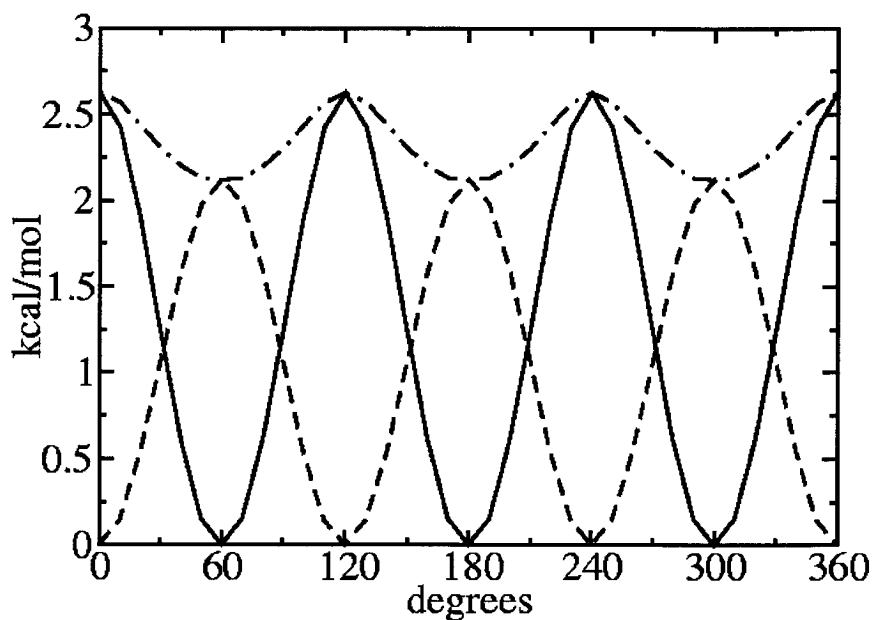


Figure 4.2: Potential energy (full line), bias potential (dashed line) and resulting potential (dashed-dotted line) for methyl group rotation in ethane.

order of  $< \approx 1$  kcal/mol.

## 4.5 The two dimensional free energy surface of peroxynitrous acid

Our second test case, peroxynitrous acid (ONOOH), is more challenging. Several different conformers, characterized by the two torsional angles ONOO ( $\phi_1$ ) and NOOH ( $\phi_2$ ), exist for this molecule [33]. A contour plot of the potential energy surface obtained at the gradient corrected DFT level using the BLYP [34] functional is shown in Figure 4.5. The locations of the minima and transition states (indicated with labels) is in good agreement with high level ab initio calculations at the QCISD(T) level [35]. Note that the surface has



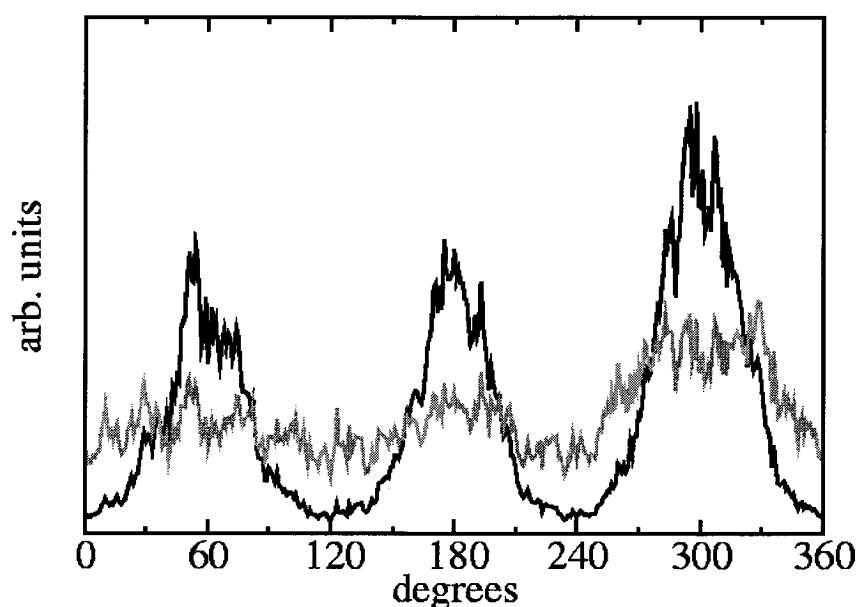


Figure 4.3: Probability density (grey) and corrected probability density (black) distribution for the torsional angle from the biased run.

an inversion center at  $(180^\circ, 180^\circ)$  due to the symmetry of the molecule. The three minima (M) and six transition states (TS) that are not symmetry equivalent, can be described by values of the angles near  $0^\circ$  (cis),  $180^\circ$  (trans),  $90^\circ$  (perp) and  $270^\circ$  (-perp). The global minimum, the cis-cis form (M1), is stabilized by an intramolecular hydrogen bond. The relative energies for the other minima are cis-perp (M2) 0.8 kcal/mol and trans-perp (M3) 3.0 kcal/mol [33]. The two barriers for cis-trans isomerization near  $\phi_1 = 90^\circ$  and  $270^\circ$  (TS2 and TS1) are high ( $\approx 15$  kcal/mol) since rotation around the central oxygen-nitrogen bond involves a partial break of the conjugated system. The barriers for rotation around  $\phi_2$  (TS3 and TS4 for the cis, and TS5 and TS6 for the trans isomer) on the other hand are much smaller ( $\approx 2.0$  kcal/mol). Given the rather complex nature of the surface, an identification of a simple reaction coordinate for the interconversion reactions between the different forms, as required for example in a thermodynamic integration approach to the

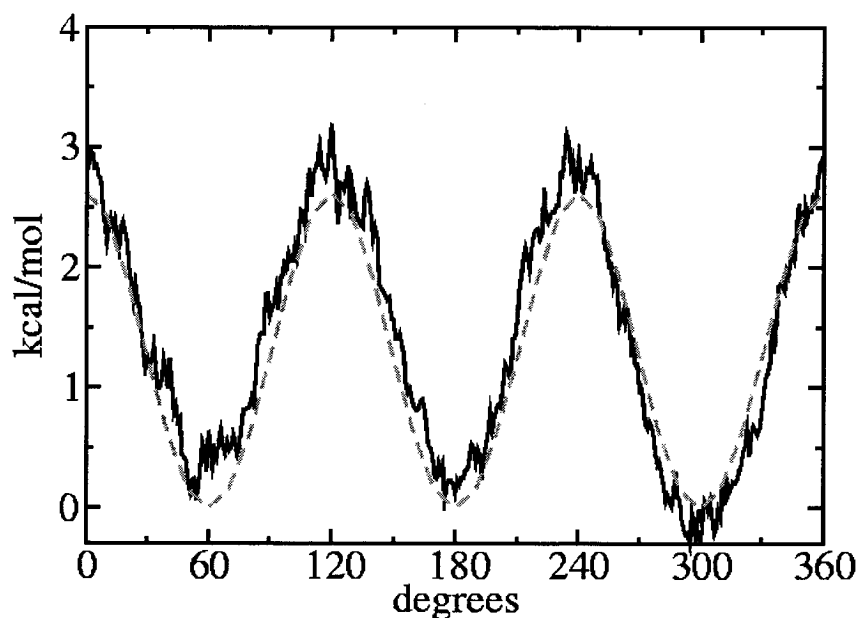


Figure 4.4: Free energy profile from the biased run (full line) in comparison with the potential energy (dashed line).

free energy, can be non-trivial. Through the calculation of the full multidimensional free energy surface such a problem can be avoided.

#### 4.5.1 Computational details

For the electronic structure calculation we used the same computational scheme as described previously [33]. The results obtained by this setup compare favorably with MP2 and QCISD(T) [35] calculations and are converged with respect to box and basis set size for the energy differences considered. MD runs were done with a time step of 5.0 a.u. and all masses were rescaled to 3.0 a.u. The system was equilibrated and afterwards let to evolve for 43 ps. The temperature of the system was controlled with the Nosé-Hoover chain thermostatting method [36, 37] at  $T=500\text{K}$ , using a chain of four thermostats with

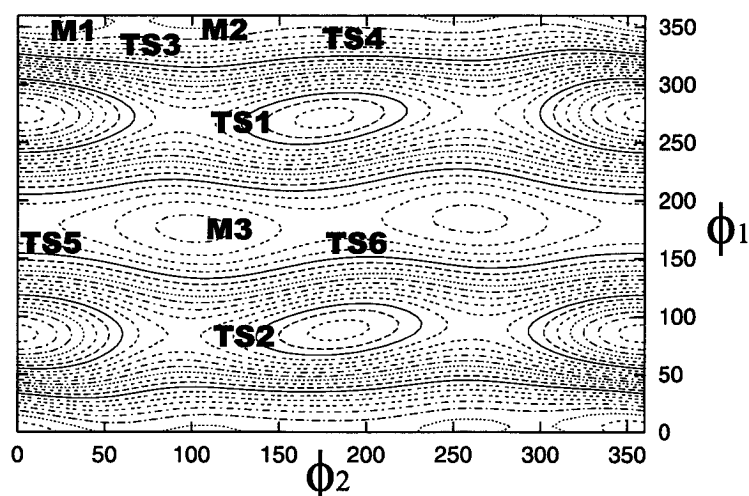


Figure 4.5: Contour plot of the potential energy surface of ONOOH as a function of the two torsional angles  $\phi_1$  and  $\phi_2$ . A definition of the labels is given in the text.

a frequency of  $500 \text{ cm}^{-1}$  for every degree of freedom. The underlying classical model for the bias potential was constructed using a 2D Fourier expansion, up to terms of  $4\phi$ , of the quantum mechanically calculated potential energy surface. The latter was obtained by optimizing the geometry at fixed torsional angles  $\phi_1$  and  $\phi_2$  on a grid with a spacing of  $15^\circ$ . The classical model reproduced the calculated potential within a maximum deviation of  $0.8 \text{ kcal/mol}$ .

#### 4.5.2 Calculation of the free energy surface from the simulation data

The fundamental quantity for the calculation of the free energy is the probability  $P(\phi_1, \phi_2)$  of finding the system in a given state. In principle the probability can be calculated as

$$P(\phi_1, \phi_2) = \lim_{\Delta t \rightarrow \infty} \frac{1}{\Delta t} \int_0^{\Delta t} \delta(\phi_1(t) - \phi_1) \delta(\phi_2(t) - \phi_2) dt, \quad (4.2)$$

however, in practice the probability has to be evaluated in a more coarse-grained way. We replace the delta functions  $\delta(x' - x)$  in Eq. 4.2 by Gaussians of the form  $\frac{1}{\sqrt{2\pi}\sigma} \exp(-\frac{1}{2}(\frac{x-x'}{\sigma})^2)$ .

In this way we have defined the smoothed probability  $P_\sigma(x)$ . The advantage is that for a larger  $\sigma$  the smooth  $P_\sigma(x)$  can be evaluated with higher statistical accuracy. However the systematic error  $P_\sigma(x) - P(x)$  grows for increasing  $\sigma$ . It is straightforward to show that for a harmonic potential  $V = \frac{1}{2}\alpha x^2$  the systematic error is negligible if we choose  $\sigma$  so that  $\frac{1}{2}\alpha\sigma^2 \ll kT$ . In this case, it can be shown that the error for the free energy estimate is also  $\sim \frac{1}{2}\alpha\sigma^2$ .

For certain choices of  $V_{bias}$  it is possible to calculate the free energy directly from  $P^{biased}(x)$ , that is the probability density on the biased potential energy surface, which allows for better statistics. It is straightforward to show that this is the case if the bias potential is only a function of those coordinates that have been chosen to span the free energy surface  $F$ , in our system  $\phi_1$  and  $\phi_2$ . The free energy can then be calculated as  $F(x) = -kT \ln(P^{biased}(x)) - V_{bias}(x)$ . The term  $-kT \ln(P^{biased}(x))$  gives the entropic part of the free energy if the bias potential is designed to be the exact negative of the potential energy of the molecule when all other degrees of freedom have been optimized. The fact that the sampling is only needed to determine the more slowly varying, entropic quantity,  $P^{biased}(x)$  can be exploited, in view of the previous analysis on smoothing, by using a much larger  $\sigma$  than would be possible when sampling directly  $P(x)$ . This guarantees faster convergence.

### 4.5.3 Results

The negative value of the model potential shown in Figure 4.5 has been used as a bias potential for our AIMD simulation. The trajectory on the biased potential energy surface is represented in torsional space in Figure 4.6. The trajectory visits the surface everywhere in a rather homogeneous way, an indication that there are no strong entropic effects, as otherwise a more inhomogeneous sampling would be expected. In order to obtain an estimate of the free energy surface we have to find the optimal smoothing parameter  $\sigma$ , and thus have to estimate the statistical uncertainty and systematic error introduced. Estimates for the error for different values of  $\sigma$  are given in Table 4.1. The systematic error (SE)

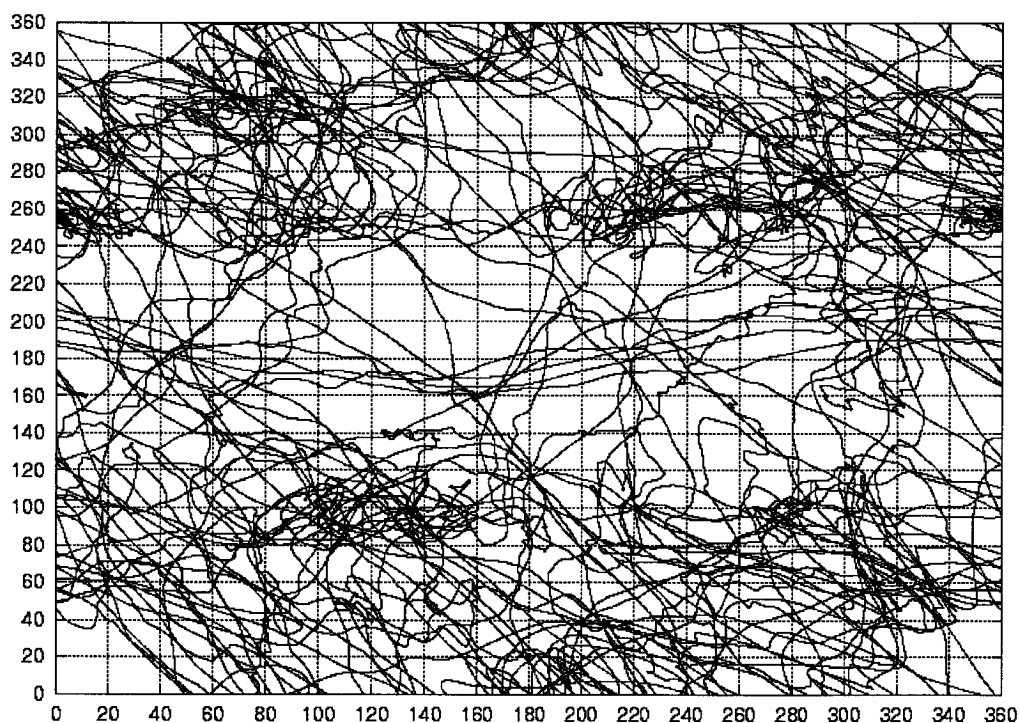


Figure 4.6: A 43 ps trajectory in torsional space.

has been estimated using  $SE \approx \frac{1}{2}\alpha\sigma^2$ , where  $\alpha$  has been estimated from the maximum curvature of  $-kT\ln(P_{10}^{biased}(x))$ , whereas the statistical error has been determined using the symmetry properties of the surface. Based on this analysis, an optimal value of  $\sigma = 20^\circ$  has been determined. For this value the estimated maximum error in the total free energy surface is  $< \approx 1$  kcal/mol, with an average deviation of only 0.4 kcal/mol. The entropic part ( $-kT\ln(P_{20}^{biased}(x))$ ) of the free energy is shown in Figure 4.7. We note that part of the fine structure is of the order of our error estimate. One can see that the compact cis-cis (with the intramolecular hydrogen bond) and the totally extended trans-trans state are entropically destabilized. On the other hand, intermediate conformations, especially near the transition states, are stabilized with respect to the potential energy. Based on the two dimensional free energy surface, one dimensional profiles can be constructed by integrating out the other variable. The profiles for cis-trans isomerisation and for hydrogen rotation, together with an estimate of the statistical error of at most 0.3 kcal/mol, are

$\sigma$	ST	SE
10	1.6	0.1
20	0.9	0.4
30	0.6	0.8

Table 4.1: Estimated statistical (ST) and systematic errors (SE) in the free energy surface (kcal/mol) for different smoothing factors sigma (degrees).

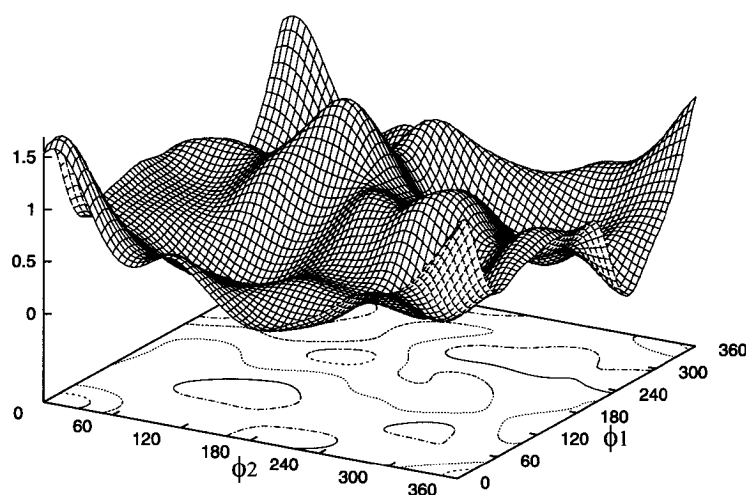


Figure 4.7: The surface represents the entropic part of the free energy ( $-kT \ln(P_{20}^{biased}(x))$ ). Energies are in kcal/mol, the contour lines are 0.5 kcal/mol apart. The profile has been shifted so that the minimum has zero energy.

shown in Figure 4.8. The free energy barrier for cis-trans isomerisation is lowered by only  $\approx 0.8$  kcal/mol, although the minimum energy configuration (cis-cis) is entropically rather strongly destabilized. This can be explained if we note that the cis state as a whole is not destabilized so much since the cis-perp state is entropically stabilized. Indeed, the free energy profile for hydrogen rotation shows that the most abundant form at 500K is likely to be the perp conformer in contrast to the 0K results.

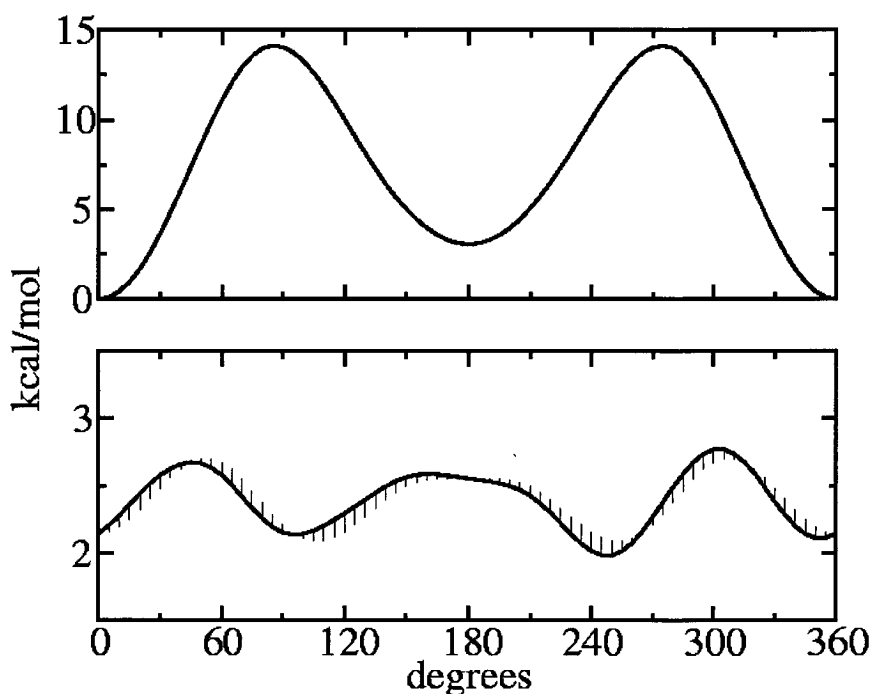


Figure 4.8: Upper panel : Free energy profile for cis-trans isomerisation. Lower panel : Free energy profile for hydrogen rotation. The vertical lines indicate the deviation from symmetry around  $180^\circ$  and are an indication of the statistical accuracy. For the upper curve they are smaller than the line thickness, and not visible.

## 4.6 Conclusions

In this paper we tested the feasibility of ab initio free energy calculations. We propose to use a bias potential to enhance sampling since in this way, the most severe bottleneck, the long equilibration time between different minima, can be overcome. This approach has the advantage that the accuracy is not limited by using a method that could introduce systematic errors such as classical MD simulations based on empirical force fields or free energy estimates based on the assumption of a quasi-harmonic potential. A simple, cost-effective, and efficient method for the construction of a bias potential, based on selected terms of classical force fields, has been proposed. We demonstrate that, for the small

systems tested here, it is possible to evaluate the full free energy surfaces with a precision of  $< \approx 1$  kcal/mol within the timescale accessible to ab initio MD. The ab initio calculation of multidimensional free energy surfaces for larger systems will still be on the limit of what is currently feasible. However, the method presented here can always be used to explore phase space more efficiently. Work is now in progress on an application of the same method for systems in aqueous solution.

## Bibliography

- [1] R. Car, and M. Parrinello, *Phys. Rev. Lett.* **55**, 2471 (1985).
- [2] see e.g. C. Cavazzoni, G. L. Chiarotti, S. Scandolo, E. Tosatti, M. Bernasconi, and M. Parrinello, *Science* **283**, 44 (1999); P. Ballone, and W. Andreoni, *Metal Clusters*, (1999), p.71; M. Benoit, D. Marx, and M. Parrinello, *Nature* **392**, 258 (1998); A. Pasquarello, M. S. Hybertsen, and R. Car, *Nature* **396**, 58 (1998); U. Rothlisberger, W. Andreoni, and M. Parrinello, *Phys. Rev. Lett.* **72**, 665 (1994)
- [3] see e.g. M. Sprik, *J. Phys. Cond. Mat.*, **12**, A161 (2000) (and references therein); M. Boero, M. Parrinello, S. Huffer, H. Weiss, *J. Am. Chem. Soc.* **122**, 501 (2000); D. Marx, M. E. Tuckerman, J. Hutter, and M. Parrinello, *Nature* **397**, 601 (1999); U. Rothlisberger, M. Sprik, and M. L. Klein, *J. Chem. Soc. Faraday Trans.* **94**, 501 (1998); A. Curioni, M. Sprik, W. Andreoni, H. Schiffer, J. Hutter and M. Parrinello, *J. Am. Chem. Soc.* **119**, 7218 (1997)
- [4] P. Carloni and U. Röthlisberger in 'Theoretical Biochemistry - Processes and Properties of Biological Systems', L. Eriksson (ed.), Elsevier Science (in press) (and references therein)
- [5] P. Hohenberg, and W. Kohn, *Phys. Rev B* **136**, 864 (1964).
- [6] W. Kohn, and L. J. Sham, *Phys. Rev. A* **140**, 1133 (1965).



- [7] D. McQuarrie, *Statistical Mechanics* (Harper and Row, New York, 1976).
- [8] G. M. Torrie, and J. P. Valleau, *J. Chem. Phys.* **66**, 1402 (1977).
- [9] E. A. Carter, G. Ciccotti, J. T. Hynes, and R. Kapral, *Chem. Phys. Lett.* **156**, 472 (1989).
- [10] M. Sprik, and G. Ciccotti, *J. Chem. Phys.* **109**, 7737 (1998).
- [11] K. Kuczera, *J. Comp. Chem.* **17**, 1726 (1996).
- [12] Y. Wang, and K. Kuczera, *Theor. Chem. Acc.* **101**, 274 (1999).
- [13] C. Bartels, and M. Karplus, *J. Comp. Chem.* **18**, 1450 (1997).
- [14] J. Apostolakis, Philippe Ferrara, and A. Caffisch, *J. Chem. Phys.* **110**, 2099 (1999).
- [15] C. Bartels, M. Schaefer, and M. Karplus, *J. Chem. Phys.* **111**, 8048 (1999).
- [16] S. Crouzy, J. Baudry, J. C. Smith, and B. Roux, *J. Comp. Chem.* **20**, 1644 (1999).
- [17] T. Huber, A. E. Torda, and W. F. van Gunsteren, *J. Comput.-Aided Mol. Design* **8**, 695 (1994).
- [18] H. Grubmüller, *Phys. Rev. E* **52**, 2893 (1995).
- [19] A. F. Voter, *J. Chem. Phys.* **106**, 4665 (1997).
- [20] A. F. Voter, *Phys. Rev. Lett.* **78**, 3908 (1997).
- [21] M. M. Steiner, P.-A. Genilloud, and J. W. Wilkins, *Phys. Rev. B* **57**, 10236 (1998).
- [22] X. G. Gong, and J. W. Wilkins, *Phys. Rev. B* **59**, 54 (1999).
- [23] A. Amadei, A. B. M. Linssen, and H. J. C. Berendsen, *Proteins: Structure, Function, and Genetics* **17**, 412 (1993).
- [24] B. Space, H. Rabitz, and A. Askar, *J. Chem. Phys.* **99**, 9070 (1993).

- [25] N. Nakajima, H. Nakamura, and A. Kidera, *J. Phys. Chem. B* **101**, 817 (1997).
- [26] C. Dellago, P. G. Bolhuis, F. S. Csajka, and D. Chandler, *J. Chem. Phys.* **108**, 1964 (1998).
- [27] M. Marchi, and P. Ballone, *J. Chem. Phys.* **110**, 3697 (1999).
- [28] We suggest, however, that it might be helpful to include also terms that do not only depend on the principal degrees of freedom that span the free energy surface. The orthogonal degrees of freedom can be biased in order to enhance their mobility, but only slightly since they should remain close to the potential energy minima. This brings additional freedom, and is at variance with previously developed classical multidimensional free energy schemes [13–16].
- [29] W. L. Jorgenson, J. Tirado-Rives, *J. Am. Chem. Soc.* **110**, 1657 (1988)
- [30] J. Hutter, P. Ballone, M. Bernasconi, P. Focher, E. Fois, M. Goedecker, M. Parrinello, and M. Tuckerman, Max-Planck-Institut für Festkörperforschung and IBM Zurich Research Laboratory **1995-96**.
- [31] Computational results in this Section are from density functional calculations with the LDA functional, a basis set of plane waves with a kinetic energy cutoff of 60 Ry, norm-conserving non local pseudo potentials and a face centered cubic super cell of edge  $a = 10 \text{ \AA}$ . The estimated barrier compares favorably with experiment (2.75 kcal/mol) [38].
- [32] It is also possible to construct a bias potential that does not depend explicitly on the torsional angle, for example, by describing the barrier for rotation in terms of van der Waals interactions between the methyl hydrogens.
- [33] K. Doclo, and U. Rothlisberger, *Chem. Phys. Lett.* **297**, 205 (1998).
- [34] A. D. Becke, *Phys. Rev. A*, **38**, 3098 (1998)

- 
- [35] M. P. McGrath, and F. S. Rowland, *J. Phys. Chem.* **98**, 1061 (1994).
- [36] S. Nosé, *J. Chem. Phys.* **81**, 511 (1984).
- [37] G. J. Martyna, M. L. Klein, and M. Tuckerman, *J. Chem. Phys.* **97**, 2635 (1992).
- [38] G. Herzberg, *Molecular spectra and molecular structure* (Krieger publishing company, Malabar, Florida, 1991).



## Chapter 5

# Accelerating rare reactive events by means of a finite electronic temperature

## Abstract

The range of chemical problems that are directly accessible to first-principles molecular dynamics simulations based on density functional theory is extended with a novel method apt to accelerate rare reactive events. The introduction of a finite electronic temperature within the Mermin formalism leads to a lowering of chemical activation barriers and thus to an exponential enhancement of the rate at which these reactions are observed during a first-principles molecular dynamics simulation. The method presented here makes direct use of the intrinsic chemical information encoded in the electronic structure, and is therefore able to lower selectively chemically relevant activation energies even in systems where many competing low-energy pathways for conformational transitions or diffusive motions are present. The performance of this new approach is demonstrated for a series of prototypical chemical reactions in gas and in condensed phase. These tests show that the activation barriers can be lowered substantially while the locations of the stationary points remain essentially unchanged with respect to the zero Kelvin potential energy surface. A typical acceleration that can be achieved is e.g. a factor of  $10^5$  for the *cis-trans* isomerization of peroxyntrous acid in aqueous solution. The electronic temperature is the only tunable parameter of this electronic bias potential, and the thermodynamic properties of the original ground state system can be recalculated on-the-fly from the trajectory of an accelerated molecular dynamics simulation.

## 5.1 Introduction

Electronic structure calculations have become an important tool for a detailed understanding of chemical reaction mechanisms. A particular versatile approach in this respect is the recently developed first-principles molecular dynamics (Car-Parrinello) method. [1,2] This technique allows for the evaluation of finite temperature properties and thus for the *in situ* study of chemical reactions in gas phase and in solution [3] within the framework of density functional theory (DFT) [4,5] or other quantum chemical electronic structure methods. [6] First-principles molecular dynamics simulations are especially valuable for complex systems in which a reaction coordinate is not known *a priori* and may involve a nontrivial combination of multiple degrees of freedom. A few snapshots of the dynamics of such a system can often guide chemical intuition into previously unexpected directions. Indeed, for systems with relatively low activation barriers, chemical reactions can occur spontaneously during a molecular dynamics (MD) run, and hence reveal direct atomistic information about the reactive process. Unfortunately, the observation of spontaneous reactions is currently only possible for fast processes with low activation barriers, since only relatively short time periods, typically 10-100 ps, can be simulated. Simulation times that are many orders of magnitude longer would be needed in order to observe chemical reactions with activation barriers of the order of 10 - 30 kcal/mol, with rates in the millisecond to hours range.

At present, slow reactions in complicated systems can only be studied efficiently if some information about a possible reaction pathway is known so that it is possible to constrain the system along an *a priori* chosen coordinate in order to guide it over the activation barrier. [7,8] Since this information is not always available, and an inappropriately chosen coordinate can even be misleading, it is of primary importance to develop methods that are able to explore possible reaction pathways and potentially reactive configurations in an efficient and unprejudiced way. It is the aim of this paper to describe a novel method that is capable to enhance specifically the sampling of rare reactive events in chemical systems.

One efficient way to increase the number of rare events during a simulation is biased sampling [9–16]. In this approach, an additional (bias) potential is added to the total Hamiltonian that guides the system through the region of interest, or helps it to explore previously unvisited regions of phase space and to overcome barriers between them. An enhanced sampling of barrier crossing events can in principle be achieved in a straightforward manner by choosing the bias potential in such a way that it lowers the height of the barriers, or equivalently, increases the energy of the respective minima configurations. Since the rates for barrier crossing depend exponentially on the barrier height, the use of bias potentials leads to dramatically improved statistics. As a result, the required computer time for a statistically meaningful sampling of the system, and accordingly, for a comprehensive understanding of its chemical reactivity, is orders of magnitude lower than in the original unbiased ensemble.

All thermodynamic averages, including free energies and rate constants within transition state theory, can be obtained exactly, since the following equation relates the thermodynamic average of a function  $f$  in the biased with the one in the unbiased system [17]:

$$\langle f(p, q) \rangle_{\beta H} = \langle f(p, q) e^{\beta' H' - \beta H} \rangle_{\beta' H'} \frac{1}{\langle e^{\beta' H' - \beta H} \rangle_{\beta' H'}} \quad (5.1)$$

where  $\beta$  and  $H$  refer to the original ensemble and  $\beta'$  and  $H'$  to the biased system. The performance of such a method depends crucially on the choice of an adequate biasing potential. Several approaches have been suggested to this purpose [9–16] but their efficiency depends strongly on the type of system under study. Most of the existing methods use properties of the potential energy surface, such as the Hessian and its derivatives, for the construction of an appropriate bias potential, and occasionally impressive gains in computational efficiency of up to ten orders of magnitude can be achieved. [13] However, for many reactive systems, the information that is locally contained in the potential energy surface near a minimum configuration is not representative for the properties of the reactive transition state and thus not sufficient for the design of a successful bias potential. The low frequency modes of the Hessian near the minimum often do not yield specific information about the possible chemical reactions of the system since these events can



involve the breaking of bonds that are initially much stiffer than the typical soft modes such as e.g. torsional modes. In realistic chemical systems many low barriers exist related to solvent motion or to the overall rotation of ligands, that only lead to new conformers. The barrier for the actual reactive process lies at much higher energy, and is therefore hard to locate. Nevertheless, if the reaction proceeds via a relatively simple, well-defined geometric pathway, it is occasionally possible to carefully design a bias potential that is optimally adapted to a particular reactive situation [9, 16]. However, this is not always possible, since a reaction pathway may be complex, and involve many degrees of freedom that are not known beforehand, or that are difficult to express in a simple geometrical way. In general, methods that are only based on the local information of the potential energy surface cannot discriminate between events of high or low chemical priority. Therefore, their efficiency for the acceleration of rare reactive events is often greatly reduced and it would be advantageous to design enhanced sampling methods that are directly based on chemical properties of the system.

A lot of information about the intrinsic chemical reactivity of a system is directly encoded in its electronic structure. This simple fact has been used by chemists for decades and lies at the roots of the overwhelming success of frontier orbital theory. [18] Within DFT, this intimate link between electronic structure and chemical properties can be formalized in the concepts of reactivity indices such as chemical hardness and softness and Fukui functions. [19, 20] For example, within a frozen orbital picture, the highest occupied orbital(s) (HOMO(s)) determine the electron-donor properties of a reactive system, whereas the lowest occupied orbital(s) (LUMO(s)) are relevant for its electron-acceptor behavior and a linear combination of HOMOs and LUMOs is relevant in the context of radical reactions. [19, 20]

This suggests that a method that uses the electronic structure to construct a bias potential could be especially efficient in exploring chemically relevant regions of phase space without having to resort to *a priori* assumptions about likely reaction pathways based on atomic

coordinates. In a similar spirit, the empirical valence bond (EVB) method introduced by Warshel uses reaction coordinates that depend on the diagonal matrix elements of the (EVB) Hamiltonian, and hence, in an empirical way, on the electronic structure. [21] However, the EVB method limits the reactive rearrangement to variations between few preselected electronic configurations. The relevant electronic states have to be chosen and parameterized manually and there is no guarantee that an important configuration does not remain unconsidered. A first-principles approach in which the system reacts in an unbiased way and chooses itself the relevant configurations would clearly be preferable.

The simple electronic bias potential we present here in the context of first-principles molecular dynamics simulations exploits the electronic structure in a straightforward way by simulating the system at an increased electronic temperature. Through the introduction of a finite electronic temperature, electron density is transferred from the highest lying donor orbitals of the entire reactive system to its lowest lying acceptor orbitals, i.e. its lowest-energy virtual states, thus enhancing its intrinsic reactivity. This particular choice of electronic bias potential can be further rationalized using concepts from chemical reactivity theory, such as the maximum hardness principle [22–26] which states that the ground state of any system has a maximal hardness. [27] This implies, that through the admixture of virtual excited states the system becomes softer, i.e. more reactive towards soft, orbital-driven reactions. This enhanced reactivity is exploited by the finite temperature bias potential we present here, which drives the system towards soft reactions. Typical hard reactions on the other hand are electrostatically driven and can often be accelerated in more obvious ways. In the next Section, we will first discuss the effect of a finite electronic temperature for a two state (HOMO-LUMO) system and proceed with the study of a series of more realistic chemical reactions. In order to examine the efficiency of this finite temperature assisted acceleration (FTAA) approach in a quantitative manner, energy profiles along simple reaction coordinates have been calculated for a set of prototypical chemical reactions in gas and condensed phase and the barrier heights at finite electronic temperature have been compared with the 0 K results.

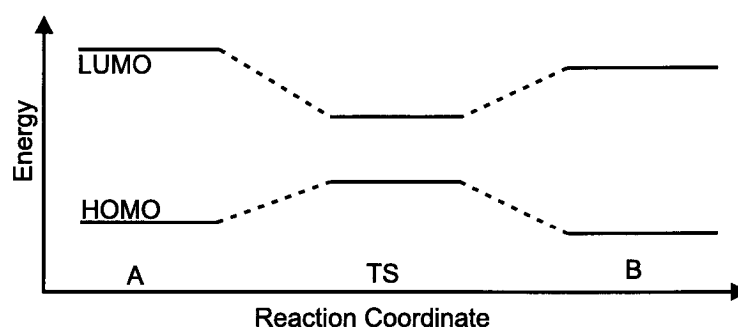


Figure 5.1: Schematic energy level diagram of a class of chemical reactions in which the smallest gap occurs near the transition state.

## 5.2 Finite electronic temperature as a chemical driving force

As a first example, we discuss the case of a simple two-level system where the chemically active orbitals are HOMO and LUMO, for example the bonding and antibonding molecular orbitals of  $H_2$ . The only possible reaction channels that are open to this system are homolytic or heterolytic breakage of the H-H bond, the former being the energetically favoured reaction path in gas phase. With increasing H-H distance, HOMO and LUMO become increasingly closer in energy until they reach complete degeneracy in the two equivalent free hydrogen radicals. A similar lowering of the HOMO-LUMO gap at the transition state can be observed more generally also for other reactions [28] leading to a characteristic energy level diagram of the type shown in Fig. 5.1. This effect can be rationalized by the qualitative argument that during a chemical reaction electron density is transferred from donor to acceptor states of the system, i.e. as discussed above, within a frozen orbital picture, from the HOMO to the LUMO. This electronic redistribution induces a destabilization of the former and a stabilization of the latter and thus a lowering of the gap. Additionally, using a finite difference and frozen orbital approximation, the hardness  $\eta$  of a system can be approximated as  $2\eta \approx \epsilon_{LUMO} - \epsilon_{HOMO}$  [23], if the system

is softer near the activation barrier, then the gap near the transition state will be smaller than the one at the equilibrium structure. By constructing a bias potential that lowers the energy of the system whenever the HOMO-LUMO gap is reduced, one can sample these regions of phase space more efficiently. A straightforward way of obtaining such a bias potential is a simulation with a finite electronic temperature.

DFT was generalized to finite electronic temperatures by Mermin [29] using a free energy functional. A simple form is given by [30]

$$F[\{R_i\}, T] = \min_{\{\psi_i\}, \{f_{ij}\}} \sum_{ij} \int f_{ji} \psi_i^* (\hat{T} + \hat{V}_{ext}) \psi_j dr + E_{Hxc}[n, T] - TS[\{f_{ij}\}]. \quad (5.2)$$

Here  $\psi$  are the orthonormal Kohn-Sham wave functions,  $n$  is the electron density,  $T$  is the electronic temperature,  $f$  is the occupation matrix,  $\hat{T}$  is the kinetic energy operator,  $\hat{V}_{ext}$  is the external potential,  $E_{Hxc}$  is the Hartree and the exchange and correlation functional, and  $S$  is the entropy term given by  $-\text{tr}(f \ln(f) + (1 - f) \ln(1 - f))$ . The solution of Eq. 5.2 implies an iterative, self-consistent computation of the wave functions and occupation numbers. The latter are calculated using the Fermi-Dirac distribution i.e.  $f_i = 1/(e^{\beta(\epsilon_i - \mu)} + 1)$ , where  $\epsilon_i$  is the eigenvalue of the wave function  $\psi_i$  and  $\mu$  is the chemical potential, which is determined by the number of electrons in the system. The free energy can be used as a potential energy surface for the dynamics of the ions, and recent advances in computational methodology made it possible to use the free energy functional for MD. [30–32] We remark that due to the entropy part of the free energy functional, the free energy of a system at a finite temperature is always lower than its (free) energy at zero temperature. However, only if the occupation numbers are significantly different from zero and one, the entropy term is non-zero. Hence, for a fixed electronic temperature the free energy will be more strongly lowered for a system with a small gap than for systems with a large gap. We can thus consider the difference between the finite temperature (FT) potential ( $V_{FT}$ ) and the zero temperature (ZT) potential ( $V_{ZT}$ ) to be a bias potential ( $V_{bias} = V_{FT} - V_{ZT}$ ) that enhances, often by many orders of magnitude, the exploration of regions with small electronic gaps. Thermodynamic averages, such as free energy differences and

rate constants in the transition state theory approximation, can be computed during a molecular dynamics run performed on the FT potential, using Eq. 5.1, where  $\beta'H' - \beta H$  is replaced by  $\beta V_{bias}$ . This requires an additional electronic structure calculation to compute the ZT energy, which can normally be done with small additional cost since the FT wave functions are a very good initial guess for the self-consistent minimization at ZT. Note that the electronic temperature can be chosen independently of the ionic temperature. In our systems, the temperature of the electrons will typically be a few thousand degrees, whereas the ions are at room temperature.

Within a frozen orbital approximation and at low temperatures (i.e. only the HOMO and LUMO are fractionally occupied), the force due to the bias potential is given by :

$$\frac{\partial V_{bias}}{\partial R} \propto \int dr \sum_{HOMO, LUMO} \frac{\partial}{\partial R} \frac{\delta f_i \psi_i^* \psi_i}{|r - R|} \quad (5.3)$$

This force is largest on the atoms where the HOMO and LUMO have a non-negligible magnitude. From a sampling point of view this is a clear advantage since only the chemically reactive part, and not the remainder of the system, is affected. We note that the driving force is an approximation to the sum of the nuclear Fukui functions ( $\Phi = (\frac{\partial F}{\partial N})_v$ , where  $F$  is the force on the nuclei) of the system. It can indeed be shown that within a frozen orbital approximation, their sum is proportional to the right hand side of equation 5.3. [33]

As for all bias potential techniques a good choice of the biasing parameters is essential. It is an advantage of FTAA that the extent in which the bias potential lowers the barrier is related to a single bias parameter, namely the electronic temperature. More importantly, a good estimate about the optimal value of this temperature can be made based on the gap of the stable system. In order to be effective, the temperature should be such that near the transition state the HOMO and LUMO are fractionally occupied. Since the gap near the transition state is generally not known, it is useful to establish an upper limit for the temperature, that will still guarantee an efficient sampling. Although the barriers are lowered with increasing temperature, a temperature that is too high will yield a too distorted potential energy surface, and configurations that are not relevant for the

ground state ensemble. As demonstrated in the next Section, we found that setting the temperature such that  $f_{LUMO} \approx 0.05$  at the equilibrium configuration gave a significant lowering of the barriers, leaving the overall positions of the minima unchanged. The given value is an empirical estimate and depends on the system under investigation, but is a useful initial guess for tuning the electronic bias.

### 5.3 Results for reactions in gas and in liquid phase

In order to probe the efficiency of a finite electronic temperature in lowering chemical activation barriers, we have applied this approach to a series of prototypical reactions in gas and condensed phase:

- (5.3.1) Homolytic bond dissociation of  $H_2$  (shown schematically in Figure 5.2a)
- (5.3.2) *Cis-trans* isomerization of ethene (shown schematically in Figure 5.2b)
- (5.3.3) Lewis acid-base reaction of sulfur dioxide and ammonia (shown schematically in Figure 5.2c)
- (5.3.4) Intramolecular proton transfer between the two tautomeric forms 2-hydroxypyridine and 2-pyridone (shown schematically in Figure 5.2d)
- (5.3.5) Conrotatory ring opening of cyclobutene to butadiene (shown schematically in Figure 5.2e)
- (5.3.6) Different reaction channels of peroxy nitrous acid :
  - (5.3.6) Dissociation of the peroxy bond (shown schematically in Figure 5.2f)
  - (5.3.6) Dissociation of the N-O single bond (shown schematically in Figure 5.2g)
  - (5.3.6-5.3.6) *Cis-trans* isomerization around the central N-O bond (in gas phase and in aqueous solution) (shown schematically in Figure 5.2h)

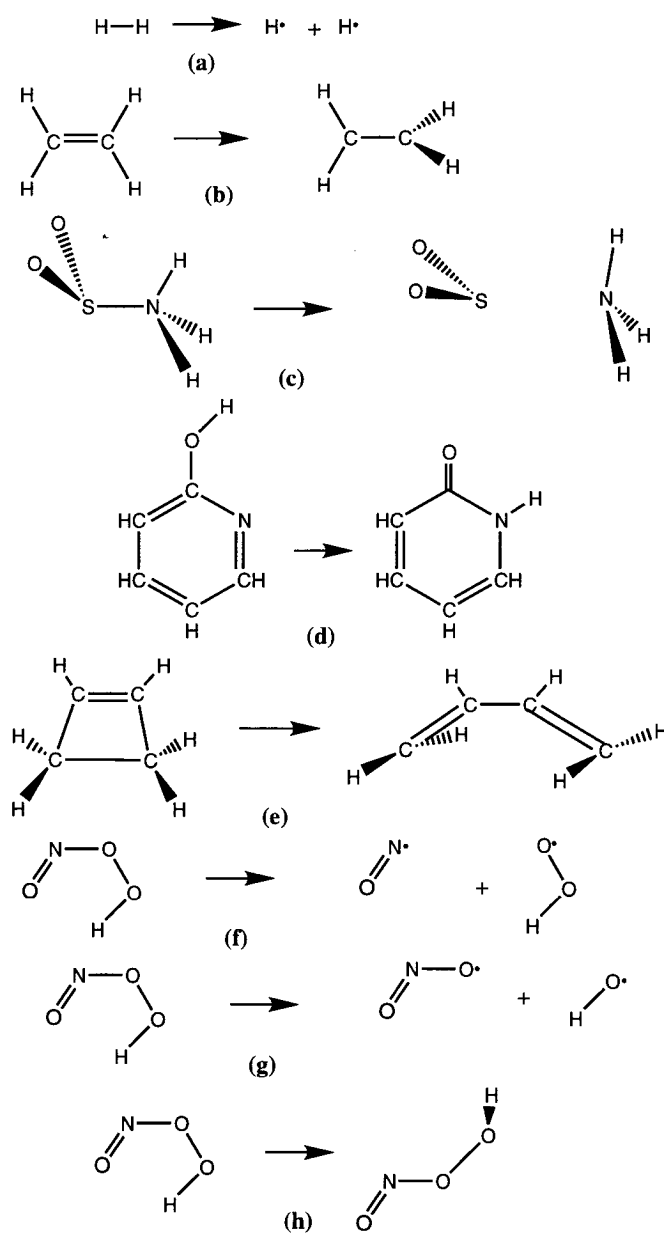


Figure 5.2: The prototypical reactions described in the text: (a)  $H_2$  dissociation; (b) *cis-trans* isomerisation in  $C_2H_4$ ; (c)  $SO_2 - NH_3$  dissociation; (d) proton transfer between 2-hydroxypyridine and 2-pyridone.; (e) Ring opening in cyclobutene; (f) N-O dissociation in peroxynitrous acid; (g) O-O dissociation in peroxynitrous acid; (h) *cis* to *trans* isomerisation in peroxynitrous acid.

The main objective of these tests was to establish if a finite electronic temperature can be used to lower significantly chemical activation barriers, or equivalently, to enhance the sampling efficiency by many orders of magnitude without changing the potential energy surface to much. For the reactions 5.3.1-5.3.6, we have therefore examined the energy profiles along appropriately chosen reaction coordinates for different electronic temperatures and compared them with the 0 Kelvin results (upper panels of Figs. 5.4-5.11). In parallel, we monitored the evolution of the eigenvalues (middle panels of Figs. 5.4-5.11) and the occupation (lower panels of Figs. 5.4-5.11) of the Kohn-Sham one-particle states along the reaction path. We would like to stress that we have chosen to follow predefined reaction pathways for these simple prototype reactions in order to facilitate the comparison of the potential energy surfaces. Such an *a priori* information however is not mandatory for general applications of FTAA that is designed to accelerate rare reactive events without any knowledge about possible atomic reaction coordinates.

The energy profiles shown in Figs. 5.4-5.11 allow an inspection of the distortions of the potential energy surfaces at different temperatures. Preserving the essential features of the potentially energy surface is important for all biasing schemes, even though Eq. 5.1 guarantees that biased sampling gives exact results. Indeed, the sampling effort increases if new minima configurations or additional channels appear on the biased potential energy surface, since the sampling probes region of phase space that are not representative for the original ground state ensemble. That the locations of the minima and transition states are basically unchanged with FTAA can be inferred for the reactions in Sec. 5.3.1-5.3.5 from the energy profiles at various electronic temperatures, calculated using the optimised zero temperature structures. A more elaborate test was performed for the systems in Sec. 5.3.6, for which the geometry along the reaction coordinate was reoptimised at every electronic temperature. It was observed that the distortions of the geometry were throughout small. In particular, the root mean square deviation (RMSD) between the low and high temperature (5000K) structures of both the stable *cis* and *trans* configurations were less than 0.02 Å. The maximum RMSD (0.07 Å) was observed at the transition state for *cis* to




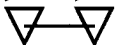
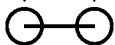
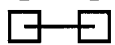
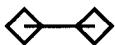
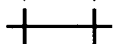
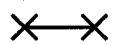

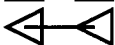
	250 K
	500 K
	1000 K
	2000 K
	4000 K
	5000 K
	6000 K
	8000 K
	16000 K

Figure 5.3: Symbols and the corresponding electronic temperature used in the Figures 5.4-5.11.

*trans* isomerisation, most of it was due to an elongation of 10 % of the N-O bond. Given that the finite temperature bias potential accelerates the *cis* to *trans* isomerisation by five orders of magnitude (*vide infra*), this change is remarkably small, and guarantees that the sampling of the modified surface and the averaging using Eq. 5.1 can be performed with high efficiency.

All the calculations were performed with the first principles molecular dynamics program CPMD [34], using finite temperature DFT [29] in the implementation of Alavi et al. [31] in the framework of pseudo potential theory, periodic boundary conditions a plane wave basis set.

### 5.3.1 Homolytic bond dissociation of $H_2$

As discussed in the previous Section,  $H_2$  can be considered as a prototypical two level (HOMO-LUMO) system with one bonding and the corresponding antibonding molecular orbital. The equilibrium structure has a large gap that gradually disappears when approaching the dissociation limit. As a consequence, even relatively high electronic temper-

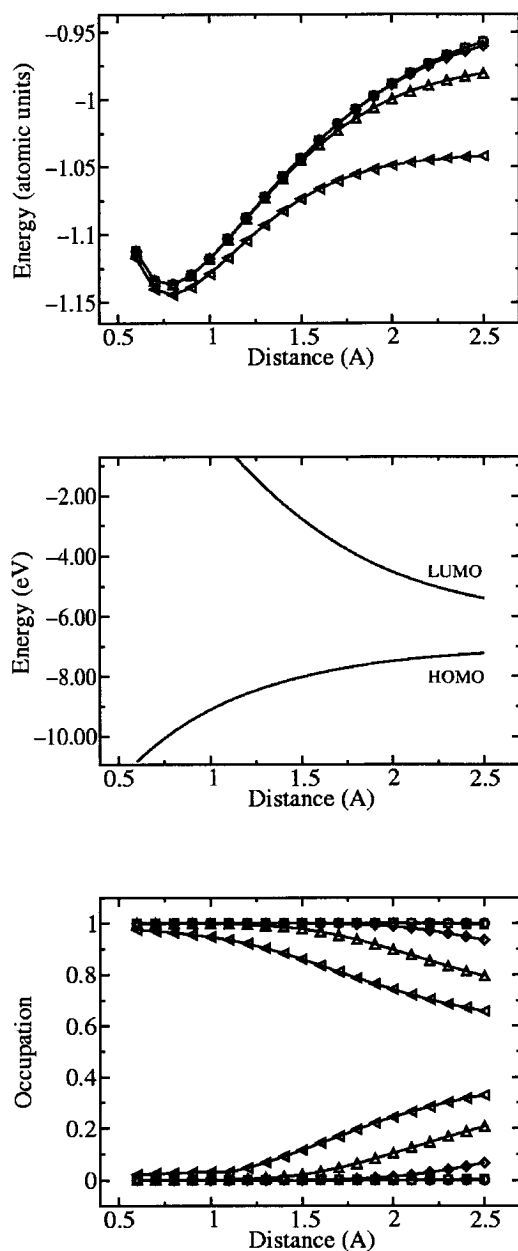


Figure 5.4: Reaction coordinate profiles for the dissociation of  $H_2$ . The reaction coordinate is the distance between the two hydrogen atoms. The upper panel shows the total energy for several values of the electronic temperature, the middle panel the evolution of the eigenvalues of the HOMO and LUMO for the zero temperature case, and the lower panel the occupation of HOMO and LUMO for several values of the electronic temperature. The different symbols correspond to different electronic temperatures as defined in Fig. 5.3.

Temperature (K)	$\Delta E$ (kcal/mol)	Enhancement
1000	0	1
2000	0	1
4000	2	70
8000	15	$6 \cdot 10^{12}$
16000	48	$1 \cdot 10^{42}$

Table 5.1: Homolytic bond dissociation of  $H_2$  at different electronic temperatures.  $\Delta E$  is the lowering of the dissociation energy in kcal/mol, and Enhancement is an estimate of the corresponding increase in sampling efficiency for a simulation at room temperature, or, equivalently, the increase in the rate constant at room temperature ( $\approx \exp(\frac{\Delta E}{kT})$ ).

atures leave the equilibrium occupation almost unaffected whereas at the same temperature the dissociated state is distinctly stabilized by a significant population of the virtual orbital. Therefore, this system constitutes a model reaction for which the enhanced sampling approach presented here can be expected to work ideally. The total energy, the eigenvalue spectrum, and the occupations during the dissociation are shown in Fig. 5.4 for different electronic temperatures. Due to the large gap in the ground state structure, we can use temperatures up to 16000K without inducing any significant changes in the equilibrium geometry. As shown in Table 5.1, the dissociation energy on the other hand is greatly reduced at finite electronic temperature, e.g. by ca. 50 kcal/mol at 16000K, leading to a drastic enhancement of sampling efficiency by a factor  $10^{42}$  at room temperature.

### 5.3.2 Rotation around the C-C bond in $C_2H_4$

The rotational barrier around the C-C bond in ethene requires an activation energy of 88 kcal/mol at the BLYP level of theory. The *cis-trans* isomerization of ethene is thus another example of a reactive rare event that is clearly beyond the time scale accessible

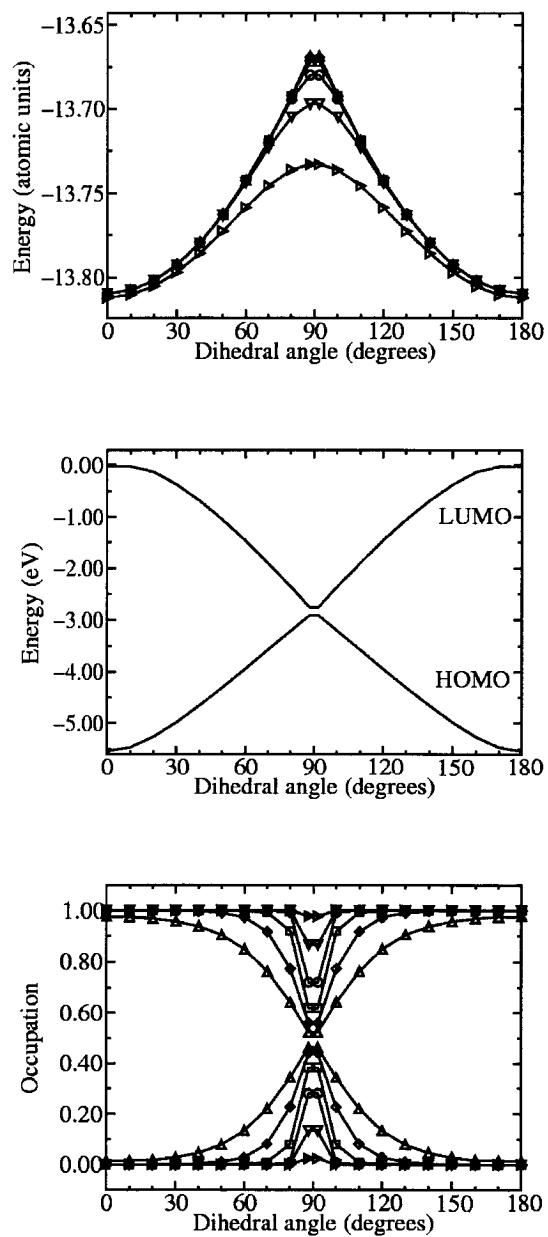


Figure 5.5: Reaction coordinate profiles for the *cis* to *trans* isomerisation of  $C_2H_4$  as a function of the dihedral angle H-C-C-H. The data is organised and labeled as in Fig. 5.4.

Temperature (K)	$\Delta E$ (kcal/mol)	Enhancement
250	0	1
500	0	2
1000	2	100
2000	7	$2 \cdot 10^6$
4000	18	$5 \cdot 10^{15}$
8000	39	$6 \cdot 10^{33}$

Table 5.2: *Cis-trans* isomerization of ethene at different electronic temperatures.  $\Delta E$  is the lowering of the activation barrier for *cis-trans* isomerization, Enhancement is an estimate of the corresponding increase in sampling efficiency for a simulation at room temperature, or, equivalently, the increase in the rate constant at room temperature ( $\approx \exp(\frac{\Delta E}{kT})$ ).

to first-principles molecular dynamics simulations. Considering only  $\pi$ -electrons, also this system can be regarded as another example of a typical 2 level (HOMO-LUMO) system, in this case involving  $\pi$  and  $\pi^*$  molecular orbitals. Similar to the situation encountered for the dissociation of  $H_2$ , these two orbitals become degenerate at the top of the rotational barrier at an H-C-C-H dihedral angle of  $90^\circ$ , i.e. also this system has a finite gap at equilibrium which vanishes at the transition state. Hence, the introduction of a finite electronic temperature has a pronounced effect on the rotational barrier (Fig. 5.5 and Table 5.2) while the location of the stationary points remains essentially untouched. Even at an electronic temperature of 8000K the population of the one-particle Kohn-Sham orbitals of the equilibrium structure is close to zero and one, i.e. the 0 Kelvin values. At the transition state on the other hand, HOMO and LUMO are equally populated and the rotational barrier is reduced by 39 kcal/mol. This lowering of the activation barrier for *cis-trans* isomerization corresponds to an impressive enhancement of the reaction rate at room temperature by roughly 34 orders of magnitude.

Temperature (K)	$\Delta E$ (kcal/mol)	Enhancement
1000	0	1
2000	0	1
4000	1	9
8000	5	$3 \cdot 10^4$

Table 5.3: Dissociation of the complex  $\text{SO}_2\text{-NH}_3$  for different electronic temperatures.  $\Delta E$  is the lowering of the dissociation energy in kcal/mol, Enhancement is an estimate of the corresponding increase in sampling efficiency for a simulation at room temperature, or, equivalently, the increase in the rate constant at room temperature ( $\approx \exp(\frac{\Delta E}{kT})$ ).

### 5.3.3 Dissociation of the Lewis acid-base complex of sulfur dioxide and ammonia

The reaction of  $\text{SO}_2$  and  $\text{NH}_3$ , is a typical example for a Lewis acid-base reaction, where the electron pair of the  $\text{NH}_3$  group is donated to the acceptor  $\text{SO}_2$ . One can therefore expect, that also this reaction is largely HOMO-LUMO dominated. As the reaction is barrierless in gas phase, we monitor here the effect on the reverse reaction, i.e. the dissociation of the Lewis acid-base complex. As in the previous examples, a considerable lowering of the dissociation barrier can be observed upon increasing the electronic temperature (Fig. 5.6 and Table 5.3). At an electronic temperature of 8000K it is basically halved. Again the HOMO-LUMO gap is reduced near the dissociation limit with respect to the value at equilibrium (Figure 5.6, middle panel) leading to a preferential lowering of the dissociated state while for all the electronic temperatures used the equilibrium distance itself is basically unaffected, i.e. the overall topology of the potential energy surface is maintained.

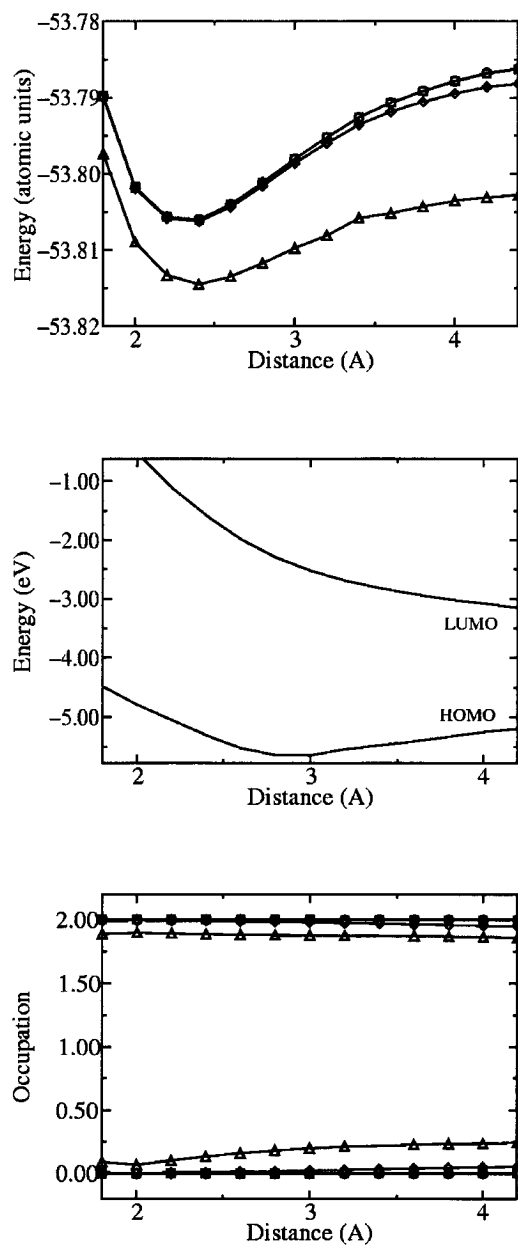


Figure 5.6: Reaction coordinate profiles for the dissociation of  $SO_2-NH_3$  with the distance between the S and N atoms as reaction coordinate. The data is organised and labeled as in Fig. 5.4.

Temperature (K)	$\Delta E_1$ (kcal/mol)	<i>Enhancement</i> <sub>1</sub>	$\Delta E_2$ (kcal/mol)	<i>Enhancement</i> <sub>2</sub>
1000	0	1	0	1
2000	0	1	0	1
4000	0	1	-0	0.9
8000	2	30	-1	0.1
16000	2	100	-3	$2 \cdot 10^{-3}$

Table 5.4: Intramolecular proton transfer between 2-hydroxypyridine and 2-pyridone.  $\Delta E_1$  and  $\Delta E_2$  are the lowering of the barrier for proton transfer from O to N and N to O, respectively. The corresponding Enhancements one and two are an estimate of the change in rate constant for the reactions at room temperature.

### 5.3.4 Intramolecular proton transfer between 2-hydroxypyridine and 2-pyridone

As a next example, we have considered the intramolecular proton transfer between the two tautomeric forms 2-hydroxypyridine and 2-pyridone in gas phase. This test system is of more complex nature, as there is no obvious direct connection between the HOMO and LUMO ( $\pi$  and  $\pi^*$  orbitals of the aromatic ring) and the proton transfer reaction which involves the breaking of the O-H  $\sigma$ -bond and the formation of an N-H bond. This is also apparent from the middle panel of Figure 5.7 that shows the evolution of the eigenvalue spectrum along an appropriately chosen reaction coordinate. There are several states near the HOMO-LUMO gap that are sensitive to changes in the reaction coordinate, the HOMO and LUMO themselves however do not experience large changes. The gap is smallest for the configuration in which the nitrogen atom is protonated, and there is no clear correlation between the magnitude of the gap, and the location of the transition state. For this system, finite electronic temperatures do not lead to a significant lowering of the reaction barrier (Figure 5.7 upper panel and Table 5.4). The largest decrease in activation energy ( $\Delta E = 2$  kcal/mol) is reached at a temperature of 8000K and a further raise does not lead to any



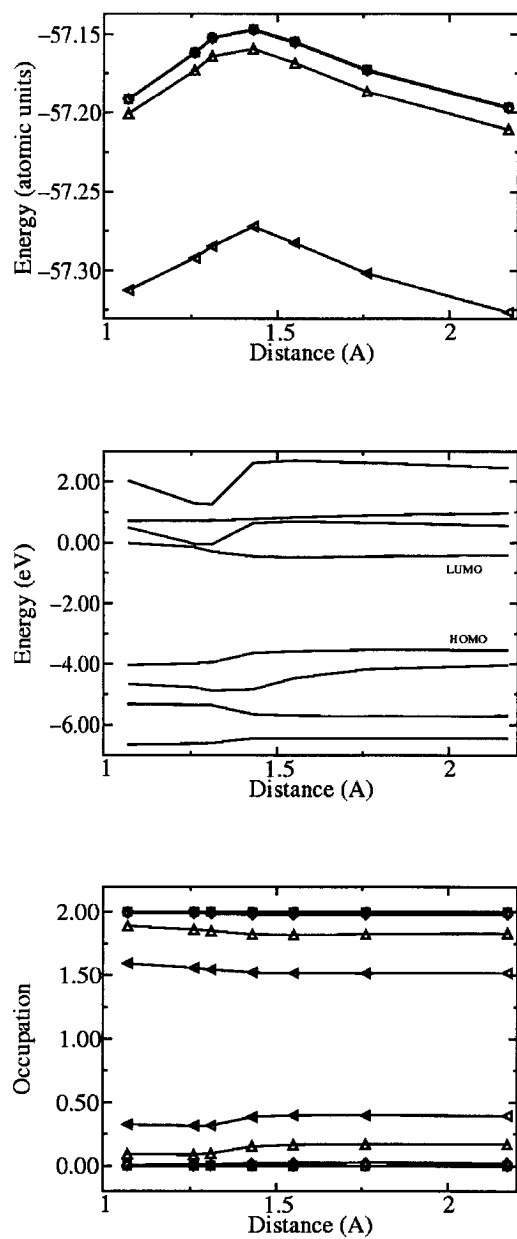


Figure 5.7: Reaction coordinate profiles for proton transfer between 2-hydroxypyridine and 2-pyridone with the oxygen-proton distance as reaction coordinate. The data is organised and labeled as in Fig. 5.4.

Temperature (K)	$\Delta E_1$ (kcal/mol)	<i>Enhancement</i> <sub>1</sub>	$\Delta E_2$ (kcal/mol)	<i>Enhancement</i> <sub>2</sub>
1000	0	1	0	1
2000	1	6	1	6
4000	1	6	1	5
8000	2	90	-1	0.3

Table 5.5: Conrotatory ring opening of cyclobutene.  $\Delta E_1$  and  $\Delta E_2$  are the lowering of the barrier for ring opening and ring closing, respectively. The corresponding Enhancements one and two are an estimate of the change in rate constant for the reactions at room temperature.

significant improvement. As is shown in Table 5.4, the net result is a marginal enhancement of the forward reaction (proton transfer from oxygen to nitrogen) and a slight slowing down of the backwards reaction (proton transfer from nitrogen to oxygen).

### 5.3.5 Conrotatory ring opening in cyclobutene

A second test case reaction of more complex nature that we have investigated is the ring opening of cyclobutene to butadiene, one of the classic examples of a symmetry controlled reaction. We have followed the symmetry-allowed, conrotatory pathway as the lowest energy reaction channel by choosing the distance of the two terminal carbon atoms as reaction coordinate. The orbital picture for the symmetry-allowed conrotatory ring opening differs distinctly from the one of the symmetry-forbidden, disrotatory reaction. Whereas for the latter, the reactive properties are dominated by the HOMO, this is not the case for the former. In the conrotatory case, the HOMO is rather insensitive to changes in the reaction coordinates but a lower lying state, namely the HOMO-1 can instead be considered as the effective frontier orbital (Figure 5.8, middle panel). As can be seen in Fig. 5.8, also the LUMO shows relatively little correlation with the reaction coordinate, resulting in a situation in which the gap is lowest for the butadiene product. As expected, no

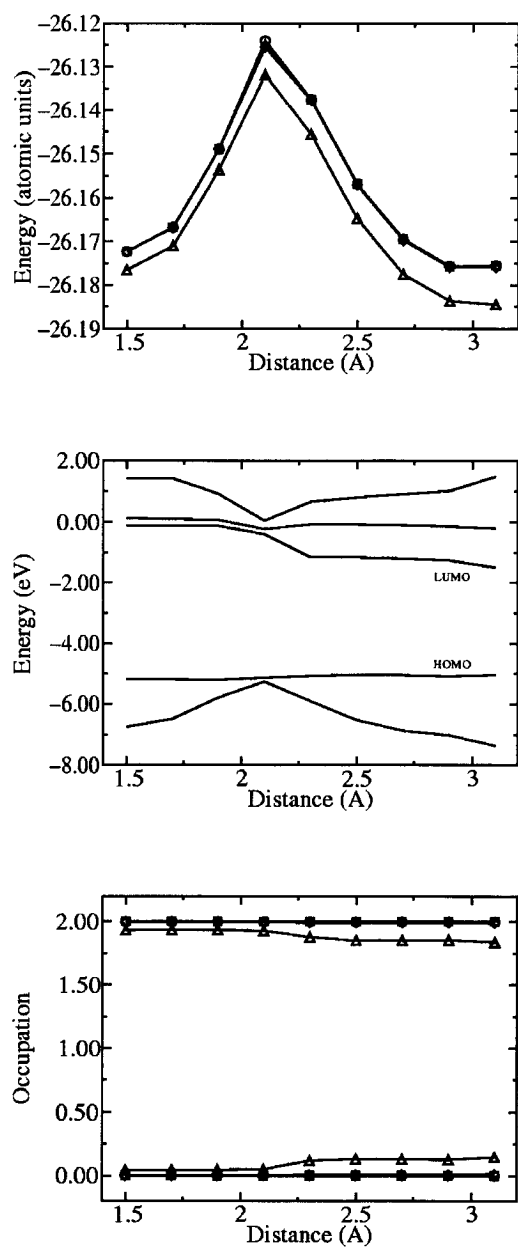


Figure 5.8: Reaction coordinate profiles for the ring opening in cyclo-butene, where the distance between the two terminal *C* atoms is the reaction coordinate. The data is organised and labeled as in Fig. 5.4.

dramatic lowering of the activation barrier is observed when a finite electronic temperature is introduced. We note that the occupation numbers are assigned using the Fermi-Dirac distribution, and hence the finite temperature mainly affects HOMO and LUMO. However, due to the fact that also the occupation of the HOMO-1, LUMO+1 and LUMO+2, are influenced by the finite temperature bias though to a lesser extent than the HOMO and LUMO themselves, a small reduction of the barrier can be detected (Table 5.5) but the overall finite temperature behaviour is generally more complex.

### 5.3.6 Peroxynitrous acid

Peroxynitrous acid is an example of a small molecule for which different reactive pathways with competitive barriers exist. It constitutes therefore an interesting test system to probe the relative efficiency of an enhanced sampling method for multiple reaction channels.

Starting from the global minimum configuration (the *cis-cis* isomer), the molecule can undergo homolytic bond breakage of either the central N-O bond or the O-O peroxy bond and dissociate into N-O• and •O-O-H or O-N-O• and •O-H, respectively. In addition, the molecule can also isomerize around the central N-O bond to a *trans-perp* form. We have determined the gas phase energy profiles at different electronic temperatures for all of the three reactions mentioned. As an important test of our method, we have also investigated the corresponding effects for the isomerisation reaction in an explicit solvent.

#### N-O bond cleavage

The first reaction channel we studied was the N-O bond cleavage of peroxynitrous acid in which the NO• and •OOH radicals are produced. As can be seen in the Fig. 5.9 (middle panel), this reaction has a strong HOMO-LUMO dependence, and accordingly, the method is able to lower the barrier significantly (Table 5.6). At the same time, the equilibrium

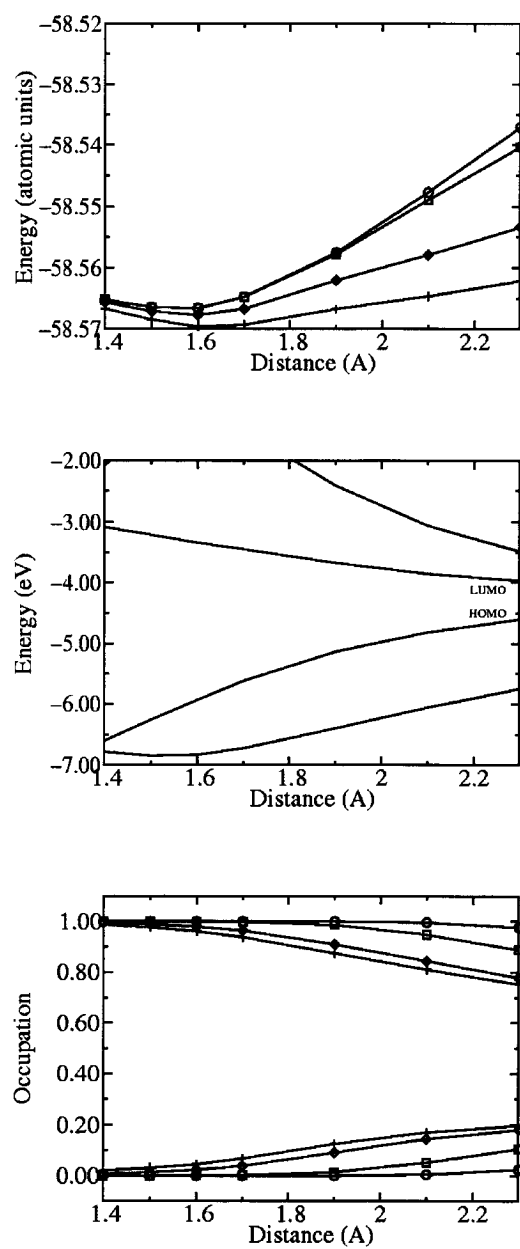


Figure 5.9: Reaction coordinate profiles for N-O bond breaking in ONOOH where the distance between the *N* and *O* atoms is the reaction coordinate. The data is organised and labeled as in Fig. 5.4.

Temperature (K)	$\Delta E$ (kcal/mol)	Enhancement
1000	0	1
2000	2	50
4000	9	$2 \cdot 10^8$
5000	14	$9 \cdot 10^{11}$

Table 5.6: N-O bond dissociation in ONOOH.  $\Delta E$  is the lowering of the dissociation energy in kcal/mol, Enhancement is an estimate of the corresponding increase in sampling efficiency for a simulation at room temperature, or, equivalently, the increase in the rate constant at room temperature ( $\approx \exp(\frac{\Delta E}{kT})$ ).

geometry is basically unchanged (RMSD of 0.014Å) with respect to the zero Kelvin results. At the highest electronic temperature, only a small barrier for dissociation remains, and we verified that during a molecular dynamics simulation the system is able to overcome the barrier and dissociate spontaneously on a subpicosecond time scale.

### O-O bond cleavage

A further reaction reaction that can take place in this system is the breakage of the peroxy bond to form  $\bullet\text{OH}$  and  $\bullet\text{ONO}$  radicals. This dissociation shows an almost equally strong HOMO-LUMO dependence (Figure 5.10, middle panel). Accordingly, also for this channel the activation energy is lowered drastically upon introduction of a finite electronic temperature (Table 5.7), and the rate is enhanced by as much as nine orders of magnitude.

### *Cis-trans* isomerization

As for the homolytic bond breakage reactions, we find a strong dependence on the electronic temperature also in the case of the *cis-trans* isomerization of peroxyxynitrous acid (Table 5.8). The characteristic evolution of the gap along the reaction coordinate (i.e. the ONOO

Temperature (K)	$\Delta E$ (kcal/mol)	Enhancement
1000	0	1
2000	1	10
4000	8	$5 \cdot 10^6$
5000	11	$8 \cdot 10^9$

Table 5.7: O-O bond dissociation in ONOOH.  $\Delta E$  is the lowering of the dissociation energy in kcal/mol, Enhancement is an estimate of the corresponding increase in sampling efficiency for a simulation at room temperature, or, equivalently, the increase in the rate constant at room temperature ( $\approx \exp(\frac{\Delta E}{kT})$ ).

Temperature (K)	$\Delta E_1$ (kcal/mol)	<i>Enhancement</i> <sub>1</sub>	$\Delta E_2$ (kcal/mol)	<i>Enhancement</i> <sub>2</sub>
1000	0	1	0	1
2000	0	1	0	1
4000	4	$1 \cdot 10^3$	3	400
5000	6	$2 \cdot 10^5$	5	$5 \cdot 10^4$

Table 5.8: *Cis-trans* isomerisation of peroxyntrous acid in gas phase.  $\Delta E_1$  and  $\Delta E_2$  are the lowering of the barrier for the rotation from *cis* to *trans* and from *trans* to *cis* respectively. The corresponding Enhancements one and two are an estimate of the change in rate constant for the reactions at room temperature.

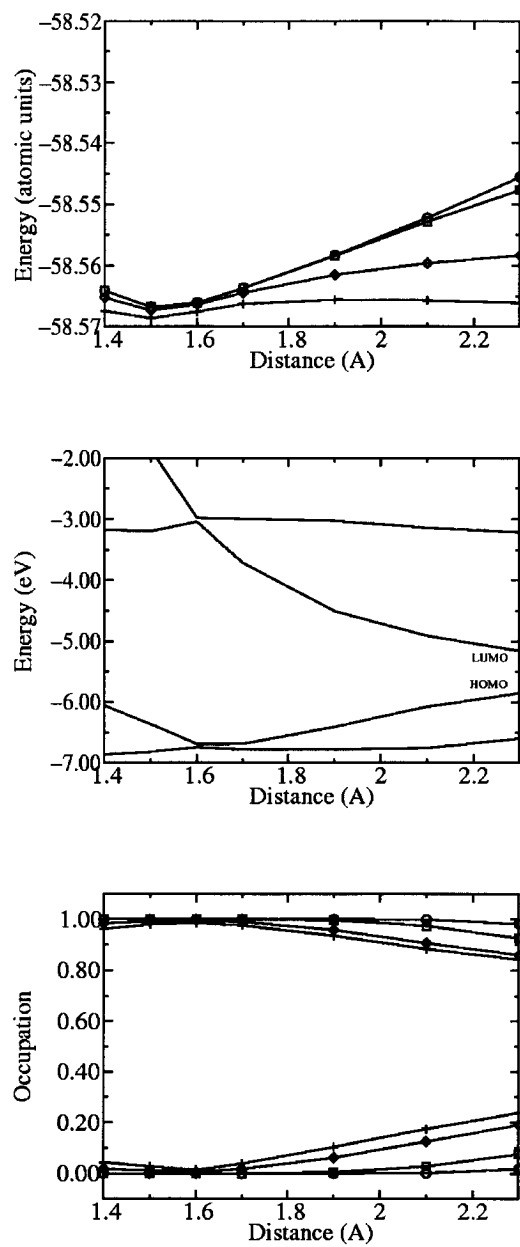


Figure 5.10: Reaction coordinate profiles for O-O bond breaking in ONOOH where the distance between the O atoms is the reaction coordinate. The data is organised and labeled as in Fig. 5.4.



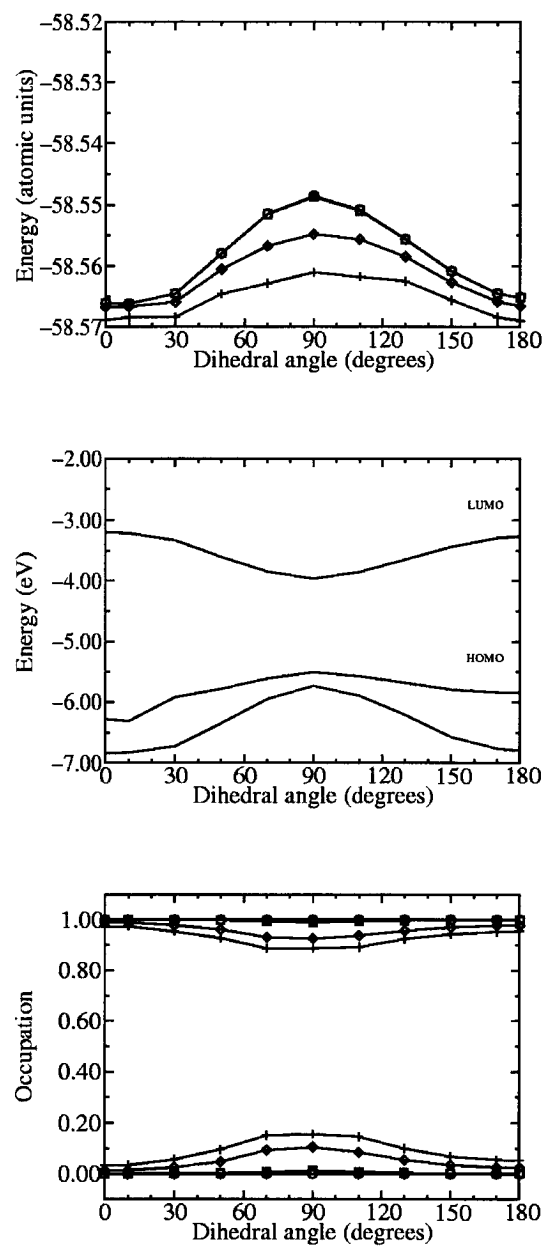


Figure 5.11: *Cis* to *trans* isomerisation in ONOOH where the dihedral angle O-N-O-O is the reaction coordinate. The data is organised and labeled as in Fig. 5.4.

dihedral angle), shown in Fig. 5.11, renders this system an almost ideal case for FTAA. Indeed, FTAA leads to a maximal lowering of 6 kcal/mol at 5000 K and therefore to an acceleration factor of approximately  $10^5$ . Moreover, this study on peroxyntrous acid also illustrates the power of FTAA in the sense that three different competitive chemical reactions can be easily accelerated significantly by a single and straightforward electronic bias. This is in contrast to a typical geometrical bias that forces the system in *a priori* selected direction.

### *Cis-trans* isomerization in solution

The acceleration of chemical events in complex systems with a rugged potential energy landscapes in which the barriers of the effective chemical events coexist with a multitude of low conformational barriers is especially challenging. Most of the existing methods lack the ability of finding relevant high lying activation barriers in a sea of less important transition states. A method that is able to enhance the sampling in a selective way for the chemical event only is therefore highly desirable. The *cis-trans* isomerisation of peroxyntrous acid in an explicit solvent of 52 water molecules at normal density, both treated at the gradient corrected DFT level constitutes thus a challenging test. We probe if the method presented here is able to lower selectively chemically relevant reactions in the presence of many chemically less relevant nearby transition states. Since the calculation of a complete free energy profile for this reaction is computationally very demanding, we decided to study the influence of the electronic temperature for selected configurations only. These configurations were obtained from a previous first principles molecular dynamics study [35] that used constrained MD to calculate the free energy profile for isomerization in aqueous solution. We used three independent configurations for several values of the reaction coordinate to calculate the average lowering of the total energy as a function of the electronic temperature. Clearly, this does not provide sufficient statistics to obtain quantitatively converged results but can give a first qualitative indication on the performance of

Temperature (K)	$\Delta E$ (kcal/mol)	Enhancement
1000	0	1
2000	0	2
4000	4	$2 \cdot 10^3$
5000	6	$2 \cdot 10^5$

Table 5.9: *Cis-trans* isomerization of peroxnitrous acid in aqueous solution.  $\Delta E$  is the lowering in activation energy in kcal/mol for conversion from the *cis* to the *trans* form, Enhancement is an estimate of the corresponding increase in sampling efficiency for a simulation at room temperature, or, equivalently, the increase in the rate constant at room temperature ( $\approx \exp(\frac{\Delta E}{kT})$ ).

the enhanced sampling approach. As shown in Fig. 5.12, the fluctuations in the observed barrier lowering are quite significant indicating the strong dynamical solvent effect on the gap of the system. The introduction of a finite electronic temperature leads to a significant lowering of the activation barrier (Table 5.9). Note, that the achieved enhancement in sampling efficiency is comparable to the values obtained for the corresponding gas phase reaction. These results indicate that the finite temperature approach is equally effective for gas phase as well as for condensed phase systems.

## 5.4 Conclusions

We have presented a novel method (finite temperature assisted acceleration, FTAA) to enhance the sampling of rare chemical events. Our approach makes direct use of the intrinsic electronic structure of the reactive system by exploiting the simple concept of a finite electronic temperature. Applying FTAA, it is possible to lower the barriers for a number of typical chemical reactions significantly. At the same time the overall topology of the potential energy surface is maintained, so that the difference between the zero temperature

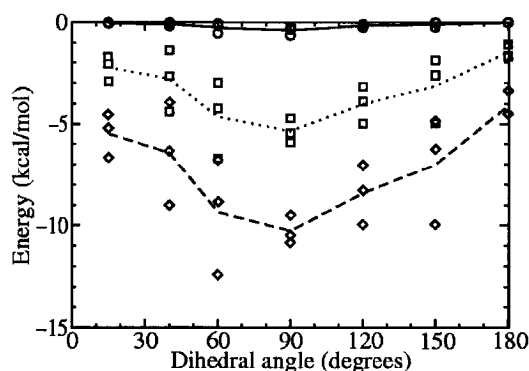


Figure 5.12: The lowering of the total energy as compared to the value at zero temperature, for selected configurations of peroxynitrous acid in solution during the *cis* to *trans* isomerisation. Different symbols represent values obtained for different electronic temperatures; Circles: 2000 K, squares: 4000K, diamonds: 5000K. The lines are drawn through the average values for the respective temperatures.

and the finite temperature potential can be used efficiently as a bias potential. Moreover, a similar reduction of activation barriers can also be achieved for solution reactions for which the barrier of the actual chemical event is competing with a large number of energetically low-lying barriers for configurational transitions. The simple method presented here works surprisingly well in the case of orbital-driven chemical reactions that are dominated by the HOMO and LUMO orbitals for which impressive acceleration factors of several orders of magnitude, often more than five, can be achieved in a straightforward manner. Advantages of the current scheme are its easy implementation, and for many electronic structure codes, its low computational cost.

## 5.5 Acknowledgements

J.V. acknowledges funding from an ETH internal grant.

## Bibliography

- [1] R. Car and M. Parrinello, *Phys. Rev. Lett.* **55**, 2471 (1985).
- [2] For a recent review of the Car-Parrinello method see, e.g.: D. Marx, J. Hutter, in *Modern Methods and Algorithms of Quantum Chemistry*, J. Grotendorst (Ed.), John von Neumann Institute for Computing, Jülich, NIC Series, **1**, 301 (2000)
- [3] For a recent review of applications of the Car-Parrinello method see, e.g.: U. Rothlisberger, in *Computational Chemistry: Reviews of Current Trends*, J. Leszczynsky (Ed.) World Scientific (in press)
- [4] P. Hohenberg and W. Kohn, *Phys. Rev. B* **136**, 864 (1964).
- [5] W. Kohn and L. J. Sham, *Phys. Rev. A* **140**, 1133 (1965).
- [6] See e.g. B. Hartke, and E.A. Carter, *J. Chem. Phys.* **97**, 6569 (1992).
- [7] E.A. Carter, G. Ciccotti, J.T. Hynes, and R. Kapral, *Chem. Phys. Lett.* **156**, 472 (1989).
- [8] M. Sprik, and G. Ciccotti, *J. Chem. Phys.* **109**, 7737 (1998).
- [9] G. M. Torrie and J. P. Valleau, *J. Chem. Phys.* **66**, 1402 (1977).
- [10] T. Huber, A. E. Torda, and W. F. van Gunsteren, *J. Comput.* **8**, 695 (1994).
- [11] H. Grubmüller, *Phys. Rev. E* **52**, 2893 (1995).
- [12] A. F. Voter, *J. Chem. Phys.* **106**, 4665 (1997).
- [13] A. F. Voter, *Phys. Rev. Lett.* **78**, 3908 (1997).
- [14] M. M. Steiner, P.-A. Genilloud, and J. W. Wilkins, *Phys. Rev. B* **57**, 10236 (1998).
- [15] X. G. Gong and J. W. Wilkins, *Phys. Rev. B* **59**, 54 (1999).

- [16] J. VandeVondele and U. Rothlisberger, *J. Chem. Phys.* **113**, 4863 (2000).
- [17] D. Chandler, *Introduction to Modern Statistical Mechanics* (Oxford University Press, New York, 1987).
- [18] K. Fukui, and H. Fujimoto, *Frontier orbitals and reaction paths* (World Scientific, Singapore, 1997).
- [19] See e.g. H. Chermette, *J. Comp. Chem.* **20**, 129 (1999).
- [20] R. G. Parr, and W. Yang, *Density-Functional Theory of Atoms and Molecules* (Oxford University Press, New York, 1989).
- [21] A. Warshel, *Computer Modeling of Chemical Reactions in Enzymes and Solutions* (John Wiley and Sons, New York, 1991).
- [22] R. G. Pearson, *J. Chem. Educ.* **64**, 561 (1987).
- [23] R. G. Pearson, *Acc. Chem. Res.* **26**, 250 (1993).
- [24] R. G. Parr, Z. ZHou, *Acc. Chem Res.* **26**, 256 (1993).
- [25] P. K. Chattaraj, H. Lee, and R. G. Parr, *J. Am. Chem. Soc.* **113**, 1855 (1991).
- [26] R. G. Parr and P. K. Chattaraj, *J. Am. Chem. Soc.* **113**, 1854 (1991).
- [27] For the formal proof, it is assumed that the chemical potential and the temperature are constant.
- [28] R. F. W. Bader, *Can. J. Chem.* **40**, 1164 (1962)
- [29] N. D. Mermin, *Phys. Rev.* **137**, A1441 (1965).
- [30] N. Marzari, D. Vanderbilt, and M. C. Payne, *Phys. Rev. Lett.* **79**, 1337 (1997).
- [31] A. Alavi, J. Kohanoff, M. Parrinello and D. Frenkel, *Phys. Rev. Lett.* **73**, 2599 (1994).
- [32] J. VandeVondele and A. De Vita, *Phys. Rev. B* **60**, 13241 (1999).

- 
- [33] F. De Proft, L. Shubin, and P. Geerlings, *J. Chem. Phys.* **108**, 7549 (1998).
- [34] CPMD, J. Hutter, A. Alavi, T. Deutsch, M. Bernasconi, St. Goedecker, D. Marx, M. Tuckerman, M. Parrinello, MPI für Festkörperforschung and IBM Zurich Research Laboratory 1995-1999
- [35] K. Doclo, and U. Rothlisberger, *J. Chem. Phys. A* **104**, 6464 (2000).





## Chapter 6

# Estimating equilibrium properties from non-Hamiltonian dynamics

## Abstract

We derive an expression that enables the accurate estimation of equilibrium properties using non-Hamiltonian dynamics. The major advantage of our scheme is that a time average over a single non-Hamiltonian trajectory can be employed instead of an ensemble average. Hence, it can directly be used in standard molecular dynamics simulations. The connection between non-Hamiltonian dynamics and equilibrium properties is established by assigning to the individual frames of the trajectory a weight that is based on the fluctuations of the phase space compression factor. Additionally, a simple scheme that takes into account only fluctuation of a given maximum duration is introduced to reduce the statistical error. By systematically extending the duration of the allowed fluctuations, increasingly accurate results can be obtained. Non-Hamiltonian dynamics schemes that are capable to enhance sampling efficiency are applied to two model systems in order to demonstrate the practical performance of our approach for the calculation of equilibrium free energy differences and probability density profiles.

## 6.1 Introduction

In a standard molecular dynamics scheme, particles are propagated using Newton's equations of motion, where the forces on the particles are derived from a potential energy function. This type of dynamics is Hamiltonian and energy conserving. Therefore, assuming ergodicity, properties of the system in the microcanonical ensemble can be extracted by averaging the quantity of interest over a single trajectory. In order to calculate properties in other ensembles with the same scheme, a more involved approach is needed. Indeed, an ensemble of systems with consistent initial conditions has to be used for the averaging process. In order to sample e.g. the canonical ensemble the initial configurations have to be Boltzmann distributed. However, current molecular dynamics simulation techniques circumvent this complexity and sample e.g. the canonical ensemble directly using a single trajectory. This is achieved by modifying the equations of motion, and adding additional forces on the particles. Methods that are e.g. aimed at sampling the canonical ensemble add friction-like forces to the equations of motion in order to ensure a given average value for the kinetic energy of the system that is consistent with the temperature of the ensemble. [1] [2] [3] [4] The freedom to add auxiliary forces to the dynamics can be exploited more generally for an efficient study of a wider range of problems with new types of molecular dynamics schemes that are designed for specific purposes. However, if additional forces are added the resulting dynamics is usually neither energy conserving nor Hamiltonian. As we will show below, the formal properties of the system change significantly in such a case, since, at variance with Hamiltonian dynamics, the phase space compression factor typically becomes non-zero. If the average phase space compression factor is negative, it is generally not known how to relate the time average over a *single* trajectory to averages over a physical ensemble.

In this paper, we want to explore the limitations and possibilities that arise whenever non-conservative or time-dependent forces, in addition to thermostats, are added to the dynamics. In particular, we are interested in this type of non-Hamiltonian molecular dy-

namics as a device for enhanced sampling aimed at bridging the time scale gap in molecular dynamics simulations. We are therefore not interested in the nonequilibrium properties of the system *per se*, but want to connect to the equilibrium properties at any instance during the non-Hamiltonian dynamics. Hence, we derive a practical relation that establishes a general connection between the average over a single non-Hamiltonian trajectory and an average in a physical ensemble. In Section 6.4, we validate our approach with numerical studies of model systems whose non-Hamiltonian dynamics has been designed with enhanced sampling applications in mind.

## 6.2 Evaluating phase space integrals using ensembles subject to compressible dynamics

In this Section, we discuss briefly how a property that is defined as the phase space average of an observable can be evaluated using an ensemble of systems subject to general dynamics. For the time independent case, if  $A(\Gamma)$  is an observable, depending on the phase space vector  $\Gamma$ , and  $f(\Gamma)$  is a probability distribution, the average value of  $A$  ( $\langle A \rangle_f$ ) is defined as [5]

$$\langle A \rangle_f = \int A(\Gamma) f(\Gamma) d\Gamma. \quad (6.1)$$

Equivalently,  $\langle A \rangle_f$  can be written as an average over an ensemble  $\{\Gamma_i\}$  of  $N$  systems, if these are distributed as  $f(\Gamma)$  and  $N$  is large.

$$\int A(\Gamma) f(\Gamma) d\Gamma = \frac{1}{N} \sum_{\{\Gamma_i\}} A(\Gamma_i). \quad (6.2)$$

If the systems evolve in time, i.e. the ensemble  $\{\Gamma_i(t)\}$  and the distribution  $f(\Gamma, t)$  are time-dependent, the equations of motion have to be specified, and they define the time-derivative of the phase space vector  $\dot{\Gamma}$ . An important characteristic quantity for the dynamics is the phase space compression factor that is defined as  $\Lambda(\Gamma) = \nabla_{\Gamma} \cdot \dot{\Gamma}$ , e.g. for Hamiltonian

dynamics :

$$\begin{aligned}
 \Gamma(t) &= (q_1(t), q_2(t), \dots, q_{3N}(t), p_1(t), p_2(t), \dots, p_{3N}(t)) \\
 \dot{\Gamma} &= \left( \frac{\partial H}{\partial p_1}, \frac{\partial H}{\partial p_2}, \dots, \frac{\partial H}{\partial p_{3N}}, -\frac{\partial H}{\partial q_1}, -\frac{\partial H}{\partial q_2}, \dots, -\frac{\partial H}{\partial q_{3N}} \right) \\
 \Lambda(\Gamma) &= \sum_{i=1}^{3N} \frac{\partial^2 H}{\partial q_i \partial p_i} - \frac{\partial^2 H}{\partial p_i \partial q_i} = 0.
 \end{aligned} \tag{6.3}$$

Since  $\Lambda(\Gamma) = 0$ , Hamiltonian dynamics is incompressible. Generally, as e.g. in the case of Nosé-Hoover dynamics [1] [2],  $\Lambda(\Gamma) \neq 0$  and the dynamics is compressible. As illustrated in Fig. 6.1, a non-zero phase space compression factor has a pronounced effect on the evolution of an ensemble. Starting from an ensemble of systems that are homogeneously distributed, it is apparent that for the incompressible case the number of systems within a finite phase space volume remains constant, whereas in the compressible case this number is free to change during the dynamics (of course, the total number of systems remains constant).

A weight  $W(\Gamma_i(t), t)$  can be assigned to every member of the ensemble so that the average over the evolved ensemble, at any time during the non-Hamiltonian evolution, equals the average over the initial (equilibrium) ensemble, i.e.

$$\int A(\Gamma) f(\Gamma) d\Gamma = \frac{1}{N} \sum_{\{\Gamma_i(0)\}} A(\Gamma_i(0)) = \frac{1}{N} \sum_{\{\Gamma_i(t)\}} A(\Gamma_i(t)) W(\Gamma_i(t), t). \tag{6.4}$$

There are two alternative ways [6] to derive the quantity  $W(\Gamma_i(t), t)$  in Eq. 6.4. The first approach is based on the observation that the local density of systems in phase space changes as a function of time (as illustrated in Fig. 6.1). The time dependent density ( $f(\Gamma, t)$ ) satisfies a generalised Liouville equation, and is given by  $\frac{df}{dt} = -f\Lambda(\Gamma)$ . [7] This equation can easily be solved for the case that  $\Lambda$  is not explicitly time dependent and yields  $f(\Gamma(t), t) = f(\Gamma(0), 0) \exp(-\int_0^t \Lambda(\Gamma(t')) dt')$ . The correct weight  $W(\Gamma_i(t), t)$  for the system  $\Gamma_i$  at time  $t$  is given by the ratio between the initial density of systems in the current point ( $\Gamma_i(t)$ ), that is  $f(\Gamma_i(t), 0)$ , and the actual density of system in the current point, that is  $f(\Gamma_i(t), t)$ . This can be written explicitly as :

$$W(\Gamma_i(t), t) = \exp\left(\int_0^t \Lambda(\Gamma_i(t')) dt'\right) \frac{f(\Gamma_i(t), 0)}{f(\Gamma_i(0), 0)}. \tag{6.5}$$

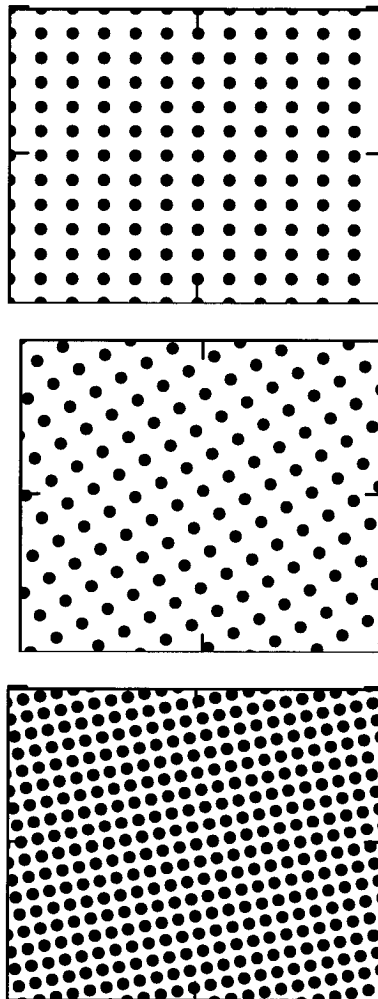


Figure 6.1: Schematic illustration of the effect of a non-zero phase space compression factor. In this representation, each point in the three panels represents the positions  $(p,q)$  in phase space of an individual system, and each panel shows the same fraction of phase space, but after different types of dynamics. Upper panel, the initial coordinates, notice that the systems are homogeneously distributed. Middle panel, coordinates after incompressible dynamics, notice that the density of points equals the density in the upper panel. Lower panel, after compressible dynamics.

In this expression, which can easily be calculated during the evolution of the system, the first factor of the integrand takes the compressibility into account, and the last factor is different from one only for non-homogeneous initial densities. The second approach to obtain  $W(\Gamma_i(t), t)$  is equivalent to assigning a phase space volume element to every member of the ensemble, and taking its size as the weight. The size of this volume element is given by the Jacobian  $J(\Gamma, t)$  of the transformation of phase space that results from the dynamics. The Jacobian  $J(\Gamma, t)$  obeys the equation  $\frac{dJ}{dt} = J\Lambda(\Gamma(t))$ . [8] Proceeding as above, this leads to the same definition of the weight as given in Eq. 6.5.

An example of a very interesting equation that can be derived using the approach outlined here, was recently published by Jarzynski [9] [10]. Jarzynski's equation relates the work ( $W$ ) done in switching a Hamiltonian in a finite time, thus not adiabatically, from  $H_{\lambda=0}$  to  $H_{\lambda=1}$  to the free energy difference between the initial and final states ( $\Delta F$ ) and is given by

$$\langle \exp(-\beta W) \rangle = \exp(-\beta \Delta F), \quad (6.6)$$

where  $\langle \dots \rangle$  denotes averaging over canonically distributed initial configurations.

For a direct, numerical, application of Eq. 6.4, it is in most cases necessary that the initial ensemble  $\{\Gamma_i\}$  is very dense to enable an accurate evaluation of the integral. This is due to the behaviour of the term  $\exp(\int_0^t \Lambda(t') dt')$ . It can be shown that for systems that are kept in a nonequilibrium steady state the phase space compression factor  $\Lambda$  is on average less than zero. [11] The effect of  $\langle \Lambda \rangle < 0$  is that the weight of a typical member of the ensemble decreases exponentially fast to zero as a function of time. Members of the ensemble that have  $\int_0^t \Lambda(t') dt' > 0$  are exponentially less probable for increasing  $t$ . [12] [13] This suggests that it is unavoidable to have a dense and extended initial ensemble, since many systems with a very low weight and very rare trajectories with a large weight have to be sampled, and hence a large amount of independent simulations have to be performed. This limits practical use of the equations in the form given above, and is the motivation for the derivation of a more practical expression in the next Section.

### 6.3 From ensemble averages to a time average

In this Section, we will propose a modified form for the weight  $W(\Gamma, t)$ , that ensures that it does not decay to zero. We will demonstrate that in this case no average over a dense initial ensemble is necessary, but that a time average over a single non-Hamiltonian trajectory can be used instead.

In the following, we employ an homogeneous initial ensemble  $\{\Gamma_i(0)\}$  for all averages, which implies that  $f(\Gamma, 0)$  factors out of Eq. 6.5. We introduce instead a phase space function  $D(\Gamma)$  so that e.g. a canonical average of an observable  $A(\Gamma)$  can be obtained as the ratio of two phase space averages  $\frac{\sum A(\Gamma_i)D(\Gamma_i)}{\sum D(\Gamma_i)}$  if  $D(\Gamma)$  is chosen to be  $\exp(-\beta H(\Gamma))$ . More importantly, we also introduce a function  $\gamma(t)$ , depending on time only, to arrive at the mathematically equivalent form

$$\begin{aligned} \frac{\int A(\Gamma)D(\Gamma)d\Gamma}{\int D(\Gamma)d\Gamma} &= \frac{\sum_{\{\Gamma_i(0)\}} A(\Gamma_i(0))D(\Gamma_i(0))}{\sum_{\{\Gamma_i(0)\}} D(\Gamma_i(0))} \\ &= \frac{\sum_{\{\Gamma_i(t)\}} A(\Gamma_i(t))D(\Gamma_i(t)) \exp(\int_0^t \Lambda(\Gamma_i(t'))dt')}{\sum_{\{\Gamma_i(t)\}} D(\Gamma_i(t)) \exp(\int_0^t \Lambda(\Gamma_i(t'))dt')} \\ &= \frac{\sum_{\{\Gamma_i(T)\}} \int_0^T A(\Gamma_i(t))D(\Gamma_i(t)) \exp(\gamma(t) + \int_0^t \Lambda(\Gamma_i(t'))dt')dt}{\sum_{\{\Gamma_i(T)\}} \int_0^T D(\Gamma_i(t)) \exp(\gamma(t) + \int_0^t \Lambda(\Gamma_i(t'))dt')dt}. \end{aligned} \quad (6.7)$$

In the last equation, we sum integrals over the trajectories of the systems, and we obtain this form by multiplying the effectively *time-independent* nominator and denominator by  $\int_0^T \exp(\gamma(t))dt$ . This expression is correct for every choice of  $\gamma(t)$ , but is particularly interesting for  $\gamma(t) = -\langle \Lambda \rangle t + c$ , where  $c$  is a constant, since for this choice, the apparent weight ( $\exp(\gamma(t) + \int_0^t \Lambda(\Gamma(t'))dt')$ ) of a given system is not exponentially decreasing, but fluctuating around a finite value. The weight is thus related to the integral of the fluctuations around the average value of the phase space compression, i.e. to  $\Lambda(t) - \langle \Lambda \rangle$ , rather than to the value  $\Lambda(t)$  itself.

At this point we replace the ensemble average in Eq. 6.7 by a time average over the



trajectory of a single system and write

$$\frac{\int A(\Gamma)D(\Gamma)d\Gamma}{\int D(\Gamma)d\Gamma} = \lim_{T \rightarrow \infty} \frac{\int_0^T A(\Gamma(t))D(\Gamma(t)) \exp(\gamma(t) + \int_0^t \Lambda(\Gamma(t'))dt')dt}{\int_0^T D(\Gamma(t)) \exp(\gamma(t) + \int_0^t \Lambda(\Gamma(t'))dt')dt}. \quad (6.8)$$

Eq. 6.8 is a practical, ad hoc, assumption, and we show in the next Section that it yields very accurate results for the model systems we studied as long as a natural condition holds; there must be a finite probability to find the system near every phase space point that is needed to evaluate the integral in the left hand side of Eq. 6.8. [14] Although certain classes of non-Hamiltonian dynamics violate this condition, a negative average phase space compression factor alone seems not to imply that this assumption is not valid. This fact is illustrated with the examples in the next Section.

As already mentioned, a functional form such as  $\gamma(t) \approx -\langle \Lambda \rangle t + c$  is mandatory to take into account all configurations in a non-Hamiltonian run. However, an attempt of using directly the form  $\gamma(t) = -\langle \Lambda \rangle t + c$  failed for the systems we studied, because of the extremely slow convergence behaviour of Eq. 6.8. This can possibly be attributed to fluctuations in  $\Lambda(t)$  that cause  $\int_0^t \Lambda(t')dt' > 0$  for all  $t$ . These fluctuations are exponentially less likely for longer  $t$ , but are on the other hand contributing with an exponentially increasing weight to the average. We require therefore an approximate form for  $\gamma(t)$  that can be made arbitrarily close to the target form  $\gamma(t) = -\langle \Lambda \rangle t + c$ , but that can be tuned in such a way as to have smaller fluctuations in the term  $\exp(\ln(D(\Gamma(t))) + \int_0^t \Lambda(t')dt' + \gamma(t))$  so that Eq. 6.8 can be sampled with high accuracy in a finite time. The following differential equation for  $\gamma(t)$  leads to the desired properties of  $\gamma(t)$

$$Q\ddot{\gamma}(t) = -\ln(D(\Gamma(t))) - \int_0^t \Lambda(t')dt' - \gamma(t) - \alpha Q\dot{\gamma}(t). \quad (6.9)$$

Here  $Q$  and  $\alpha$  are constants that play the role of a generalised mass and friction coefficient, respectively. By construction, the solution  $\gamma(t)$  of this equation follows closely the value of  $-\ln(D(\Gamma(t))) - \int_0^t \Lambda(t')dt'$ . However, the characteristic frequency ( $\omega^2 = \frac{1}{Q}$ ) of Eq. 6.9 will determine the allowed temporal length of the fluctuations in  $-\ln(D(\Gamma(t))) - \int_0^t \Lambda(t')dt' - \gamma(t)$ . The characteristic time window can be tuned through the adjustable parameter  $Q$ .

Since  $\lim_{Q \rightarrow \infty} \gamma(t) = -\langle \Lambda \rangle t + c$ , the target functional form of  $\gamma(t)$  can be reached in a continuous way. Only in this limit  $\gamma(t)$  as defined by Eq. 6.9 is independent of  $\Gamma$ , as assumed in the derivation of Eq. 6.7. We note that inclusion of the term  $\ln(D(\Gamma(t)))$  is not absolutely necessary for obtaining the target functional form in the limit of large  $Q$ , and in fact any phase space function could be used instead. However, for intermediate values of  $Q$  a lower systematic error is obtained if this term is included. We demonstrate this feature by means of numerical examples in the next Section for dynamics where  $\langle \Lambda \rangle \neq 0$ . The importance of this term can also be shown straightforwardly for standard Nosé-Hoover dynamics. [1] [2] In this case  $-\ln(D(\Gamma(t))) - \int_0^t \Lambda(t') dt'$  is a constant, and Eq. 6.9 yields  $\gamma(t) = c$  for all values of  $Q$ , so that Eq. 6.8 is exact.

It is of practical importance that the weight of a configuration can be calculated independently and at no additional cost for several values of  $Q$ . Given a trajectory of a certain length, the value of  $Q$  that minimises both the statistical and the systematic error can be determined a posteriori. The evaluation of the weight is straightforward since it involves solving a single differential equation, independent of the system size. Eq. 6.8 together with Eq. 6.9 form the central results of this article, and will be illustrated numerically with two applications on model systems in the following Section.

## 6.4 Numerical studies of two model systems

### 6.4.1 Estimating free energy differences

In the first application, we calculate the free energy difference between two single particle Hamiltonians,  $H_{min} = \frac{p^2}{2m} + \frac{1}{2}k_{min}q^2$  and  $H_{max} = \frac{p^2}{2m} + \frac{1}{2}k_{max}q^2$ , where  $k_{min}$  and  $k_{max}$  are arbitrary force constants of a harmonic potential. We introduce non-Hamiltonian conditions for this system by deriving forces from a time-dependent potential that varies continuously between two harmonic wells. This type of dynamics could be of use for the

calculation of relative binding affinities for a large set of ligands, since a single trajectory based on a Hamiltonian that is designed to vary between prototypical ligands in the set might contain a broader range of configurations and thus enhance the sampling efficiency. Since the time dependence is continuous, rapid and thus non-adiabatic, we introduce a thermostat to keep the energy of the system bounded. We have adopted the following set of equations for an extended system  $(x_1, \dots, x_6)$ .

$$\begin{aligned}
 \dot{x}_1 &= x_6^2 - K - x_1 x_2 \\
 \dot{x}_2 &= x_1^2 - K - x_2 x_3 \\
 \dot{x}_3 &= x_2^2 - K - x_3 x_4 \\
 \dot{x}_4 &= x_3^2 - K \\
 \dot{x}_5 &= x_6 \\
 \dot{x}_6 &= -(k_1 + k_2(1 + \cos(\omega_k t)))x_5 - x_6 x_1
 \end{aligned} \tag{6.10}$$

The variables  $x_1, \dots, x_4$  are thermostating variables as in the Nosé-Hoover chain method [15],  $x_5$  is the position and  $x_6$  is the momentum of a particle,  $K$  determines the temperature, and  $k_1, k_2$  and  $\omega_k$  are constants that describe a time dependent harmonic force. All masses are of unit value. The associated phase space compression factor is given by  $\Lambda = -x_2 - x_3 - x_4 - x_1$ . Since, for a non-zero switching frequency  $\omega_k$ , work is continuously performed on the system,  $\Lambda$  is on average negative.

Within the extended system, it is possible to calculate the free energy difference between the two original Hamiltonians in the canonical ensemble as

$$\begin{aligned}
 \exp(\beta\Delta F) &= \frac{\int \exp(-\beta H_{min}) dq dp}{\int \exp(-\beta H_{max}) dq dp} \\
 &= \frac{\int \exp(-\frac{\beta}{2}(x_1^2 + x_2^2 + x_3^2 + x_4^2 + k_{min}x_5^2 + x_6^2)) dx_1 \cdots dx_6}{\int \exp(-\frac{\beta}{2}(x_1^2 + x_2^2 + x_3^2 + x_4^2 + k_{max}x_5^2 + x_6^2)) dx_1 \cdots dx_6} \\
 &\approx \frac{\int_0^T \exp(-\frac{\beta}{2}(x_1^2 + x_2^2 + x_3^2 + x_4^2 + k_{min}x_5^2 + x_6^2) + \gamma(t) + \int_0^t \Lambda(t') dt') dt}{\int_0^T \exp(-\frac{\beta}{2}(x_1^2 + x_2^2 + x_3^2 + x_4^2 + k_{max}x_5^2 + x_6^2) + \gamma(t) + \int_0^t \Lambda(t') dt') dt}
 \end{aligned} \tag{6.11}$$

where  $\gamma(t)$  is calculated using Eq. 6.9, with additional parameters  $Q$  and  $\alpha$ . The latter was chosen as to have an almost critical damping of the system for all values of  $Q$ .

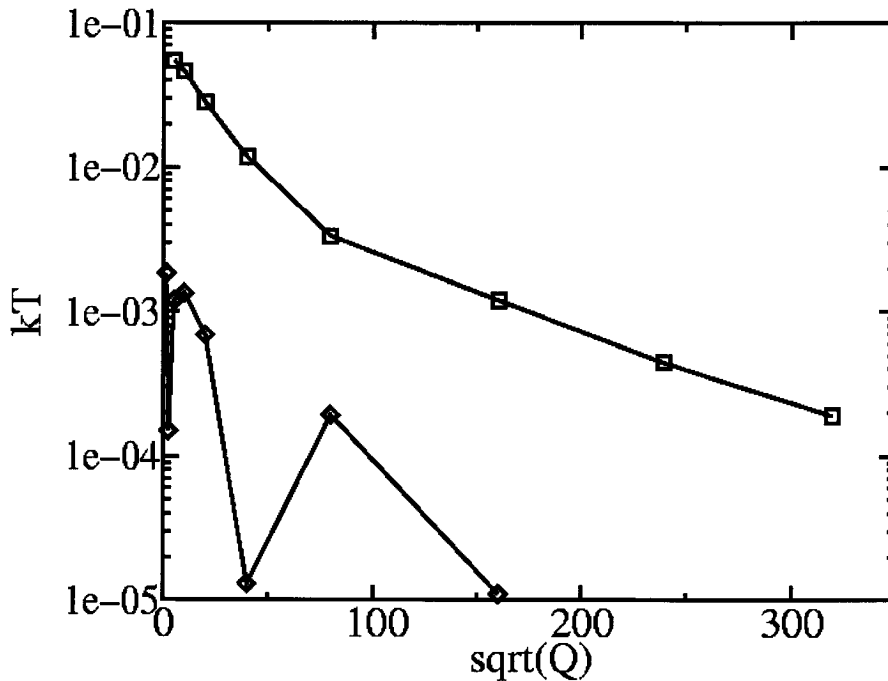


Figure 6.2: Model system A (see text): absolute value of the difference between the exact and the estimated free energy difference. Squares : without the term  $\ln(D(\Gamma))$ ; diamonds : with the term  $\ln(D(\Gamma))$ . The latter does not converge monotonically, hence some results are accidentally closer to the exact result.

The equations of motion were solved numerically using a Runge-Kutta fourth order integrator [16] [17] [18]. After equilibration, we performed the averaging over the trajectory as given by Eq. 6.11 until the statistical error was negligible. For a fixed set of parameters ( $k_{min} = 6, k_{max} = 14, \beta = 1, K = 1, k_1 = 10, k_2 = 4, \omega_k = 0.1$ ) we performed a series of simulations with different values of  $Q$  and compared the estimated free energy differences with the analytic result. Furthermore we have also run simulations with and without the term  $\ln(D(\Gamma))$  in Eq. 6.9, in order to judge its effect on the convergence behaviour. Fig. 6.2 shows the difference between the exact result and our estimate. Considering the fact that an accuracy of  $10^{-3}$  kT in a free energy difference is extremely small for all practical purposes, we can see that the error that might be introduced by Eq. 6.8 and Eq. 6.9 is

negligible in both cases. It is also clear that inclusion of the term  $\ln(D(\Gamma))$  improves the error for a given value of  $Q$  by approximately an order of magnitude. We would like to point out that the data suggests that the error decreases roughly exponentially with  $Q$ .

### 6.4.2 Spatial probability distributions

In the second example, we calculate the spatial probability distribution of a system that is subject to a non-conservative force, in particular, we scale the force on one of the two particles. Since interparticle forces are present, this introduces a non-conservative force. Preliminary tests showed that this approach might be a powerful scheme for enhanced sampling simulations, since the mobility of the particles that are subject to this scaled force can be greatly improved. We define the following equations of motion:

$$\begin{aligned}
 \dot{x}_1 &= x_4^2 + x_6^2 - 2K - x_1x_2 \\
 \dot{x}_2 &= x_1^2 - K \\
 \dot{x}_3 &= x_4 \\
 \dot{x}_4 &= -x_3 - a(x_3 - x_5 - 1) - x_1x_4 \\
 \dot{x}_5 &= x_6 \\
 \dot{x}_6 &= -x_5 + 1(x_3 - x_5 - 1) - x_1x_6
 \end{aligned} \tag{6.12}$$

where the variables  $x_1, x_2$  are thermostating variables of a Nosé-Hoover chain,  $x_3, x_4$  and  $x_5, x_6$  are position and momenta of the first and second particle, and the constant  $K$  determines the temperature. The parameter  $a$  can be used to change the force acting on the particles from conservative ( $a = 1$ ) to non-conservative ( $a \neq 1$ ). In Fig. 6.3, we show the distribution  $\delta(x_3 - x)\delta(x_5)$  for various values of  $a$ , both before and after applying the weighting procedure. It is clear that the non-Hamiltonian dynamics influences the uncorrected distribution functions significantly, especially if  $a$  deviates strongly from one. Instead, the curves of the weighted approach reproduce the target distribution closely for values of  $a$  that are above 0.4, but the curve with  $a = 0.3$  clearly deviates from the target

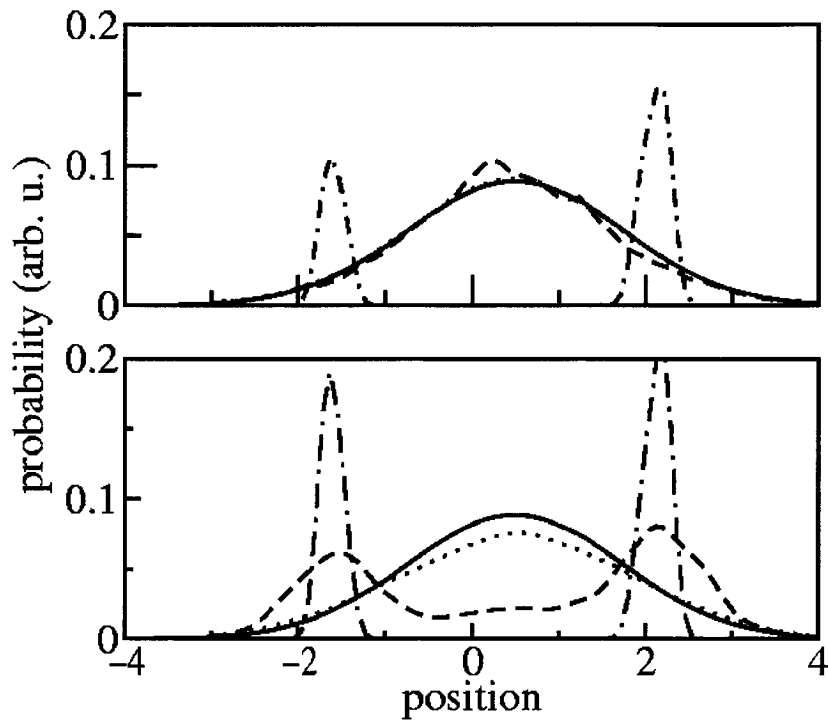


Figure 6.3: Model system B (see text): the distribution functions  $\delta(x_3 - x)\delta(x_5)$  for several values of the parameter  $a$ . The lower panel shows the uncorrected distributions, the upper panel shows the results after weighting. The solid line represents the equilibrium distribution function, whereas the dotted, the dashed, and the dashed-dotted line were obtained with  $a=0.8, 0.5, 0.3$  respectively. Notice that in the upper panel the dotted line is almost indistinguishable from the solid line.

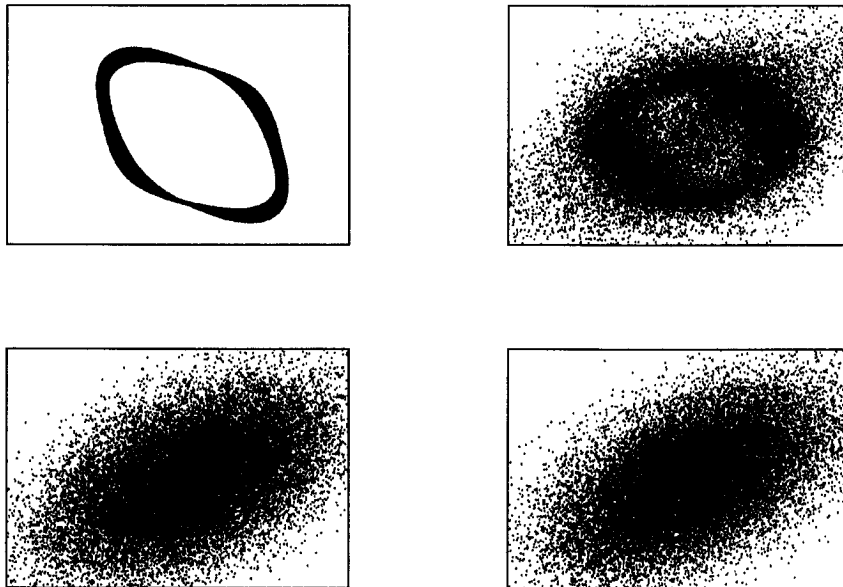


Figure 6.4: The trajectory in phase space of the second model discussed in the text. The points represent the coordinates of the particles  $(x_3, x_5)$ . Each panel shows a trajectory of equal length, but for different values of the parameter  $a$ . From left to right, from top to bottom  $a = 0.3$ ,  $a = 0.5$ ,  $a = 0.8$ ,  $a = 1.0$ .

distribution. In Fig. 6.4 independent points of the trajectory are shown for several values of  $a$ , and it can be seen that this trajectory is confined to a limiting cycle for  $a = 0.3$ , whereas for the other values the distribution is clearly inhomogeneous, but there is a non-zero probability to find the system everywhere in phase space. With this example, we want to demonstrate that, for certain choices of the parameters of a non-Hamiltonian dynamics run, the system can get trapped on a limiting cycle. Such a behaviour would invalidate the use of Eq. 6.8, but can be considered less likely for larger systems. [19]

For the same system, and for an intermediate value of  $a$  ( $a=0.8$ ), we show in Fig. 6.5 the convergence to the target distribution, as measured by the root mean square difference between the distribution functions. Also in this case, the convergence with respect to  $Q$  seems roughly exponential. The difference between the obtained distribution function and

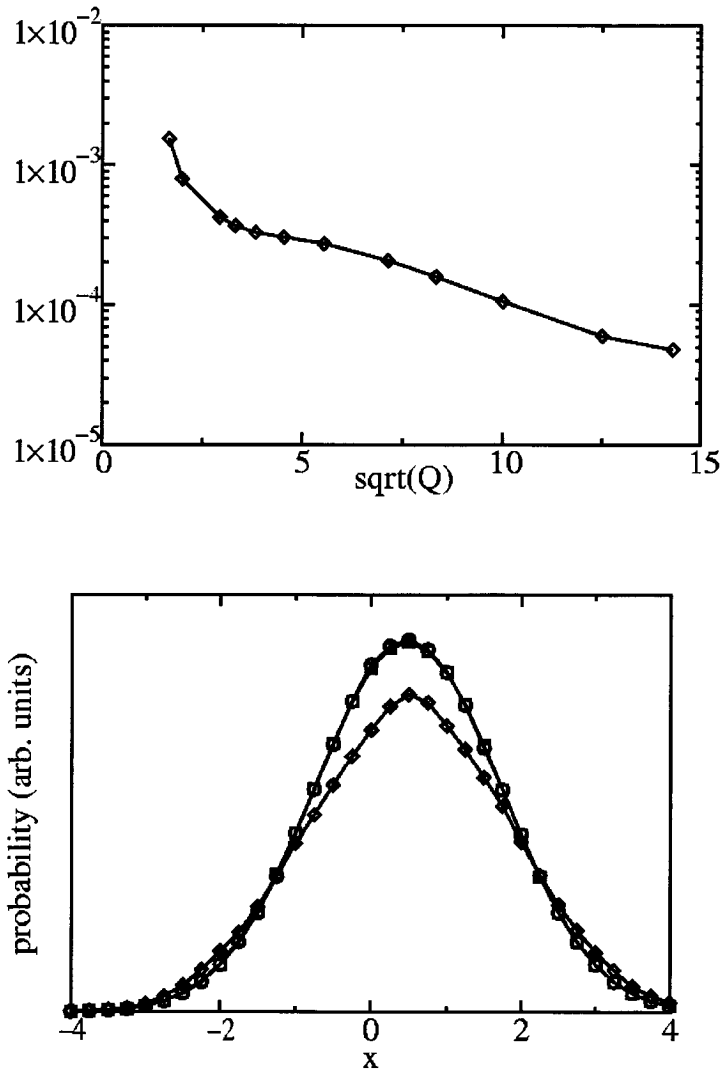


Figure 6.5: Model system B with  $a = 0.8$  : the upper panel shows the rmsd between the equilibrium distribution function and the non-Hamiltonian distribution function after weighting for several values of the parameter  $Q$ . The lower panel shows how closely the equilibrium distribution (circles) is matched by the corrected non-Hamiltonian distribution (squares), as compared to the uncorrected non-Hamiltonian distribution (diamonds).



the target function can hardly be discerned.

## 6.5 Conclusions

We have established a connection between the average over a single non-Hamiltonian trajectory and equilibrium properties. This has been achieved by weighting each of the configurations of the non-Hamiltonian run with a simple weight that is based on the fluctuations of the phase-space-compression factor. This weight can be calculated a posteriori without a significant computational cost and contains a single parameter that has to be adjusted in order to obtain statistically converged results. The assumption underlying our approach should be considered as a practical one, but the model systems we have studied show that very accurate estimates can be made with this scheme, and thus provide an indirect confirmation of the simple picture we have presented.

We are therefore confident that this scheme opens the way to applications that extend beyond the chosen model systems. We are currently developing non-Hamiltonian enhanced sampling techniques where forces that do not derive from a potential are introduced to provoke transitions between stable states, and to increase the statistics for the sampling of rare events.

## 6.6 Acknowledgements

We are indebted to Philippe Hünenberger, Alessandro Laio, Michel Mareschal, and Mark Tuckerman for their helpful comments on the manuscript. J.V. acknowledges funding from an ETH internal grant.

## Bibliography

- [1] S. Nosé, J. Chem. Phys. **81**, 511 (1984).
- [2] W.G. Hoover, Phys. Rev. A **31**, 1695 (1985).
- [3] H.J.C. Berendsen, J.P.M. Postma, W.F. van Gunsteren, A. Di Nola, and J.R. Haak, J. Chem. Phys. **81**, 3684 (1984).
- [4] A. Bulgac and D. Kusnezov, Phys. Rev. A **42**, 5045 (1990).
- [5] See e.g. M.P. Allen and D.J. Tildesley, *Computer Simulation of Liquids* (Clarendon press, Oxford, 1987).
- [6] We provide two different derivations of the weight in Eq. 6.4, based on two different, controversial formulations (see e.g. references [20] [21] [22] [23]). As mentioned in the text, the same conclusions can be reached, using either of the two alternative formulations.
- [7] See e.g. D.J. Evans and G.P. Morriss, *Statistical Mechanics of Nonequilibrium Liquids* (Academic Press, London, 1990), an electronic version can be found at <http://rsc.anu.edu.au/~evans/evansmorrissbook.htm> .
- [8] See e.g. M.E. Tuckerman, C. J. Mundy, and G.J. Martyna, Europhys. Lett. **45**, 149 (1999).
- [9] C. Jarzynski, Phys. Rev. Lett. **78**, 2690 (1997).
- [10] C. Jarzynski, Phys. Rev. E **56**, 5018 (1997).
- [11] B.L. Holian, G. Ciccotti, W.G. Hoover, B. Moran, and H.A. Posch, Phys. Rev. A **39**, 5414 (1989).
- [12] D.J. Evans, E.G.D. Cohen and G.P. Morriss, Phys. Rev. Lett. **71**, 2401 (1993).
- [13] D.J. Evans and D.J. Searles, Phys. Rev. E **50**, 1645 (1994).

- [14] This implies that the system reaches a steady state.
- [15] G.J. Martyna, M.L. Klein, and M. Tuckerman, *J. Chem. Phys.* **97**, 2635 (1992).
- [16] W.H. Press, S.A. Teukolsky, W.T. Vetterling, and B.P. Flannery *Numerical Recipes in C* (Cambridge University Press, Cambridge, 1994).
- [17] The source code that can be used to reproduce the example in this Section can be obtained from J.V. or directly at <http://www.rac.ethz.ch/vondele/psc/>
- [18] Note that the discretisation error can be considered as an additional force in the dynamical equations, and could, in principle, be accounted for with our scheme. Given the accuracy of our results as shown in Fig. 6.2, we consider this a minor issue.
- [19] This is in an analogy to the Nosé-Hoover method which is known to have difficulties to generate the canonical distribution for low dimensional or stiff problems, but performs well, especially in the formulation of ref. [15], once the dimensionality of phase space is increased.
- [20] M.E. Tuckerman, C.J. Mundy, and M.L. Klein, *Phys. Rev. Lett.* **78**, 2042 (1997).
- [21] W.G. Hoover, D.J. Evans, H.A. Posch, B.L. Holian, G.P. Morriss, and *Phys. Rev. Lett.* **80**, 4103 (1998).
- [22] P. Reimann, *Phys. Rev. Lett.* **80**, 4104 (1998).
- [23] M.E. Tuckerman, C.J. Mundy, and M.L. Klein, *Phys. Rev. Lett.* **80**, 4105 (1998).



## Chapter 7

# Canonical adiabatic free energy sampling (CAFES): a novel method for the exploration of free energy surfaces

## Abstract

We present a novel method, canonical adiabatic free energy sampling (CAFES), that allows for the efficient exploration of the free energy surface of a subsystem (S) embedded in an environment (E) using molecular dynamics simulations. The dynamics of S is decoupled from the environment by introducing fictitious masses that ensure that S evolves slowly and adiabatically on the potential of mean force generated by E. In addition, the decoupling enables the use of different temperatures for the two parts of the system without introducing an irreversible heat flow. Using a higher temperature for the subsystem, a high efficiency for the sampling of rare events is obtained. The scheme is tested for a conformational analysis of a Gly-Ala dipeptide in aqueous solution, and enables the observation of rare conformational transitions that naturally occur on a millisecond time scale within few nanoseconds of simulation. The same method has also been applied in a hybrid Car-Parrinello/classical molecular dynamics simulation of the proton-catalyzed conversion of 2-bromoethanol to dibromoethane in water. Applying the CAFES method, anchimeric assistance and the occurrence of a bromonium ion intermediate could be observed repeatedly.

## 7.1 Introduction

A central goal of chemical research is the elucidation of chemical reactions on the atomistic level. Molecular dynamics (MD) simulations are a promising theoretical tool for this. Indeed, the introduction of Density Functional Theory [1] (DFT) in molecular dynamics by Car and Parrinello, [2] combined with the novel hybrid quantum mechanical/molecular mechanical (QMMM) approaches, [3] made it possible to have accurate dynamics of large systems for tens of picoseconds. If these large systems could be simulated for times that are comparable to experimental ones, a richness of chemical reactions could be observed directly, with atomistic detail and without introducing prior knowledge, using computer experiments. However, a simulation length of tens of picoseconds is at the limit of what is routinely feasible for *ab initio* MD at this moment, and this is still many orders of magnitude away from the millisecond to hour timescale that is typical for many chemical reactions. Hence, chemical reactions are seldomly observed spontaneously during MD.

To overcome this limitation and to get closer to the goal of observing rare, unknown reactions during MD simulations, there has been an intensive search for methods that can significantly extend the time scale, or enhance the sampling efficiency of MD simulations. [4] These methods typically try to increase the rate constant for possible reactions (activated events) in the system by modifying the potential energy surface (PES) in a well controlled way so that the free energy of activation is lowered. Since the rate depends exponentially on the activation energy, the probability that a reaction happens spontaneously during an MD simulation on the modified PES can be orders of magnitude larger. Efficient and general recipes to modify the PES exist for small systems, or for systems where a precise geometrical reaction coordinate is known, but these recipes often fail for (bio)chemical systems. These difficult systems typically contain a large number of degrees of freedom, for example the solvent, that are subject to anharmonic motion and have low barriers, whereas the chemically interesting degrees of freedom might be rather stiff and have a high free energy of activation. General methods usually fail for this kind of system because the

effort is not focussed on, for example, the active site, but is equally distributed over the full system. This reduces significantly the efficiency of the sampling, since a phase space with many degrees of freedom has to be explored. At the same time, such a large phase space is often not necessary for many interesting problems, since the chemical events are limited to a small subsystem, such as the solute in solution, or the active site in a protein.

The method presented here focusses the sampling effort and differentiates between a reactive subsystem (S, f.e. the solute or the active site), and an environment (E, f.e. the solvent or a protein). We do this by decoupling adiabatically the dynamics of the subsystem and the environment in such a way that the subsystem performs a dynamics on its free energy surface (FES), thereby taking in a precise way the effect of the environment into account. This decoupling allows us to use a temperature  $T^S$  for the reactive system that is different from the temperature of the environment ( $T^E$ ). By significantly increasing the temperature of the reactive system, it samples more efficiently its free energy surface. Since increasing the temperature can be done without using prior information, CAFES can be used for the exploration of an unknown free energy surface, ideally providing sufficiently many transitions so that the previously unknown reaction mechanism can be understood. Notice that for a standard MD simulation a significant increase of the temperature is normally not possible for a complex system, since e.g. a solvent would evaporate or a protein would unfold, leading to an unphysical system. It is crucial that the environment remains, as in the CAFES method, at the physical temperature. The increase in the rate for reactive events can then be estimated by  $\frac{\exp(-\Delta G\beta^S)}{\exp(-\Delta G\beta^E)}$ , the ratio of the rate constants at the respective temperatures, where  $\Delta G$  is a typical activation free energy and  $\beta^X = \frac{1}{kT^X}$ . E.g. for a reaction with an activation energy of 20 kcal/mol and  $T^E=300\text{K}$  using  $T^S=1200\text{K}$  yields an increase of efficiency of  $10^{10}$ . This is sufficient to bridge the gap between the nanosecond timescale of simulation, and the second timescale of experiment. Even higher efficiencies can be obtained if the system has a larger activation energy or if the temperature  $T^S$  is increased further. We remark that these apparently high temperatures  $T^S$  are in the same energetic range as the spontaneous local fluctuations that make these rare events happen



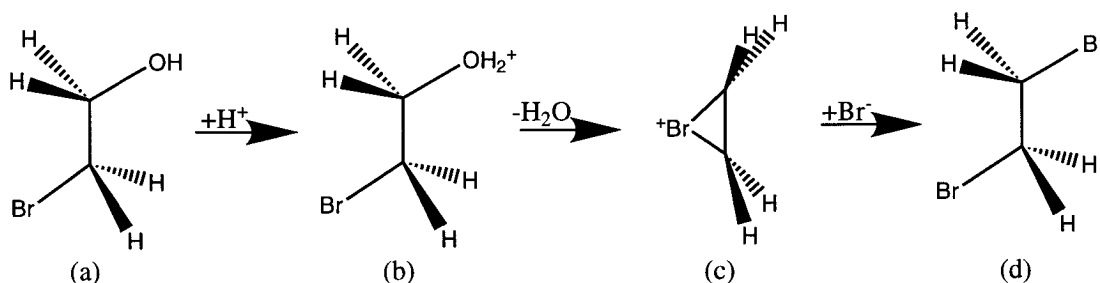


Figure 7.1: The reaction of 2-bromoethanol (a) with bromine to yield dibromoethane (d), involving as a key intermediate, after dissociation of the  $H_2O$  group from the protonated 2-bromoethanol (b), the bromonium ion (c).

in reality, and must be compared to the activation energy.

As we show in the next Section, the strength of our method lies in its formulation as a combined dynamical scheme where both the subsystem and the environment are propagated simultaneously, but are adiabatically decoupled, leading to a computationally efficient method. The performance of this scheme is demonstrated by conformational sampling, and the acceleration of reactive events. The complex nature of reactive, solvated systems, which involve high activation barriers within a sea of low barriers, makes them especially challenging for any sampling method. The first test involved the calculation of the free energy surface of a dipeptide in solution, where free energy profiles can be compared with those from standard simulation methods. The results on this system clearly indicate that new conformations can be found efficiently and accurately, even though naturally the interconversion would occur on time scales that are orders of magnitude beyond what is achievable by standard molecular dynamics simulations. Furthermore, we successfully applied our method, within a QM/MM framework, to the study of the reaction of 2-bromoethanol with bromine in solution which yields dibromoethane as shown in Fig. 7.1. In particular, we focussed on the second elementary step that involves  $H_2O$  as a leaving group, and a bromonium ion as a key intermediate. The suggestion of the existence of a bromonium intermediate dates back from the 30s. This intermediate accounts for the

stereochemistry of bromine additions to olefins and explained why substitution with retention of configuration is possible. [5] [6] [7] Furthermore, the described reaction is the textbook example of neighboring group participation or anchimeric assistance, [8] [9] and this provides an additional reason for its study. Using the CAFES method and over 200 ps of mixed classical/Car-Parrinello molecular dynamics, we were able to observe several times the formation of the bromonium ion, and hence confirmed its role as an intermediate and the mechanism of this fundamental reaction.

## 7.2 Formulation of the method

Central to our method is the partitioning into two subsystems, the reactive subsystem and the environment, that are kept at different temperatures. In the following, we superscript quantities that belong to the reactive subsystem and the environment with  $R$  and  $E$  respectively. In particular, we denote the momenta with  $(\{p_i^S, p_j^E\})$ , the positions with  $(\{q_i^S, q_j^E\})$  and the mass of all atoms with  $(\{m_i^S, m_j^E\})$ , where  $i$  and  $j$  run over the atoms ( $N^S, N^E$ ) of each system. In order to achieve canonical sampling for each system, we use Nosé-Hoover thermostats, [10] [11] implying thermostating variables  $(\{p_\eta^S, \eta^S, Q^S, p_\eta^E, \eta^E, Q^E\})$ , and temperatures  $(\{T^S, T^E\})$ . For a given potential energy  $V(\{q_i^S, q_j^E\})$  we define the following dynamics where  $X$  stands for both  $R$  and  $E$  :

$$\begin{aligned} \dot{q}_i^X &= \frac{p_i^X}{m_i^X} \\ \dot{p}_i^X &= -\frac{\partial V}{\partial q_i^X} - p_i^X \frac{p_\eta^X}{Q^X} \\ \dot{p}_\eta^X &= \sum_i^{N^X} \frac{(p_i^X)^2}{m_i^X} - 3N^X kT^X \quad \text{with } i : 1 \dots N^X \\ \dot{\eta}^X &= \frac{p_\eta^X}{Q^X} \end{aligned}$$

These equations are a straightforward generalisation, of the Nosé-Hoover equations, with two independent thermostats, and conserve the quantity

$$V(\{q_i^S, q_j^E\}) + \sum_i^{N^S} \frac{(p_i^S)^2}{2m_i^S} + \sum_i^{N^E} \frac{(p_i^E)^2}{2m_i^E} + \frac{(p_\eta^S)^2}{2Q^S} + \frac{(p_\eta^E)^2}{2Q^E} \\ + 3N^S \eta^S kT^S + 3N^E \eta^E kT^E.$$

The use of two thermostats introduces additional freedom that can be exploited to enhance sampling efficiency. In our approach,  $T^E$  is set to the physical temperature, whereas  $T^S$  is tuned to optimize the sampling. Two thermostats have been used in an MD based docking strategy before, but without an adiabatic decoupling, and hence with a continuous heat flow, and without a well defined sampling probability distribution. [12] The crucial step, which is needed to obtain the dynamics of the reactive system on its free energy surface at the specified temperature, is the rescaling of the masses so that  $\frac{m^E}{m^S} \ll 1$ . In this way, a clear difference between the frequency spectrum of the reactive system and the environment is introduced, and in particular, the reactive system has become slowly varying, as compared to the fast motion of the environment. This has two important consequences that we address in detail below : (1) The systems are decoupled and can be in equilibrium although they have different temperatures; (2) The slowly moving system feels an average force, and its dynamics is on its free energy surface (FES) as determined by the environment.

We would like to point out the close analogy between this approach, which treats the reactive system in the average field of the decoupled environment, and the Car-Parrinello method [2] [13], which considers the ions in the average field of the decoupled electronic degrees of freedom, hence the arguments to validate the Car-Parrinello method can be adapted to the current method. As shown in Ref. [14] for the CP method, the following intuitive statements, which are exact in the limit of perfectly decoupled systems, hold accurately in case the systems have well separated frequencies: (1) There exist adiabatic invariants and this implies that the irreversible energy flow between the two systems is close to zero. Therefore, the systems are in equilibrium, and since we use Nosé-Hoover

thermostats, equilibrate at the specified temperatures. This implies that the fast degrees of freedom ( $p^E, q^E$ ) sample the canonical distribution at temperature  $T^E$  for every configuration ( $\{p^S, q^S\}$ ) of the reactive system. (2) The dynamics of the slow degrees approximates the one resulting from a Hamiltonian with an effectively averaged potential. This potential, which we denote by  $V_{MF}^{\beta^E}(q^S)$ , is, for a full decoupling, given by

$$\exp(-\beta^E V_{MF}^{\beta^E}(q^S)) = \frac{\int \exp(-\beta^E V(q^S, q^E)) dq^E}{\int \exp(-\beta^E V(q^S, q^E)) dq^E dq^S}.$$

This potential of mean force equals the physical free energy surface of the reactive system. An enhanced canonical sampling of this free energy surface can be obtained by taking  $T^S > T^E$ . Since we assume adiabatic evolution and hence equilibrium sampling, the probability distribution of the full system in configuration space is given by

$$\begin{aligned} \rho(q^S, q^E) &= \frac{\exp(-(\beta^S - \beta^E)V_{MF}^{\beta^E}(q^S))}{\int \exp(-\beta^S V_{MF}^{\beta^E}(q^S)) dq^S} \times \\ &\quad \times \frac{\exp(-\beta^E V(q^S, q^E))}{\int \exp(-\beta^E V(q^S, q^E)) dq^S dq^E} \end{aligned}$$

This explicit form allows us to calculate thermodynamic properties from a trajectory generated with CAFES. In the next Section, we discuss how the ratio of the masses  $\frac{m^E}{m^S}$  can be tuned in order to achieve an efficient and accurate sampling.

### 7.3 Determination of the mass ratio

The ratio of the masses  $\frac{m^E}{m^S}$  determines the degree of decoupling between the subsystems, and hence the accuracy of the method. Rescaling the masses of the reactive system by a factor  $\alpha \gg 1$  increases the cost of the simulation because the total time ( $t$ ) needed for averaging over the trajectory grows as  $t \propto \sqrt{\alpha}$ . [15] Accuracy has therefore to be traded for efficiency, and we show below that  $\alpha = 100$  is a reasonable choice for the system we studied, but the appropriate choice of the masses might depend on the desired accuracy, and on the system and property that is being studied. Our choice of mass ratio brings the

overall efficiency down by about a factor of ten, which is little compared to the exponential gain implied by our method, and still produces qualitatively accurate free energy profiles for both the minima and the transition states in the system. A precise number for the free energy barrier might afterwards be generated more efficiently with techniques that use this reaction coordinate [4] and, starting from a reactive trajectory as generated by our method, a study of the dynamical effects of the crossing could be undertaken using the transition path sampling method. [16]

A reasonable setting for the masses of the CAFES system can only be determined by studying a realistic molecular system. We address this question with classical molecular dynamics simulations of a zwitterionic Gly-Ala dipeptide solvated in water. Our computational setup is based on the GROMOS96 force field [17], using SPC water (1720 molecules), flexible bonds, and P3M with a  $32^3$  mesh to compute the electrostatic interactions [18]. We used the hybrid classical/quantum interface to the program CPMD [19] [20] in the fully classical mode, extended to incorporate the CAFES equations, in a generalised form where every atom is coupled to a chain of Nosé-Hoover thermostats. [21] We performed CAFES simulations where the full peptide was treated as the 'reactive' system and was thermostated at 1200 K, whereas the solvent was kept at 300 K. We did not optimise the frequency of the Nosé-Hoover thermostats and kept all chains at a frequency of  $1000 \text{ cm}^{-1}$ . We multiplied the masses of the peptide by a factor of 1, 3, 10, and 100 and ran those systems for 1.4, 2.3, 3.1, and 10.7 ns respectively. As mentioned before, the simulation time should increase with the square root of the mass factor to obtain comparable statistics. The reference calculation was a standard molecular dynamics simulation of 3.1 ns. For these systems, we compared the free energy profiles (given by  $FE(\theta) = -kT \ln(p(\theta))$ ) for the torsional angle ( $\theta$ ). The probability density  $p(\theta)$  for the torsional angle can be computed exactly from the probability density of the CAFES subsystem ( $\rho^S(q^S)$ ) as  $p(\theta) = \alpha \int \delta(\theta'(q^S) - \theta) [\rho^S(q^S)]^{\frac{T^S}{T^E}} dq^S$ , where  $\alpha$  is a normalisation constant. We used instead the more convenient, approximate expression  $p(\theta) \approx \alpha (\int \delta(\theta'(q^S) - \theta) \rho^S(q^S) dq^S)^{\frac{T^S}{T^E}}$ , that neglects contributions of cross terms within the reactive system to the free energy. The advantage of this expression is that it

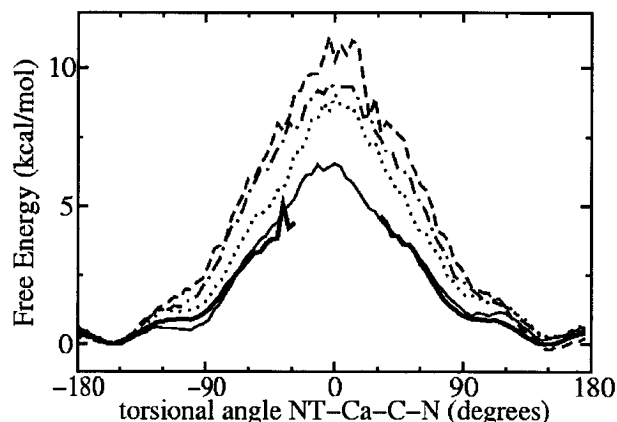


Figure 7.2: In the figure, we compare the peptide torsional ( $\text{NT-C}_\alpha\text{-C-N}$ ) free energy profiles calculated with the CAFES method, for several scaling factors of the peptide masses. The solid, dotted, dash-dotted, and dashed line represent the results for scaled masses by a factor of 100, 10, 3, and 1 respectively. The thick solid line is based on the MD reference trajectory that is well reproduced by the heaviest system. Notice that the MD trajectory did not cross the barrier.

can be computed directly as an average over the trajectory. In Fig. 7.2 the calculated free energy profiles are shown. Notice that a straightforward MD simulation of 3.1 ns sampled the free energy surface up to energies of about 5 kcal/mol only. The fact that the relatively small barrier of approximately 6 kcal/mol has never been crossed clearly indicates the limitations of standard MD simulations for the exploration of rare events. At variance with this, all CAFES simulations sample the complete torsional angle profile. Most importantly, it can be seen that the free energy profile of the MD simulation is better reproduced with increasing mass. Using a factor of 100 for the mass ratio, the difference between the MD profile and the CAFES profile is small compared to typical errors due to the empirical force field (or even DFT) description of the system. We remark that the convergence is such that the barrier appears higher for the lighter systems. This can probably be attributed to the energy flow between the reactive system and the environment

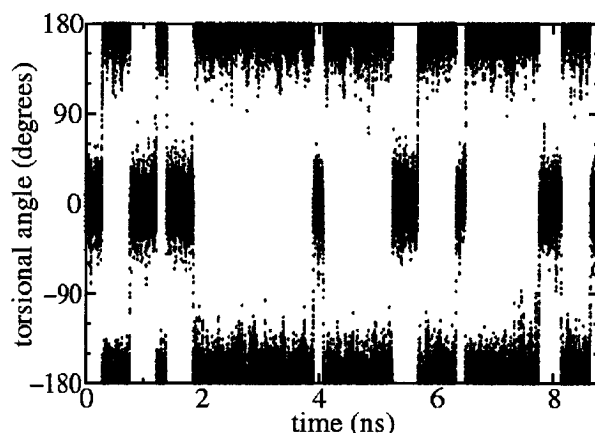


Figure 7.3: The figure shows the time evolution of the torsional angle over the peptide bond ( $C_\alpha$ -C-N- $C_\alpha$ ) during CAFES dynamics (mass factor 100). Torsional transitions, which are naturally in the millisecond time range, happen several times within the few nanoseconds shown.

that effectively cools the lighter, more coupled systems more, reducing the probability to find them near the barrier. In Fig. 7.3, we show the time evolution of the torsional angle over the peptide bond ( $C_\alpha - N - C - C_\alpha$ ), and several *cis* to *trans* torsional transitions can be observed within a few nanoseconds of simulation. This result underlines the sampling efficiency of our method, since this transition can be estimated to be in the millisecond range, and hence inaccessible with standard molecular dynamics techniques. Indeed, using a bias potential approach, we found a barrier of  $15 \pm 0.1$  kcal/mol for this transition, which agrees with the CAFES results within the statistical error ( $\pm 3$  kcal/mol). Unexpectedly, the unusual *cis* conformer was found to be lower in energy by about 0.6 kcal/mol. The latter can be explained by the strong charge-charge interaction of the end groups that are at closer distance in the *cis* conformation. The fact that an unexpected transition can lead to an unexpected global minimum illustrates the usefulness of a sampling approach that leaves, contrary to e.g. constrained dynamics, considerable freedom in the sampling.

## 7.4 The formation of a bromonium ion intermediate and anchimeric assistance in 2-bromoethanol

In this section, we use the CAFES method to explore the reactivity of a solute in solution. In particular, we address the question of whether the bromonium ion is formed as an intermediate in the conversion of 2-bromoethanol to dibromoethane as described in Fig. 7.1. We performed an exploration of the free energy surface using the CAFES method, starting from the protonated form of the reactant (Fig. 7.1b) to arrive at a bromonium ion intermediate (Fig. 7.1c). The computational setup is based on the hybrid Car-Parrinello/Classical code, [19] [20] where the protonated 2-Bromoethanol is described quantum mechanically, and the solvent classically, using 218 SPC water molecules in periodic boundary conditions, and one counter ion. The van der Waals interaction between the QM and MM atoms is based on the GROMOS96 force field, [17] and the Coulomb interaction between the QM and MM part is explicitly taken into account with the scheme described in ref. [22]. The quantum system is treated at the DFT [1] level with the Becke-Perdew exchange [23] and correlation functionals, [24] Martin-Trouillers pseudopotentials, [25] a plane wave basis set with a 70 Ry cutoff, a cubic quantum box with an edge of 16 a.u., decoupled from its images, [26] a timestep of 5 a.u. and a fictitious electron mass of 600 a.u. [19] Notice that it is not possible for the classical solvent to bind covalently with the solute. However, this limitation becomes important only after the  $H_2O$  group has left, and is therefore of minor importance for the part of the reaction under study. The heavy atoms of the bromoethanol molecule are taken as the reactive subsystem, with the masses scaled by a factor of 100, coupled to a Nosé-Hoover chain thermostat with a frequency of  $1000\text{ cm}^{-1}$  and a temperature of 2000 K. The solvent molecules and the hydrogens of the solute were at 300K. Keeping the hydrogens of the solute at room temperature allows us to concentrate on the forward step of the reaction, since the backwards step, which is the deprotonation, is not accelerated. We verified using a standard MD simulation that the distribution of the O-H distance in the solute was unaffected by this setup, even though there is a bonded



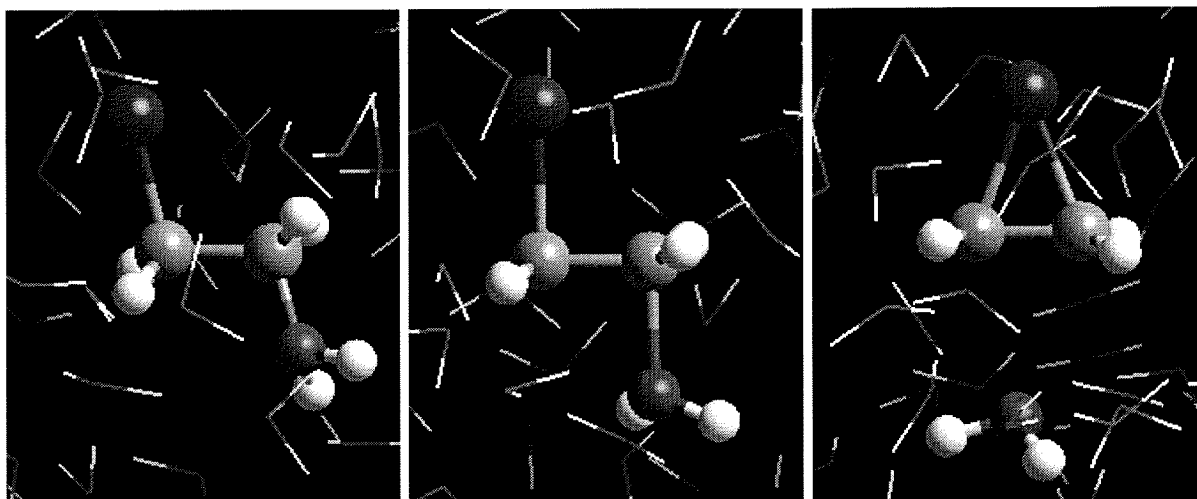


Figure 7.4: The figure shows three consecutive snapshots of the dynamics taken during the reaction. From left to right : 1) Initial configuration, the protonated 2-bromoethanol molecule (ball and sticks) is treated quantum mechanically, whereas the water solvent (lines) is treated classically. 2) A typical configuration just before the water molecule leaves the solute, notice that the C-O bond is elongated, and that both the Br-C-C and the C-C-O angle are close to 90 degrees. 3) The final state of the reaction, where the bromonium ion intermediate is formed.

interaction between the CAFES system and the environment. Independent frames of the reference trajectory were used to start CAFES simulations for a total time of 203 ps of QM/MM Car-Parrinello molecular dynamics simulations.

During these simulations, four reactive events were observed in which the water molecule leaves the solute and a bromonium ion intermediate is formed. One of the reactive events is shown in Fig. 7.4. Based on these four events, a qualitative understanding of how the reaction proceeds can be gained. In particular, we did not observe any dissociation without the formation of the bromonium ion, pointing at the importance of this structure for an energetic stabilisation of the reaction. In addition, we were also able to observe several torsional transitions around the C-C bond, resulting from the fact that the dynamics

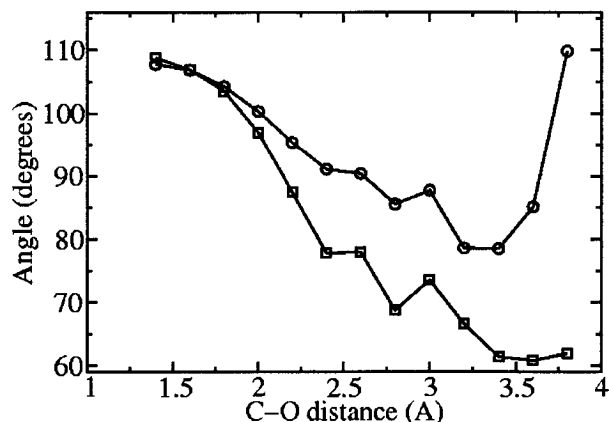


Figure 7.5: Average value of the Br-C-C angle (squares), and the C-C-O angle (circles) as a function of the C-O distance. When the water dissociates, the system ends up in the bromonium state, as indicated by the small Br-C-C angle (60 degrees). Interestingly, both angles are strongly correlated with the distance, and in particular, become acute. Notice that for longer distances, the average of the C-C-O angle is not well defined, since the water molecule diffuses away.

samples freely the CAFES subsystem. We estimate that the relative free energy of the *trans* and *gauche* conformation, as well as the torsional barriers, can be determined with a statistical accuracy of about 1 kcal/mol. The *trans* conformer was observed slightly more than either of the two *gauche* conformers, however, the energy difference between *trans* and *gauche* is very small, and presumably statistically insignificant. The barrier for isomerisation from *trans* to *gauche* is estimated to be about 5 kcal/mol, whereas the *cis* configuration is at the top of a barrier of about 9 kcal/mol. This implies that crossing it with direct molecular dynamics would require a microsecond simulation. We notice that although the system spends the majority of the time in the *gauche* states, the dissociation reaction happens only when the system is in the *trans* state, which is consistent with the fact that it is more difficult to form the bromonium ion starting from the *gauche* configuration. In order to address the extend of the cooperativity between the leaving of the  $H_2O$  group

and the formation of the bromonium ion, we show in Fig. 7.5 a correlation plot between the C-O distance and the average Br-C-C and C-C-O angles. This figure clearly indicates that the dissociation happens in a concerted way with the bending of both angles and thus that an appropriate reaction coordinate for this reaction should include all of them. The second snapshot of Fig. 7.4 shows a typical configuration during the dissociation, and the bending of both angles can be clearly seen. The anchimeric assistance of the bromine follows from the fact that a bromonium ion is formed upon dissociation and that the Br-C-C bend is clearly correlated with the C-O distance during the dissociation. This strong coupling indicates that the rate at which the  $H_2O$  group leaves the solute depends on the properties of the neighboring group. We notice that the average value of the C-C-O bond is  $80^\circ$  to  $90^\circ$  when the water molecule leaves the solute, indicating that the water molecule leaves in such a way as to maximize the overlap of one of its lone pairs with the p-orbital of the carbon atom. Despite the multidimensional character of the reaction coordinate, the simplest way to present the energetics of the reaction is still to use an approximate one dimensional reaction coordinate, and to calculate a free energy profile for this degree of freedom. We calculated, based on our CAFES trajectory, the free energy profile for the dissociation using the C-O distance as an approximate reaction coordinate, and the binned data, together with a Morse potential fitted to this data, are shown in Fig. 7.6. The Morse potential fits very well the shape of the free energy profile up to the more or less flat dissociation region, and can be used to estimate the free energy of dissociation as  $23 \pm 2$  kcal/mol.

## 7.5 Summary and conclusions

CAFES, a novel method for the efficient exploration of free energy surfaces has been presented. In this method, the system is partitioned in a reactive subsystem and an environment, and analogy to the Car-Parrinello method, a fictitious mass is used to decouple adiabatically the two systems. In this way, the dynamics of the slowly moving, reactive

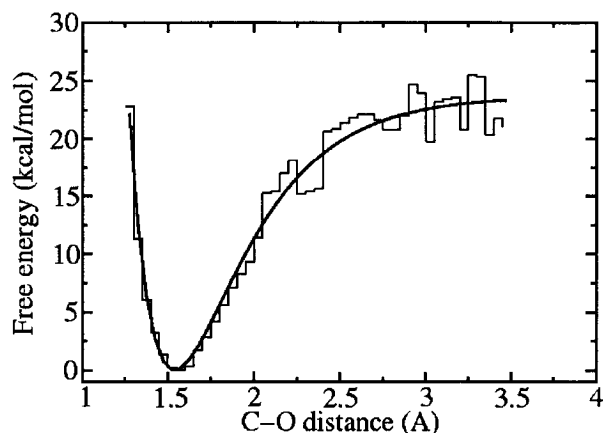


Figure 7.6: The free energy profile for the water dissociation, using the C-O distance as an approximate one dimensional reaction coordinate. The solid curve is a Morse potential fitted to the binned data.

system is on its potential of mean force due to the environment, and additionally, two different temperatures can be introduced without introducing a irreversible heat flow between the systems. The freedom to assign different temperatures can be used to enhance specifically the sampling of the reactive subsystem by increasing its temperature, and hence to accelerate transitions on its free energy surface. If the subsystems are decoupled by using a sufficiently large fictitious mass, a well defined canonical distribution is sampled. We notice that the CAFES method can also be used in a simulated annealing approach, and in particular, for  $T^S$  close to zero, the 'reactive' system goes to a minimum on its free energy surface. If a sufficiently slow cooling is used, the system might find its global free energy minimum. The method can be applied in various MD schemes and here we presented applications using classical molecular dynamics and hybrid Car-Parrinello molecular dynamics. In the first study, the conformation flexibility of a small peptide in solution was enhanced significantly, and transitions that are naturally in the millisecond range were observed during a few nanoseconds of simulation. At the same time, we verified that the free energy profiles generated by the CAFES method were equivalent to those generated

by standard molecular dynamics simulations. For the second application we used 200 ps of Car-Parrinello/classical molecular dynamics simulation, one of the longest *ab initio* simulations performed so far, to probe the reactivity of a protonated 2-bromoethanol molecule in solution. During this simulation, the water molecule dissociates and surpasses a barrier of approximately 23 kcal/mol. During these events, the anchimeric assistance of the bromine was observed several times, and the bromonium ion intermediate was found to be the key intermediate for all the observed dissociations. Previously, such events were inaccessible to straightforward molecular dynamics simulations. These studies demonstrate therefore that the CAFES method is a general and efficient scheme that can reveal unknown reaction pathways and intermediates in complex systems.

## 7.6 Acknowledgements

J.V. acknowledges funding from an ETH internal grant.

## Bibliography

- [1] W. Kohn, and L. Sham, *Phys. Rev.* **140**, A1133 (1965).
- [2] R. Car and M. Parrinello, *Phys. Rev. Lett.* **55**, 2471 (1985).
- [3] For a monograph see *Combined quantum mechanical and molecular mechanical methods*, J. Gao, M.A. Thompson (Ed.) (Oxford University Press, 1998).
- [4] See e.g. G. M. Torrie and J. P. Valleau, *J. Chem. Phys.* **66**, 1402 (1977); T. Huber, A. E. Torda, and W. F. van Gunsteren, *J. Comput.* **8**, 695 (1994); H. Grubmüller, *Phys. Rev. E* **52**, 2893 (1995); A. F. Voter, *Phys. Rev. Lett.* **78**, 3908 (1997); M. M. Steiner, P.-A. Genilloud, and J. W. Wilkins, *Phys. Rev. B* **57**, 10236 (1998); J. VandeVondele and U. Rothlisberger, *J. Chem. Phys.* **113**, 4863 (2000).

- [5] I. Roberts, and G.E. Kimball, *J. Am. Chem. Soc.* **59**, 947 (1937).
- [6] S. Winstein, and H.J. Lucas, *J. Am. Chem. Soc.* **61**, 1576 (1939).
- [7] S. Winstein, and H.J. Lucas, *J. Am. Chem. Soc.* **61**, 2845 (1939).
- [8] See e.g. J. March, *Advanced organic chemistry* (Wiley, New York, 1992).
- [9] For a monograph, see B. Capon, and S.P. McManus, *Neighboring Group Participation* (Plenum Press, New York, 1976).
- [10] S. Nosé, *J. Chem. Phys.* **81**, 511 (1984).
- [11] W.G. Hoover, *Phys. Rev. A* **31**, 1695 (1985).
- [12] A. Di Nola, D. Roccatano, and H.J.C. Berendsen, *Proteins* **19**, 174 (1994).
- [13] P. E. Blochl and M. Parrinello, *Phys. Rev. B* **45**, 9413 (1992).
- [14] G. Pastore, E. Smargiassi, and F. Buda, *Phys. Rev. A* **44**, 6334 (1991).
- [15] It is equivalent to make the environment lighter by a factor  $\alpha \ll 1$ , and this would imply a timestep ( $\Delta t$ ) that scales as  $\Delta t \propto \sqrt{\alpha}$ .
- [16] C. Dellago, P.G. Bolhuis, F. S. Csajka, and D. Chandler, *J. Chem. Phys.* **108**, 1964 (1998).
- [17] W.R.P. Scott, P.H. Hünenberger, H.G. Tironi, A. Mark, S.R. Billeter, J. Fennen, A.E. Torda, T. Huber, P. Krüger, and W.F. van Gunsteren, *J. Phys. Chem. A* **103**, 3596 (1999).
- [18] P. Hünenberger, *J. Chem. Phys.* **23**, 10464 (2000).
- [19] CPMD, J. Hutter, A. Alavi, T. Deutsch, M. Bernasconi, St. Goedecker, D. Marx, M. Tuckerman, M. Parrinello, MPI für Festkörperforschung and IBM Zurich Research Laboratory 1995-1999

- 
- [20] J. VandeVondele, A. Laio, and U. Rothlisberger, *to be published*.
- [21] G.J. Martyna, M.L. Klein, and M. Tuckerman, *J. Chem. Phys.* **97**, 2635 (1992).
- [22] A. Laio, J. VandeVondele, and U. Rothlisberger, *to be published*.
- [23] A.D. Becke, *Phys. Rev. A* **38**, 3098 (1998).
- [24] J.P. Perdew, *Phys. Rev. B* **33**, 8822 (1986).
- [25] N. Trouiller, and J.L. Martins, *Phys. Rev. B* **43**, 1993 (1991).
- [26] G. Martyna, and M. Tuckerman, *J. Chem. Phys.* **110**, 1810 (1999).





## Chapter 8

# Summary and outlook

## 8.1 Summary

In this thesis, novel methods have been presented that can significantly extend the length and time scales of *ab initio* molecular dynamics.

The length scales have been extended by introducing a QM/MM scheme that combines the Car-Parrinello method with a classical molecular dynamics approach based on empirical potentials. This technique effectively allows the simulation of reactive events in large systems, with a cost that is related only to the size of the reactive part and this allows an efficient treatment of the effect of e.g. protein and solvent environment. The interface between the QM and the MM part of the system has been constructed carefully so that a balanced interaction has been obtained. The computational efficiency of the underlying Car-Parrinello and classical methods has been maintained. Using this method, copper binding to the prion protein has been investigated and a possible binding site has been presented.

Various sampling methods have been introduced in order to bridge the time scale gap in MD simulations. These methods significantly extend the range of events that can be observed in molecular dynamics simulations. The classical bias potential technique can be used to efficiently generate free energy surfaces of *ab initio* quality, provided that a good (classical) estimate of the dominant interactions is available. The finite electronic temperature scheme is most promising for the study of systems where an unknown, electronically driven rearrangement, might take place. Non-Hamiltonian dynamics was linked to equilibrium properties as an essential step towards novel schemes that employ general forces to enhance sampling efficiency. Finally, the CAFES method can be used quite generally to explore the reactivity and the conformational flexibility of a given subsystem in an environment. We note that these schemes, with exception of the finite electronic temperature scheme, can also be applied in classical molecular dynamics simulations. All the methods that have been presented here have shown to yield increases in sampling efficiency by

several orders of magnitude.

We can therefore conclude that the combination of the QM/MM scheme and the sampling methods presented here, makes *ab initio* molecular dynamics an even more powerful approach to study the reactivity of complex systems.

## 8.2 Outlook

The subject of this thesis allows for, and requires, experimenting with methods and systems. The result of this experimenting is presented here in the form of several novel schemes. Some of these methods are already in practical use, and thus new ideas about how to apply and extend the schemes have appeared meanwhile. Other methods might still require additional applications before an in depth understanding of their merits and limitations can be obtained. Ultimately, I would like to suggest some directions that could be explored in future work :

- The QM/MM approach in its current form requires van der Waals parameters for the atoms of the QM system. QM species with van der Waals properties that change during the course of a reaction, e.g. change their ionic state, have to be sufficiently far from the QM/MM border. This is a limitation that could be removed from the scheme, but requires additional parameters for the classical system. It would be interesting to see if these parameters could be determined in an *ab initio* way.
- For QM/MM simulations of solutes in solution, an automatic scheme to deal with the diffusion of QM solvent molecules would be very valuable.
- Enhanced sampling simulations can be significantly more efficient, and hence should become part of the standard repertoire of simulation tools. However, in order to achieve this, a larger number of illustrative applications to complex systems has to be performed.

- The enhanced sampling schemes in this thesis are mainly focused on accelerating activated events. It would be interesting to see if similar ideas could be used to improve the conformational dynamics of systems that have slow and low-frequency modes, that are not necessarily activated.
- The introduction of a finite electronic temperature is an interesting first step towards a novel class of sampling methods that can use as much chemical information as can be deduced directly from the electronic structure of the reactive system. Using other reactivity indicators such as e.g. the vibronic coupling constants could be valuable as well.
- The use of non-Hamiltonian dynamics for the evaluation of equilibrium properties might require additional investigation in order to judge the practical applicability. However, the question of whether *dynamical* properties could be estimated from non-Hamiltonian dynamics is appealing and challenging as well.
- The CAFES method seems promising since it is easily applicable and well tested. Additionally, the combined dynamical scheme with the adiabatic separation can also be seen as a general method to reduce a complex, highly dimensional system to a lower dimensional one in an efficient way. Other ways of exploring this simplification could yield several useful molecular dynamics schemes.

## **Curriculum Vitae Joost VandeVondele**

- 1975            Born on the 28th of May, Sint-Amandsberg (Ghent), Belgium
- 1980 - 1987    Primary education
- 1987 - 1993    Diploma in science-mathematics  
                  Sint-Lievens College Ghent
- 1993 - 1998    Academic degree in engineering with specialisation in physics  
                  University of Ghent (RUG)
- 1996 - 1997    Student exchange year  
                  Swiss Federal Institute of Technology Lausanne (EPFL)
- 1998 - 2001    Doctoral studies  
                  Swiss Federal Institute of Technology Zurich (ETHZ)